Title: Palaeotectonic setting of the south-eastern Kédougou-Kéniéba Inlier, West Africa: new insights from igneous trace element geochemistry and U-Pb zircon ages

Author: James S. Lambert-Smith David M. Lawrence Wolfgang Müller Peter J. Treloar

PII: S0301-9268(15)00348-4
DOI: http://dx.doi.org/doi:10.1016/j.precamres.2015.10.013
Reference: PRECAM 4384

To appear in: *Precambrian Research*

Received date: 14-1-2015
Revised date: 7-10-2015
Accepted date: 17-10-2015

Please cite this article as: Lambert-Smith, J.S., Lawrence, D.M., Müller, W., Treloar, P.J.,Palaeotectonic setting of the south-eastern Kédougou-Kéniéba Inlier, West Africa: new insights from igneous trace element geochemistry and U-Pb zircon ages, *Precambrian Research* (2015), http://dx.doi.org/10.1016/j.precamres.2015.10.013

Palaeotectonic setting of the south-eastern Kédougou-Kéniéba Inlier, West Africa: new insights from igneous trace element geochemistry and U-Pb zircon ages

James S. Lambert-Smith[1*]; David M. Lawrence[2]; Wolfgang Müller[3]; Peter J. Treloar[1]

[1]School of Geography, Geology and the Environment, Kingston University London, Kingston upon Thames, Surrey, KT1 2EE, UK

[2]Randgold Resources Ltd, 3rd Floor, Unity Chambers, 28 Halkett Street, St Helier, Jersey, JE24W

[3]Department of Earth Sciences, Royal Holloway, University of London, Egham, Surrey, TW20 0EX

*Corresponding author (Telephone: +44 (0) 208417 9000 Ext. 62880; Email: J.S.Lambert-Smith@kingston.ac.uk)

Abstract

New U-Pb zircon ages and geochemistry from the eastern Kédougou-Kéniéba Inlier are presented and integrated with published data to generate a revised tectonic framework for the westernmost Birimian terranes. The Falémé Volcanic Belt and Kofi Series are highly prospective, hosting several multi-million ounce gold deposits and a significant iron ore resource, but remain under-researched. It is therefore important to constrain the fundamental geological setting.

The igneous rocks of the eastern Kédougou-Kéniéba Inlier are dominantly of high-K calc-alkaline affinity, with fractionated REE patterns and negative Nb-Ta anomalies. The plutonic rocks in the Falémé Belt are dioritic to granodioritic in composition, with moderately fractionated REE patterns and metaluminous A/CNK signatures. Felsic, peraluminous granite stocks, dykes and plutons with fractionated REE patterns and negative Eu, Ti and P anomalies intruded both the Falémé Belt and Kofi Series. Albitisation masks the affinity

of some units, although use of the Th-Co diagram shows that prior to albitisation, all igneous unitsbelonged to the high-K calc-alkaline series. New U-Pb age data for the Boboti and Balangouma plutons indicate crystallisation at 2088.5 ± 8.5 Ma and at 2112 ± 13 Ma, respectively. Inherited zircons in the Boboti pluton indicate magmatic activity in the Falémé Belt at 2218 ± 83 Ma coincided with the oldest dated units in the Mako Belt to the West.

Systematic changes in Dy/Yb, Sm/La, Nb/Zr, Rb concentration, Eu-anomaly and εNd_t over ~200 Ma reveal that the tectonic setting in the KKI evolved from a volcanic island arc environment to an active continental margin. Crustal thickening, as a result of a shift to collisional tectonic setting, combined with magmatic differentiation, led to the generation of peraluminous, granitic melts with a significant crustal component. A small suite of more basic intrusive and extrusive rocks on the eastern margin of the Dialé-Daléma basin are highly metaluminous and display limited LILE enrichment, with normalised HREE values close to unity. The Daléma igneous rocks may have formed in an extensional back arc, related to the arc system.

Key Words

Kédougou-Kéniéba Inlier; Birimian; geochemistry; U-Pb zircon ages; palaeotectonic setting

1 Introduction

The Birimian terranes of the West African Craton are considered to be an important record of crustal growth in the Palaeoproterozoic (Boher et al., 1992; Doumbia et al., 1998; Gasquet et al., 2003). The exact tectonic setting and geodynamic processes that gave rise to the Birimian terranes remain a subject of debate. In part this is because of the complex nature of the terranes, but also due to gaps in the geochemical and chronological datasets. The Kédougou-Kéniéba Inlier (KKI; Figure 1) represents the westernmost outcrop of the Birimian in the Leo-Man shield, and is separated from the majority of the Palaeoproterozoic terranes by the overlying Neoproterozoic sandstones of the Taoudeni Basin. The western part of the KKI is well studied, with most attention given to the Mako Volcanic Belt (MVB; Figure 1) in Eastern Senegal (e.g., Debat

et al., 1984; Abouchami et al., 1990; Ledru et al., 1991; Dia, et al., 1997; Diallo, 2001; Gueye et al., 2008; Ngom et al., 2009; Treloar et al., 2014). By comparison, the eastern KKI (the Falémé Volcanic Belt and Kofi Series; Figure 1) is under-researched, despite hosting several world-class Au deposits, including the Loulo, Gounkoto, Sadiola and Tabakoto gold mines all of which are situated east of the Senegal-Mali Shear Zone (SMSZ; Bassot and Dommanget, 1986; Dommanget et al., 1993; Lawrence et al., 2013a and b). In addition to Au mineralisation, several magnetite-skarn deposits are hosted in the Falémé Volcanic Belt (FVB; Schwartz and Melcher, 2004). The KKI is clearly a highly prospective region in the Birimian; it is therefore important to constrain the fundamental geological setting.

The majority of geochemical studies in the KKI have focused on the tholeiitic lavas and belt-hosted granitoid plutons in the MVB (Debat et al., 1984; Abouchami et al., 1990; Boher et al., 1992; Diallo, 2001; Pawlig et al., 2006). Schwartz and Melcher (2004) published a geochemical study of the FVB, which concentrated on the genesis of the skarn-style iron ore deposits. However, niether the extensive Balangouma pluton in the north of the belt (Figure 2), or the numerous minor stocks and dykes throughout the FVB and Kofi Series have been studied geochemically. These lithologies are dominantly unaltered by hydrothermal processes, with well-preserved primary textures, despite greenschist facies metamorphism. However, some rocks in the area have been albitised due to hydrothermal fluid-rock interactions. This may hide the true tectonic and petrogenetic affinity of these lithologies, leading to incorrect conclusions as to their genesis.

Here we use new geochronological and geochemical datasets, combined with published data, to construct an improved geotectonic framework for the KKI, with an emphasis on the Falémé Volcanic Belt and Kofi Series. We aim to integrate trace element geochemistry with geochronology to show the secular evolution of Birimian magmas from primitive island arc granitoids to evolved syn-collisional granites. This reflects the shift from an ocean island arc setting to an accretionary regime with associated crustal thickening. In addition we aim to examine the key geochemical characteristics of altered igneous lithologies

and show that Na-rich igneous rocks in the KKI are the product of albitisation of high-K calc-alkaline lithologies.

2 Geology of the Birimian of West Africa

The West African Craton (WAC) consists of Archaean and Palaeoproterozoic terranes; stable since ~2 Ga, they provide a valuable record of crustal growth processes and contain notable mineral wealth. The WAC is divided into three domains: 1) The Reguibat Rise in northern Africa; 2) The Leo-Man Rise in sub-Saharan West Africa and, 3) The Kayes and Kédougou-Kéniéba Inliers in the Sahel region, North West of the Leo-Man Rise. The Reguibat and Leo-Man rises both share contacts with Archaean continental nuclei and are collectively referred to as the Baoulé-Mossi Domain. The Birimian terranes consist of narrow, linear to arcuate, N to NNE trending volcanic belts, separated by broad sedimentary basins. The volcanic rocks are interpreted to be the base of the sequence, with coeval to slightly younger metasedimentary rocks (Béziat et al., 2000; Pouclet et al, 2006; Roddaz et al., 2007). The terranes were accreted and cratonised during a period of SE to NW directed crustal shortening, metamorphism and magmatic accretion from 2120 to 2080 Ma known as the Eburnean orogeny (Bonhomme, 1962; Oberthür et al., 1998; Feybesse et al., 2006). Peak metamorphic conditions were reached in the Ashanti belt of Ghana at ~2100 Ma based on U-Pb ages of metamorphic titanite (Oberthür et al., 1998). Peak metamorphic conditions are widely reported as amphibolite facies (500–600°C; 4–6 kbar; John et al., 1999; White et al., 2013), although greenschist facies assemblages are dominant across the region (Hirdes et al., 1996).

The volcanic belts consist of tholeiitic lavas and associated mafic intrusions interbedded with minor sequences of immature sedimentary, volcaniclastic and carbonate rocks. The sedimentary basins comprise isoclinally folded and deformed sequences of greywacke, argillite and arkose with calc-alkaline volcanic sequences. Extensive suites of plutonic rocks have intruded both units, and range in composition from tholeiitic gabbro to high-K calc-alkaline granite. The majority of plutonic rocks are grouped by their host

terranes; i.e. 'belt-' and 'basin-type', and a post-Eburnean K-rich series (Leube et al., 1990; Hirdes et al., 1992).

The Birimian terranes formed over a period of ~180 Ma, between 2266 and 2088 Ma (Perrouty et al., 2012; White et al., 2014 and references therein; Parra-Avila et al., 2015). This period is divided into two phases, the age and terminology of each differs throughout the Birimian. In South western Ghana the Eburnean I (2266-2150 Ma) precedes the Eburnean II (2216-2088 Ma) (Allibone et al., 2002). In northern Ghana, the earlier event is referred to as the Eoeburnean (2195–2150 Ma) and the latter as the Eburnean (2148–2090 Ma) (de Kock et al., 2011). In Burkina Faso the Eburnean (2130 – 1980 Ma) is preceded by the Tangaean event (2170-2130 Ma) (Tshibubudze et al., 2009; Hein, 2010). Broadly speaking, the earlier event, in each case, consists of volcanism, granitoid emplacement and fold, thrust tectonics. This is followed by emplacement of younger granitoids, strike-slip deformation and mineralisation in the latter event. U-Pb zircon ages show that the Eburnean I encompasses early volcanism, between 2266 ± 2 and 2132 ± 3 Ma (Taylor et al., 1992; Loh et al., 1999), and early plutonism, from 2213 ± 3 to 2151 ± 7 Ma (Dia et al., 1997; Gueye et al., 2007; White et al., 2014 and references therein). Tshibubudze et al., (in press) suggest that the three early events are broadly the same tectonic event. U-Pb dating of detrital zircons shows that sedimentation was coeval with magmatism in the volcanic belts, from 2135 ± 5 Ma in Ghana (Oberthür et al., 1998; Davis et al., 1994) and from 2164.7 ± 0.9 Ma in the KKI (Hirdes and Davis et al., 2002). The Eburnean represents the final phase of magmatism in Ghana, where basin-type plutons were intruded between 2116 ± 2 and 2088 ± 1 Ma (U-Pb zircon) (Hirdes et al., 1992; Davis et al., 1994).

Though there are variations, models for crustal growth in the Birimian largely involve the development of juvenile volcanic arc magmas in an oceanic setting (Sylvester and Attoh, 1992; Dia et al., 1997; Pawlig et al., 2006; Soumaila et al., 2008; Baratoux et al., 2011). Recent P-T-t reconstructions in metasedimentary rocks record blueschist-facies metamorphic conditions diagnostic of subduction environments (Ganne et al., 2011).

3 Lithostratigraphy of the KKI

The stratigraphy of the KKI from west to east consists of: 1) bimodal volcanics intruded by numerous plutonic complexes in the MVB; 2) detrital sedimentary rocks of the Dialé-Daléma basin, which are intruded by the Saraya batholith; 3) calc-alkaline volcaniclastic rocks of the FVB and; 4) siliciclastic sedimentary rocks of the Kofi Series, unconformably overlain by Neoproterozoic sedimentary rocks to the east (Figure 1). Age data for the KKI are summarised in Table 1.

3.1 The Mako Volcanic Belt

The MVB is a NNE trending ~20-40 km wide band of bimodal volcanic rocks which crop out in the west of the KKI. They are overlain to the west by the Pan-African Mauritanides belt. The Main Transcurrent Shear Zone (MTZ) marks the eastern edge of the MVB, with the Dialé-Daléma basin to the east (Figure 2). The lowermost units in the west consist of thick flows of massive and pillowed tholeiitic basalt. These are associated with dolerites and gabbros and intercalated with thin felsic tuffs, pyroclastites, rhyolites and minor clastic and carbonaceous sedimentary rocks (Dioh et al., 2006), which become more prominent to the east. The age of the Mako tholeiitic basalts is poorly constrained. Dia (1988) reported a whole-rock Pb-Pb age of 2195 ± 118 Ma. Given this large error, the upper age limit for the Sandikounda amphibolite-gneiss complex (SAG; Figure 1) is interpreted to be the younger age limit for their eruption as it intrudes the lava sequences. The volcanic sequence is capped by andesitic lava, tuff and pyroclastic rocks (Dia, et al., 1997; Ngom et al., 2009). An andesite flow in the east of the MVB yielded a Sm-Nd whole-rock age of 2160 ± 16 Ma (Boher et al., 1992).

The MVB is intruded by a plutonic complex known as the Kakadian batholith (Dia, 1985; Hirdes and Davis, 2002; Dioh et al., 2006; Gueye et al., 2007). The batholith is composed of three units in the north (Figure 1); 1) the Sandikounda amphibolite-gneiss complex (SAG); 2) the Sandikounda Layered Plutonic Complex (SLPC); and 3) the Laminia-Kaourou Plutonic Complex (LKPC). The south of the batholith is known as the Badon batholith. The SAG consists of tonalitic to dioritic gneiss containing amphibolite enclaves. This is the oldest unit in the north of the batholith. U-Pb data indicate crystallisation at 2205 ± 15 Ma (Gueye et al.,

2007). The SLPC crystallised between 2171 ± 9 and 2158 ± 8 Ma (Pb-Pb and U-Pb zircon data; Dia et al., 1997; Goujou et al., 2010), and is composed of layered hornblende-gabbro, diorite, migmatite and hornblendite, with xenoliths of wherlite and pyroxenite. Elements of the SLPC intruded the SAG (Gueye et al., 2008). The LKPC consists of the Laminia and Kaourou plutons. Tonalite and granodiorite of the Laminia pluton were emplaced at 2138 ± 12 and 2105 ± 8 Ma (Pb-Pb zircon data; Dia et al., 1997; Gueye et al., 2008). The porphyritic monzogranite of the Kaourou pluton is younger at 2079 ± 6 Ma (Pb-Pb zircon data; Dia et al., 1997). Both plutons contain xenoliths of Mako volcanic rocks and the SLPC (Dia et al., 1997). The Badon batholith is composed of biotite-granodiorite; magmatic emplacement occurred at a similar time to the SAG at 2198 ± 2 Ma (Pb-Pb zircon data; Gueye et al., 2007). To the south east of the Badon batholith, the Mako belt was intruded by the Soukouta granite-granodiorite complex at 2142 ± 7 Ma (U-Pb zircon; Delor et al., 2010). Delor et al., (2010) and Goujou et al., (2010) dated (U-Pb zircon) a series of granitic plutons, which intruded the MVB between 2142 ±7 Ma and 2102 ±8 Ma. The minor Mamakono and Tinkoto plutons intruded the MVB at 2076 ± 3 Ma and 2074 ± 5 Ma, respectively (U-Pb and Pb-Pb zircon data; Hirdes and Davis, 2002; Gueye et al., 2007). Ar-Ar and K-Ar studies on hornblende by Gueye et al. (2007) showed that the SAG and Tinkoto plutons cooled to ~550 °C by 2112 ± 12 Ma and 2051 ± 16 Ma, respectively. The Badon batholith cooled to below ~300°C at 2098 ± 20 Ma (Ar-Ar and K-Ar in biotite; Gueye et al., 2007).

3.2 The Dialé-Daléma series

Cropping out to the east of the MVB, the Dialé-Daléma series consists of a thick sequence of isoclinally folded volcanoclastic, siliciclastic and minor carbonate rocks centrally intruded by the Saraya Batholith (Hirdes and Davis, 2002; Gueye et al., 2008; Figure 1). The dominant volcanoclastic component of the Dialé-Daléma sediments suggests that they represent a lateral facies equivalent of the MVB. Subordinate basalts are interbedded in the westernmost sequence (Diallo, 2001), where the youngest detrital zircons yield a maximum U-Pb age of 2165 ± 0.9 Ma (Hirdes and Davis, 2002). The Saraya batholith consists of several plutonic bodies, composed of biotite-muscovite-adamellite granite. These bodies were emplaced between

2079 ± 2 Ma and 2061 ± 15 Ma (U-Pb zircon and monazite) and place a lower limit on sedimentation in the Dialé-Dalemé Basin (Hirdes and Davis, 2002; Delor et al., 2010).

3.3 The Falémé Volcanic Belt

The Falémé Volcanic Belt crops out to the east of the Daléma basin (Hirdes and Davis, 2002; Lawrence et al., 2103a). The FVB is a ~16 km wide NNE trending belt of volcanic and intrusive rocks. Outcrop is dominated by plutonic rocks, consisting of two plutonic complexes, each >100 km^2: 1) the Balangouma pluton in the north; and 2) the Boboti pluton in the centre and south of the belt. Several smaller plutons crop out in the southern and eastern regions of the FVB, including the South Falémé (Hirdes and Davis, 2002) and Garaboureya plutons (Figure 2). The volcanic sequences comprise pillowed andesite flows, subordinate rhyodacite lavas and pyroclastic rocks. These are interbedded with volcanoclastic rocks, wackes and carbonate rocks (Hirdes and Davis, 2002; Schwartz and Melcher, 2004). Magnetite skarn deposits are hosted in several of the smaller plutons and carbonate rocks (Schwartz and Melcher, 2004). Limited age data are available for the volcanic sequence in the FVB. U-Pb zircon ages date a several volcanic and sub-volcanic rhyolite units at 2099 ± 4 Ma, 2082 ± 8 Ma and 2064 ± 30 Ma, with inheritance at 2155 ± 34 Ma (Hirdes and Davis, 2002). Further U-Pb zircon geochronological data from the Boboti pluton and the South Falémé tonalite show ages of 2080.2 ± 0.9 Ma and 2081.5 ± 1.1 Ma, respectively (Hirdes and Davis, 2002).

3.4 The Kofi Series

The Senegal-Mali Shear Zone (SMSZ) is a sinistral brittle-ductile shear zone that forms a 1-10 km wide N-S trending corridor of varying deformation styles, and separates the Kofi Series from the FVB. Secondary and higher order splays off the SMSZ host the major Au deposits in the Kofi Series, including Gara, Yalea, Sadiola, Yatela and Gounkoto (Dommanget, et al., 1993; Lawrence et al., 2013a and b). The Kofi Basin is made up of detrital sedimentary and carbonate rocks and breccias intruded by minor mafic dykes and small intermediate to felsic stocks. The sedimentary rocks in the Kofi Series are dominantly wackes, with end member sandstone (rare) and argillite (common). Wackes and argillites are typically interbedded on a small scale (10s cm), although both rock types occur as thicker units (10s m), with gradational changes from quartz

wacke through to argillite common. The siliciclastic component of wackes varies between quartz and feldspar rich, with clasts showing a large range in size (fine sand to pebbles) and shape (angular to well rounded). Certain packages of quartz wacke, particularly in the west of the series have been intensely tourmalinised (Lawrence et al., 2013a), while others have been albitised. The Kofi Series is carbonate-rich to the west, with proximity to the Falémé Volcanic Belt (Figure 1). These carbonate rocks are dominantly dolomitic marls. Silicic clasts are composed of fine grained and sub angular quartz and feldspar. All sedimentary lithologies in the Kofi Series show poly-phase deformation generated during the Eburnean orogeny (Dabo and Aïfa, 2010). The igneous rocks that intruded the Kofi Series include dolerite to monzodiorite dykes and small stocks of quartz feldspar porphyry. Two larger plutons of monzogranite composition also intruded the Kofi Series, namely the Gamaye and Yatea plutons.

The age of deposition in the Kofi Series is constrained by detrital zircons and intrusive plutonic rocks. Tourmalinized quartz wacke at the Gara deposit include a detrital zircon dated by Pb-Pb at 2093 ± 7 Ma (Boher et al., 1992). An older, deltaic deposit on the margin of the FVB yields a U-Pb detrital zircon age of 2125 ± 27 Ma (Boher et al., 1992), though it is unclear whether this belongs to the Kofi Series or the FVB. The Gamaye pluton has been dated at 2045 ± 27 Ma using the Rb-Sr whole-rock isochron method, providing a broad lower age limit for sedimentation (Bassot and Cean-Vachette, 1984).

4 Methods

4.1 Mineral chemistry and petrography

Major and trace-element mineral compositions were determined using an Oxford Instruments X-ACT Energy Dispersive System (EDS) detector mounted on a Zeiss EVO 50 Scanning Electron Microscope (SEM) at Kingston University London. EDS operation employed an accelerating voltage of 20 kV, a beam current of 1.5 na, and a detector process time of 4. Data collection and reduction was handled using the Oxford Instruments INCA analytical suite. The detection limit for all elements was approximately 0.20 wt %.

4.2 Geochemistry

Geochemical sample preparation and analyses were conducted at Kingston University. Rock pulps were desiccated overnight at 60 °C, then tested for loss on ignition (LOI) at 900 °C. 0.25 g of each sample was mixed with 1.25 g of lithium metaborate ($LiBO_2$) flux and fused in graphite crucibles at 1050 °C. The melt was then dissolved in 150 ml of 0.5M nitric acid (HNO_3), filtered, and diluted to a concentration of 0.3M HNO_3.

Analysis of major elements was conducted using a JY Ultima 2C inductively coupled plasma atomic emission spectrometer (ICP-AES). Standard reference materials: GSJ JR2 (rhyolite), USGS BCR-2 (basalt), USGS AVG-2 (andesite) and USGS BHVO-2 (basalt), were prepared and run as unknowns to monitor accuracy and precision. Measured values were within 3 % of the recommended values and the precision was better than 3 % (1 SD). USGS W-2 (Centerville diabase) was analysed every five samples to monitor instrumental drift.

Analysis of trace and rare earth elements (REEs) employed an Agilent 7500c quadrupole inductively coupled plasma mass spectrometer (ICP-MS). Samples, standards and blanks were prepared as above, and then diluted x25 in 0.5 % HCl and 1 % HNO_3. Instrumental drift was monitored by regular analysis of a 10 ppb multi-element solution. Accuracy and precision were determined from analysis of the standard reference materials: USGS AGV-2, GSJ JR-2, USGS BHVO-2, USGS BCR-2, GSJ JP-1, GSJ JA-2, TDB, WMG-1, GH, BR, Bt-Mica-Fe and Phl-Mica-Mg. Total accuracy was <3 % and precision was <4% (1SD).

4.3 Geochronology

Laser ablation inductively coupled mass spectrometry (LA-ICP-MS) was conducted on magmatic zircons from four samples of the Falémé Volcanic Belt. Zircons were separated using conventional methods at Kingston University. Zircons were mounted in 25 mm epoxy resin blocks, polished, and examined under SEM-CL to identify internal zonation and mineral inclusions.

LA-ICP-MS analysis was conducted at the Department of Earth Sciences, Royal Holloway University of London using a 193 nm excimer laser-ablation system featuring a two-volume Laurin LA cell coupled to an

Agilent 7500ce quadrupole ICP-MS (Müller et al., 2009) (Table 2). Using GeoStar software, ~150 spots analysis points of both unknowns (~100) and reference materials (standards; ~50) were selected, which comprise one 'run'. The primary standard GJ-1 (600.7 Ma, based on Jackson et al., 2004) was analysed every seventh analysis to monitor both downhole as well as long-term elemental fractionation. Acquisition time was 30 seconds per spot with 15 seconds background before and after, pulse rate was 5 Hz, spot size was 34 µm and laser fluence on target (energy density) was 3 J/cm^2. The standards Temora-2 (416.78 ± 0.33Ma; Black et al., 2004), 91500 (1065.4 ± 0.3 Ma; Wiedenbeck et al., 1995), Mud Tank (732 ± 5 Ma; Black and Gulson, 1978) and Plešovice (337.13 ± 0.37 Ma; Sláma et al., 2008) were analysed as unknowns in order to ensure accuracy and reproducibility. Reduction of raw analytical data was performed using the Iolite software package® (Paton et al., 2010) in Wavemetrics Igor Pro® by applying exponential downhole fractionation and long-term spline data derived from the primary standard to both unknowns and secondary standards; no common-Pb correction was required. Approximate U, Th, Pb concentrations and Th/U-ratios are based on using the generally fewer 91500 analyses as calibration standard. Isochron diagrams, concordia, discordia and weighted mean U-Pb and Pb-Pb ages were calculated using the Isoplot 4.15 Excel macro (Ludwig, 2003).

Analyses of four international zircon standards were conducted to assess the accuracy and precision of the instrument. Thirty seven analyses of Plešovice yielded a concordant age of 336.1 ± 1.4Ma (MSWD=0.73); this gives an error of 0.3 % and precisionof 0.8 % (2 SD). Twenty nine analyses of the 91500 standard yielded a concordant age of 1053.8 ± 8.7 Ma (MSWD=0.9); this gives an error of 1.1 % and precision of 1.7 % (2 SD). Seventeen analyses of Temora-2 yielded a weighted average age of 410.7 ± 2.6 Ma (MSWD=1.2), with error of 1.5 % and precision of 1.3 % (2 SD). Mud Tank yielded a concordant age of 715 ± 11 Ma (MSWD=0.74); with error of 2.3 % and precision of 3.1 % (2 SD). Low U concentration in Mud Tank may contribute to higher error and uncertainty. The unknowns contained significantly higher concentrations of U; therefore Mud Tank can be disregarded when calculating accuracy and precision. Long-term reproducibility of $^{238}U/^{206}Pb$ ages based on Plesovice and 91500 zircons is ± 1.5 % (2 RSD). Analytical data for zircon satndards is presented in Table 3.

5 Petrographic data

5.1 The Falémé Volcanic Rocks

The earliest volcanism in the FVB is recorded by fine-grained porphyritic andesites that crop out in the Kabe West area, south of the Balangouma pluton. These plagioclase-amphibole porphyries contain abundant euhedral albite (15 %) and amphibole (15 %) phenocrysts (0.5-2 mm). The groundmass is made up of finer, bladed albite (60 %) with minor anhedral quartz (5 %). Albite is strongly sericitised (5 %) and amphibole is replaced by actinolite. Along the eastern margin of the Boboti pluton, porphyritic and equigranular andesite overlies albitised sub-volcanic diorite (Figure 3A). The andesites contain albite phenocrysts (10 %) and a groundmass of albite (65 %) and actinolite (25 %), with accessory rutile, ilmenite, apatite and zircon. The diorite is equigranular, medium to coarse-grained and richer in amphibole (35 %) and rutile than the andesite.

5.2 The Daléma Suite

This small suite of intrusive and extrusive rocks crop out over ~3 km^2 on the eastern margin of the Dialé-Daléma basin, west of the Balangouma pluton. In this location, a fine-grained porphyritic basaltic-andesite (Figure 3B) contains phenocrysts of plagioclase (10 %), olivine (10 %) and trace clinopyroxene. Plagioclase is dominant and occurs as 0.5 to 3 mm laths and rare coarse tabular crystals. Olivine is fine to medium grained and subhedral, with embayments and inclusions of the groundmass common. The groundmass (75 %) is very fine and contains a high proportion of magnetite (5 %), with plagioclase, olivine and accessory pyrite. To the north, a phaneritic gabbroic diorite (Figure 3C) contains phenocrysts of oligoclase (50 %) (An_{23}) (up to 7 mm), magnesio-hornblende and tschermakite (35 %) (Both ~1.5 cm). These are replaced by biotite (10 %) and minor chlorite with associated ilmenite and titanite. Minor quartz and K-feldspar (~5 %) occur in the groundmass, with allanite, chalcopyrite, apatite, pyrite, gypsum and zircon. In the same locality, a gabbroic diorite porphyry (Figure 3D) contains 1-6 mm, subhedral phenocrysts of oligoclase (10 %), biotite (5 %) and actinolite (5 %). The groundmass is composed of oligoclase (32 %) (An_{22}), biotite (5 %), amphibole (40 %) and quartz (2-3 %), with minor clinopyroxene, K-feldspar, zircon and apatite.

5.3 The Balangouma Pluton

The Balangouma pluton occupies the majority (~200 km^2) of the northern FVB and is composed of intermediate to felsic lithologies. The northern lobe of the pluton crops out to the north west of the Gara mine has been sheared out along the SMSZ. The main unit varies slightly in composition between monzodiorite, monzonite, quartz monzonite and granodiorite, but the bulk of the pluton is a coarse-grained, mesocratic quartz monzodiorite (Figure 3E). This contains coarse (5-7 mm) K-feldspar (2 %) and ~1 mm oligoclase (5 %) (An_{26}) phenocrysts. These minerals are also present in the medium grained groundmass (13 % and 25 %, respectively) together with biotite (26 %), quartz (9 %), augite (5 %) ($Wo_{30}En_{40}Fs_{30}$) and hornblende (5 %). Pyroxenes and amphiboles are partially chloritised (10 %). Accessory phases include apatite, titanite, zircon and Cr-rich haematite. This unit is cross cut by 20-30 cm wide aplite dykes (Figure 3G) composed of medium grained intergrown plagioclase (10 %), K-feldspar (35 %) and quartz (50 %). Fine-grained (<100 μm) biotite (2 %) emphasises a weak shear fabric. Similar units crop out throughout the pluton as meter-scale stocks.

5.4 The Boboti Pluton

The Boboti pluton (~187 km^2) makes up the central intrusive complex of the FVB. Schwartz and Melcher, (2004) and Dioh et al., (2006) describe the Boboti pluton as a clinopyroxene-hornblende-bearing granodiorite. Field mapping and sampling from outcrop in the southern Boboti pluton has revealed it to be more complex and composed of a number of intermediate to felsic intrusive stocks. Lithologies range in composition from diorite to monzogranite.

The southern body of the pluton is a coarse porphyritic quartz monzodiorite with 7-8 mm phenocrysts of albite (5 %), and ~2 mm phenocrysts of biotite and pyroxene (1 %) (Figure 4A). The groundmass is composed of sericitized albite (35 %), K-feldspar (25 %), quartz (10 %), clino- and orthopyroxene (10 %), biotite (9 %) and actinolite (3 %). Pyroxenes have been largely replaced by titanite (1 %) and V-Cr-bearing magnetite (1 %). Accessory phases include apatite, ilmenite, chalcopyrite, monazite and zircon. Minor bodies of monzogranite (Figure 4B), ~1-2 km^2 in extent, intruded the centre of the southern Boboti pluton. These are

equigranular (400 - 600 µm) with rare 2-3 mm plagioclase phenocrysts. Quartz (31 %), albite (32 %) and K-feldspar (29 %) make up the groundmass, with minor intergrown muscovite (1 %) and biotite (1 %). Unevenly distributed clusters of <100 µm euhedral tourmaline (1 %) grains are present throughout the rock. Accessory minerals include epidote, ilmenite, zircon, apatite and titanite. Extensive outcrops of porphyritic pyroxene-bearing quartz diorite (Figure 4C) occur to the west (Sample BOP4 in Figure 2). This is medium to coarse-grained with 4 mm albite phenocrysts (7 %), with finer biotite (1 %) and actinolite phenocrysts (<1 %). The groundmass is composed of albite (70 %), quartz (5 %), clino- and orthopyroxene (6 %), biotite (4 %), actinolite (2 %) and K-feldspar (1 %). Pyroxene grains contain abundant inclusions of titanite (2 %) and magnetite (1 %). Accessory phases include apatite, chalcopyrite, monazite and zircon.

5.5 Minor Falémé Intrusive rocks

To the south of the Balangouma pluton several small plutons crop out just north of the Kouroudiako magnetite skarn deposit in the Kabe West target area (Figures 2, 4D and 4E). These consist of medium to coarse-grained quartz diorite with minor carbonate-chlorite-epidote alteration and magnetite-pyrite mineralisation. Phenocrysts of plagioclase (1-6 mm) and actinolite (~1 mm) occur within a fine to medium grained groundmass of plagioclase, K-feldspar, quartz, biotite and minor orthopyroxene. To the west, several medium-grained dioritic plutons host a magnetite skarn deposit at Karakaene Ndi. These have a hiatal seriate texture, with medium to coarse-grained albite, biotite, actinolite and quartz in the groundmass. Biotite and actinolite replace primary hornblende. All the diorite plutons in this area have been albitised (feldspars have been altered to albite), with the characteristic assemblage of carbonate-chlorite-haematite in the groundmass.

The south Falémé pluton, south east of the Boboti pluton, is exposed along the Falémé River. It consists of albitised diorites, magmatic breccias, and a small suite of diorites. Fine-grained diorite porphyry contains phenocrysts of coarse euhedral albite (~1 cm) and medium-grained, subhedral actinolite. The groundmass comprises plagioclase and actinolite with accessory rutile.

5.6 Igneous rocks of the Kofi Series

5.6.1 The Yatea granite and North Gara stock

The Yatea granite, which crops out in the east of the Kofi Series, is of similar affinity to a small stock which crops out just north of the Gara mine. Both bodies are pink coloured, medium-grained (1-3 mm) monzogranite (Figure 4F). Orthoclase and microcline (45 %) are dominant over plagioclase (up to 25 %). The mafic assemblage is dominated by biotite (<10 %). Accessory phases include magnetite, monazite and titanite.

5.6.2 The Gamaye pluton

The Gamaye pluton is the largest igneous body exposed in the Kofi Series (~138 km^2). It is composed of monzogranite (Figure 4G), which is porphyritic in the south and equigranular in the north. The pluton is cross-cut by tourmaline bearing pegmatite dykes. The northern part of the pluton is composed of phaneritic monzogranite. The mineralogy consists of medium grained (200 - 500 µm), subhedral albite (35 %), K-feldspar (30 %), quartz (27 %) and biotite (8 %). Accessory minerals include muscovite, allanite and apatite (200 - 400 µm), zircon, rutile and magnetite. Tourmaline is disseminated in 1-5 cm halos around pegmatite dykes. Feldspars are weakly sericitized. This unit becomes porphyritic ~15 km to the SE (MOU2; Figure 2). K-feldspar forms subhedral poikilitic phenocrysts (up to 7 mm), and contains inclusions of quartz, plagioclase and biotite. Sub-rounded, 1 to 15 cm mafic enclaves are present throughout the unit. A series of coarse-grained pegmatite dykes cross cut the pluton. These are 1-30 cm wide and composed of 10-15 mm albite, quartz and K-feldspar, and ~200 µm muscovite. Some dykes contain very coarse (up to 8 mm) tourmaline crystals. These are typically subhedral, with inclusions of quartz and apatite. Thin (1-2 mm) tourmaline veins cross cut the dykes.

5.6.3 Minor intrusive rocks in the Kofi Series

The Kofi Series is intruded by numerous discordant dykes (typically <5 m) and small (sub-km scale) plutons. Some units are extremely fine-grained. These minor igneous units are typically intermediate, diorite

361 to quartz monzodiorite in composition, though mafic dykes are also present. Many lithologies have been
362 albitised to variable degrees.

363 Small stocks of biotite-quartz-feldspar porphyry (QFP; Figure 4H) occur in the vicinity of the Gamaye
364 pluton. Quartz (16 %), plagioclase (16 %) and K-feldspar (2 %) phenocrysts are up to 8 mm, while biotite
365 phenocrysts (6 %) measure ~1 mm. The groundmass (~60 % of the rock) is composed of <20 µm mineral
366 phases (likely quartz, plagioclase, k-feldspar and biotite). Feldspars show weak to moderate sericite
367 alteration. Intensely albitised QFP stocks occur near the Baqata and Kolya target areas (Figure 2). These
368 contain coarse (up to 7 mm) relict phenocrysts of quartz and feldspar, the latter having been replaced by
369 glomeroblastic albite. The groundmass is composed of secondary <100 µm albite with interstitial ankerite
370 and very fine –grained haematite. Albite is weakly sericitized.

371 Medium to coarse grained quartz monzodiorite dykes have intruded the footwall of the Gounkoto
372 deposit. These contain phenocrysts of plagioclase (5 %) and amphibole (replaced by actinolite) in a
373 groundmass of plagioclase (60 %), k-feldspar (5 %), quartz (10 %), actinolite (10 %) and biotite (10 %).
374 Accessory phases include augite (primary), apatite, tourmaline, ilmenite, rutile, monazite and chromite. In
375 addition, dykes of medium grained diorite occur throughout the Kofi Series. The mineralogy consists of
376 plagioclase (75 %), biotite (20 %) and K-feldspar (5 %) with accessory rutile and pyrite. It is possible that
377 these were originally monzodiorite dykes which have undergone weak albitisation.

378 Mafic dykes 0.5 to 13 m wide have intruded the wall-rock at both the Gara and Yalea Au deposits. These
379 are discontinuous, deformed and metamorphosed, forming sharp contacts with the host sediments. The
380 intensity of alteration makes primary compositions difficult to identify.

381 ***5.6.4 Hydrothermal albitite***

382 Albitite crops out primarily at two localities within the Kofi Series, one at Baqata on the Bambadji permit
383 and one 15 km to north, in the Falémé River, near Kolya. In outcrop the unit is massive and blocky, with no
384 definable sedimentary or igneous textures. The lithology is composed dominantly of equigranular albite (85-

95 %) with accessory quartz, chlorite, apatite, rutile, allanite, zircon and biotite. Chlorite is associated with fractures cross cutting the groundmass. It is likely that this unit is the result of extreme alteration of an igneous protolith and therefore represents the most intense example of the sodic alteration seen in this region.

5.6.5 Post-Birimian dolerite dykes

These dolerite dykes cross cut all lithologies in the KKI and show no clear evidence of deformation or hydrothermal alteration. These are more continuous than the Birimian dykes and vary in thickness from 2-200 m. Mineralogy consists of bytownite (An_{71-79}), clinopyroxene and rare orthopyroxene. Similar dykes elsewhere in the WAC belong to the 200 Ma Central Atlantic Magmatic Province (CAMP; Jessell et al., 2015) ± . Though some CAMP-aged dykes are no doubt present, the mafic dykes in the KKI are dominantly older. Mafic dyke swarms with ages of ~1350-1400 Ma are most abundant, but ages of ~900 Ma and 1150 Ma are also present (K-Ar whole-rock data; Delor et al., 2010).

6 Geochemistry

A total of 42 fresh (unaltered) and albitised whole-rock samples were analysed for major and trace element concentrations. Only samples with minimal weathered crust and hydrothermal alteration were selected for analysis, with the exception of 14 samples of albitised igneous rocks. These were included to investigate the geochemical characteristics of the regional sodic alteration. All trace element data has been normalized against Normal-Mid Ocean Ridge Basalt concentrations (N-MORB; data from Sun and McDonough, 1989). Whole rock geochemical data is summarised in tables 4, 5, 6 and 7.

The geochemical data from the FVB and Kofi Series show a suite of igneous rocks with high-K calc-alkaline affinities (Figure 5A and B) with compositions ranging from gabbroic through to granitic (Figure 6). The FVB is dominated by large plutons of intermediate composition, with metaluminous A/CNK values (mean = 0.8; Figure 7), relatively little REE fractionation (mean La/Lu = 22.3) and very minor Eu anomalies (Eu/Eu* = 0.9; Figure 8). The small suite of felsic stocks that intruded the Balangouma and Boboti plutons are

409 more evolved (SiO_2 >73 %), with moderately fractionated REE patterns (mean La/Lu = 50), peraluminous
410 A/CNK values (mean =1.2) and more distinct negative Eu anomalies (mean Eu/Eu* = 0.6; Figure 8C). By
411 comparison to the FVB, the Kofi Series contains less exposure of igneous rock. These are dominantly highly
412 fractionated (mean La/Lu=113), peraluminous (mean A/CNK = 1.1) granites of similar affinity to the minor
413 felsic stocks of the FVB. Minor dykes and plutons of more intermediate compositions are largely albitised;
414 these exhibit metaluminous A/CNK values (mean of 0.99) and relatively little REE fractionation (La/Lu of
415 19.9). The rocks of the Daléma igneous suite form a separate group, consisting of unevolved gabbros and
416 dolerites with highly metaluminous A/NK and A/CNK values (Figure 7) and low La/Lu ratios (mean = 9.4).

417 All samples show enrichment in the light ion lithophile (LILE) elements, with granitic samples showing
418 considerably higher enrichment in both the Kofi Series and the FVB (Figure 8). All rocks from both terranes
419 show consistent negative Nb and Ta anomalies (Figure 8D to F). In addition, granitic rocks from the Falémé
420 Belt and Kofi Series show pronounced negative Ti and P anomalies (Figure 8F).

421 Albitised samples show consistently high Na_2O concentrations (mean =7.8 wt. %), with correspondingly
422 low concentrations of most other major elements, most notably K_2O (mean = 0.6 wt. %). As a result of this,
423 the albitised samples lie in the tholeiitic series of the K_2O versus SiO_2 diagram (Figure 5A) and also
424 consistently plot above the alkaline-sub-alkaline divide on the TAS diagram (Figure 6); unaltered samples are
425 consistently of sub-alkali affinity. Use of the Th-Co diagram of Hastie et al. (2007) reveals that the albitised
426 samples should indeed belong to the calc-alkaline and high-K calc-alkaline series (Figure 5B), as do the
427 unaltered rocks of the eastern KKI. A/NK values in albitised rocks are significantly lower than in unaltered
428 rocks, yet A/CNK values are unperturbed (Figure 7). This reflects albitisation of both plagioclase (loss of Ca^{2+})
429 and K-feldspar (loss of K^+), and likely replacement of other alkali-bearing mineral species (e.g. biotite).
430 Albitised rocks plot in the alkaline field of the TAS diagram as a direct result of Na metasomatism.

431 **7 LA-ICP-MS U-Pb Zircon Geochronology**

7.1 Boboti Pluton

7.1.1 BOP1A

Sample BOP1A was obtained from the Southern part of the Boboti pluton. This unit is a coarse quartz monzodiorite with albite, biotite and pyroxene phenocrysts (Figure 4A). A total of 71 zircon grains were analysed (84 spots in total). These were stubby, subhedral, fine-grained (<150 µm) and highly fractured. Growth zones revealed under SEM-CL are well developed in some grains and almost absent in others (Figure 9A, B, C and D). A systematic relationship between zonation, apparent age and the degree of discordance was not observed. Forty three analyses produced concordant ages within a 2σ error ellipse (Figure 10A); 19 of these were highly concordant (Figure 10B and C). The majority of the data (70 spots) formed a clear discordia trending toward the origin. This is interpreted to be caused by recent Pb-loss attributed to surface weathering. Analytical data for sample BOP1A is presented in Table 8.

A regression line fitted to the 70 concordant and discordant spots intersects the isochron at 2088.5 ± 8.5 Ma (MSWD=2.2), with a lower intercept around the origin (-5 Ma; Figure 10A). This corresponds well with a weighted average $^{206}Pb/^{238}U$ age from the 19 most concordant spots of 2093 ± 9.6 Ma (MSWD=1.6; Figure 10B) and a weighted average $^{207}Pb/^{206}Pb$ age of 2085 ± 11 Ma (MSWD=6.3; Figure 10C). In order to minimize the rejection of data points the upper discordia intercept of 2088.5 ± 8.5 Ma is interpreted to represent the age of magmatic emplacement.

In addition to the main population, 2 small grain populations show evidence for inheritance of older material at ~2200 Ma and 3000 Ma (Figure 11A and B). Two zircon grains 9 and 22 yield partially concordant (~99 %) $^{206}Pb/^{238}U$ ages at 2209 ± 34 Ma and 2215 ± 35 Ma respectively (Figure 9C and D). These yield a concordia age of 2226 ± 13 Ma (MSWD of 1.4; Figure 11A). CL imaging show bright cores with diffuse zonation surrounded by a dark 2-10 µm rim. Two grains (zircons 75 and 73; Figure 9E and F) yielded concordant $^{206}Pb/^{238}U$ ages at 3000 ± 120 and 3380 ± 160 Ma respectively (Figure 11B) and Pb-Pb ages of 2865 ± 84 Ma and 3152 ± 94 Ma. Both the Archaean aged grains are fractured and feature a luminescent,

finely zoned core and with a dark rim (Figure 11B). These cores may be the inherited component, with the dark rim a later overgrowth related to magmatism at ~2 Ga.

These new data broadly agree with the published age of emplacement for the Boboti pluton at 2080.2 ± 0.9 Ma (Hirdes and Davies, 2002). However, our data show a more protracted period of emplacement with a more widely distributed age population and additional evidence of inheritance from early magmatism and possible Archaean material.

7.2 Balangouma Pluton

7.2.1 CLIB01

Sample CLIB01 from the Balangouma pluton to the north west of the Loulo mine camp is a coarse grained, mesocratic quartz monzodiorite with coarse (5-7 mm) K-feldspar phenocrysts (Figure 3E). A total of 81 grains were analysed (94 spots in total). The majority of spots produced highly discordant ages. Grains were stubby, subhedral, fine-grained (<150 µm) and highly fractured (Figure 9G and H). As with sample BOP1A, growth zonation appears to bears no relationship to the age or concordance of the grains. Analyses of the cores and rims of zircons are also consistently within error of each other. Analytical data for sample CLIB01 is presented in Table 9.

A discordia line was fitted to a subset of 43 spots with an upper intercept of 2105.6 ± 9.8 Ma (MSWD=5.8) and a lower intercept at 28 ± 57 Ma (Figure 12A). The lower intercept near the origin implies that recent Pb-loss is responsible for the discordance. A weighted mean $^{207}Pb/^{206}Pb$ age of 2098 ± 6.3 Ma (MSWD=4.6; Figure 12B) corresponds well to the upper intercept age as does a weighted mean $^{206}Pb/^{238}U$ age calculated from the most concordant spots (n=7) of 2097 ± 25 Ma (MSWD=3.9; Figure 12C). The age of magmatic emplacement is best represented by the upper intercept of the discordia, with an age of 2105.6 ± 9.8 Ma. This sample showed no evidence of inheritance.

7.2.2 CLIB05

Sample CLIB05 was collected from the Balangouma pluton around 8.5 km south of CLIB01. This sample is a coarse grained quartz monzonite with K-feldspar phenocrysts (Figure 3F). A total of 69 zircon grains were analysed (81 spots in total). Grains were subhedral, fractured and fine grained (<150 μm). Examination under SEM-CL reveals fine concentric zonation in the majority of zircon grains (Figure 9I and J). Some grains show small, anhedral cores lacking zoning; spot analyses of these cores tend to yield discordant ages. Analytical data for sample CLIB05 is presented in Table 10.

A significant number of analysed spots produced highly discordant ages, generating a discordia with an upper intercept of 2118 ± 16 Ma (MSWD=2.3; n=43) and a lower intercept around 100 Ma (Figure 13A). A weighted average of the 13 most concordant $^{206}Pb/^{238}U$ ages yields a younger age of 2054 ± 24 Ma (MSWD=0.58; Figure 13B), however the weighted average for the equivalent $^{207}Pb/^{206}Pb$ ages gives an age of 2096.5 ± 9.3 Ma (MSWD=1.4; Figure 13C), which broadly agrees with the upper intercept of the discordia. This weighted average $^{207}Pb/^{206}Pb$ age remains relatively consistent even if a limited number of analyses are rejected, giving an average age of 2103 ± 20 Ma, though this does produce a very high MSWD of 26 (n=57; Figure 13D). On the basis of this broad agreement it seems likely that the upper discordia intercept age of 2118 ± 16 Ma represents the age of magmatic emplacement for this sample.

7.2.3 CLIB07

Sample CLIB07 was collected from an outcrop approximately 1.2 km to the northwest of CLIB05 in the Balangouma pluton. The sample is a coarse porphyritic monzonite (Figure 3H). A total of 59 zircon grains were analysed (70 spots in total). Grains are euhedral, fine (<150 μm) and highly fractured with rare inclusions of apatite and quartz (Figure 9K and L). As with other samples, growth zonation shows no clear relationship to the age or concordance of spots. Where cores and rims have been analysed, $^{206}Pb/^{238}U$ ages are consistently within error of each other. Analytical data for sample CLIB07 is presented in Table 11.

The analyzed grains produced highly discordant ages for a large number of spots. A set of 56 spots form a discordia with an upper intercept at 2113 ± 15 Ma and a lower intercept at 76 Ma (MSWD=1.4; Figure 14A). This corresponds well to the weighted mean $^{207}Pb/^{206}Pb$ age for the same spots of 2102 ± 8.2 Ma

(MSWD=7.3; Figure 14B). In addition the weighted mean of the $^{206}Pb/^{238}U$ ages of the 9 most concordant spots yields an age of 2086 ± 23 Ma (MSWD=0.27; Figure 14C). The upper discordia intercept is accepted as the most probable age for magmatic emplacement for this sample at 2113 ± 15 Ma. This is on the basis of the overlapping mean U-Pb and Pb-Pb ages and the minimal rejection of data points in order to construct a robust discordia. No evidence of inheritance was found in this sample.

Given that the overall reproducibility of our method is ±1.5 % (2 RSD), the three ages of emplacement for the Balangouma pluton are analytically indistinguishable. We therefore favour an unweighted mean age for each of these units (represented by CLIB01, 05 and 07) of 2112 ± 13 Ma.

8 Discussion

8.1 Tectonic setting of the KKI

The Falémé Volcanic Belt and the Kofi Series consist of high-K and uppermost calc-alkaline series volcanic and magmatic rocks with fractionated REE patterns, and immature, siliciclastic sedimentary rocks. This suggests an island arc or active continental margin setting, an interpretation further supported by persistent depletion in Nb-Ta relative to HFS elements (Figure 8). This phenomenon is attributed to magmas derived from partial melting of sub-arc mantle wedge. This is due to the insolubility of Nb and Ta in slab-derived aqueous fluids and strong partitioning into residual rutile (Brenan et al., 1994; Baier et al., 2008). Calc-alkaline volcanic and plutonic rocks in the MVB display similar LREE and LILE enrichment, and negative Nb anomalies (Boher et al., 1992; Dioh et al., 2006; Pawlig et al., 2006) suggesting a similar tectonic setting.

The least evolved rocks in the region belong to the Daléma Suite. The tectonic setting in which this unit formed is unclear; Nb-Ta depletion and high Th/La and positive Ce/Ce* inherited from subducted sediment (Plank, 2005; Hastie et al., 2013; Figure 15) all point to a volcanic arc environment. The Dy/Dy*-Dy/Yb diagram of Davidson et al. (2013; Figure16) is of use here as it can represent the shape of a REE pattern in a single point. This highlights the slight LREE-enriched MORB character in the Daléma samples. LILE

527 enrichment and near-MORB HREE values (Figure 8) suggest a possible extensional (back-arc) setting. Back-
528 arc rocks commonly feature arc-like chemistries modified by an invading fertile mantle source below the
529 spreading centre (Taylor and Martinez, 2003).

530 The less evolved rocks, dominantly present in the FVB (typically silica oversaturated syeno-diorites),
531 show characteristics typical of volcanic arc granites (Figure 17). These include the predominance of
532 amphibole, biotite and pyroxene in ferromagnesian mineral assemblages, depleted medium to HREE (Figure
533 8; a function of amphibole fractionation) and metaluminous A/CNK (Figure 7; c.f. Pearce, 1996). Minor
534 negative P anomalies and enrichment in Zr and Hf compared to other HFS elements (Figure 8E), respectively
535 indicate minor apatite fractionation and zircon accumulation (Pearce et al., 1984). Th/La-Ce/Ce* ratios
536 (Hastie et al., 2013; Figure 16) indicate that the arc rocks in the eastern KKI contain a mix of slab derived
537 components. These are dominated by volcanic and continental detritus, with minor contribution from
538 hydrogenous Fe–Mn oxides linked to slow sedimentation rates.

539 The felsic rocks (granites *sensu stricto*) of the FVB and Kofi Series feature negative Eu, Ti and P
540 anomalies, not observed in the intermediate lithologies (Figure 8) and classify as syn-collision granites
541 (Figure 17). Negative Eu anomalism indicates that plagioclase fractionation took place under relatively
542 reduced conditions (increasing Eu^{2+}/Eu^{3+}) during magma evolution (Drake, 1975). Similarly, depletions in Ti
543 and P indicate fractionation of apatite and Ti oxides. The Dy/Dy*-Dy/Yb diagram (Figure 15) indicates that
544 felsic rock in the study area have incorporated significant amounts of sediment (Davidson et al., 2013).

545 Overall, the igneous rocks of the south-eastern KKI represent a volcanic arc, developed above a
546 subducting oceanic plate. This subsequently evolved into a collisional setting. The Dy/Dy*-Dy/Yb diagram
547 (Figure 15) adequately represents the evolution of the arc system, with the Daléma igneous rocks plotting in
548 the E-MORB field and the Balangouma pluton and some of the more intermediate intrusions in the Kofi
549 showing upper continental crust compositions. The bulk of the data sit along the trend of increasing
550 sediment incorporation, with the most felsic, peraluminous rocks showing the highest Dy/Yb values. The
551 Th/La-Ce/Ce* diagram (Figure 16) shows that the mantle wedge below the arc has a significant contribution

552 of continental detritus and hydrogenous Fe–Mn oxides as well as minor volcanic detritus from the
553 downgoing slab.

554 The MVB differs significantly from the FVB, due to the presence of a lower sequence of tholeiitic igneous
555 rocks. It is generally agreed (Abouchami et al., 1990; Diallo, 2001), due to the presence of pillow lavas,
556 turbidite sequences, a lack of significantly older inherited material and consistently positive $\varepsilon_{Nd}t$ values (+4.9;
557 Ngom et al., 2009) that these tholeiites are juvenile. However, there is debate over specific tectonic setting
558 being attributed to either: 1) intra-plate oceanic plateau (Abouchami et al., 1990; Boher et al., 1992; Ngom
559 et al., 2009); or 2) an immature oceanic island arc (Sylvester and Attoh, 1992; Dia et al., 1997; Diallo, 2001;
560 Pawlig et al., 2006). Abouchami et al. (1990) and Boher et al. (1991) suggested an oceanic plateau setting
561 based on low Ti concentrations, LREE depletion and pronounced negative Ce anomalies, placing the MVB
562 tholeiites between MORB and island arc compositions. Sylvester and Attoh (1992) observed that the Mako
563 and other Birimian belts show petrogenetic similarities with modern island arcs. The granitic rocks (*sensu*
564 *lato*; >5 % quartz) in the MVB are characterised by persistent negative Nb-Ta anomalies and LILE enrichment
565 (Boher et al., 1992; Dioh et al., 2006; Pawlig et al., 2006). Dioh et al. (2006) reported that the majority of
566 calc-alkaline and high-K intrusive rocks in the MVB classify as volcanic arc granites. A small subset lies along
567 the divide between volcanic arc and syn-collisional granite, including granites (*sensu stricto*) from the
568 Kéniéba pluton. These share geochemical characteristics with syn-collisional granites in the FVB and Kofi
569 Series, including peraluminous A/CNK values (1.03-1.04), negative Eu anomalies (0.72-0.81) and high Dy/Yb
570 values (~3.2). These points suggest that, despite the absence of tholeiites in the FVB, plutonic rocks in the
571 western KKI developed in very similar tectonic settings to those in the east, evolving from juvenile volcanic
572 arc to a collisional setting.

573 **8.2 Geochronological framework for the Kédougou-Kéniéba Inlier**

574 New U-Pb zircon age data presented here show that the Balangouma pluton crystallised at 2112 ± 13
575 Ma (Table 1; Figure 18). Additionally, evidence of inherited zircon cores from the ~2085 Ma Boboti pluton
576 (Hirdes and Davis, 2002 and this study), suggest an earlier phase of magmatism in the FVB at ca. 2226 ± 13

577 Ma (Figure 18). This suggests the presence of underlying basement material which predates the SAG in the
578 Mako Belt at 2213 ± 3 Ma (Gueye et al., 2007).

579 In general, the intermediate to felsic rocks in the KKI are the younger units. They are also the most likely
580 to yield useable zircons for accurate and precise dating. The geochronological data presented here,
581 combined with existing data, allows the synthesis of a geochronological framework for the KKI. Much of the
582 available age data imply diachroneity, with the westernmost MVB containing the oldest units (the SAG and
583 Badon pluton; Figure 18); the FVB, sedimentary basins and silicic intrusive rocks are generally younger.
584 Inherited grains found in several units of the FVB indicate that volcanism may have occurred simultaneously
585 in both the Falémé and MVBs. The following sequence of events can be determined from the available data
586 (Figure 18):

587 1. The intrusion of the SAG and elements of the Badon pluton occurred between 2213 ± 3 Ma and 2194
588 ± 4 Ma (Dia et al., 1997; Gueye et al., 2007). The Mako tholeiitic lavas are assumed to be older.
589 However, it is possible that tholeiitic volcanism was cogenetic with emplacement of the SAG or
590 Badon pluton (Pawlig et al., 2006). Inherited zircon grains from the Boboti pluton imply
591 magmatism may have occurred at some time prior in the FVB at ~2226 Ma.

592 2. The SLPC intruded the Mako volcanics and the SAG between 2171 ± 9 Ma and 2158 ± 8 Ma (Dia et
593 al., 1997; Goujou et al., 2010) within the time frame for possible calc-alkaline magmatism in the
594 FVB at 2155 ± 34 Ma, based on inherited zircon grains from a rhyolite flow (Hirdes and Davis,
595 2002). Sedimentation began in the westernmost Dialé-Daléma basin at 2164.7 ± 0.9 Ma (Hirdes
596 and Davis, 2002), coinciding with andesitic volcanism at 2160 ± 16 Ma (Boher et al., 1992).

597 3. The southern portion of the MVB was intruded by the Soukouta granite at 2142 ± 7 Ma. The oldest
598 component of the LKPC was emplaced over 33 Ma, from 2138 ± 6 Ma to 2105 ± 8 Ma (Dia, 1988;
599 Dia et al., 1987). The latter stages of emplacement overlap with the main phase of magmatism in

600 the FVB. The SAG cooled below 550 °C at 2112 ± 12 Ma (Gueye et al., 2007. Deltaic deposits
601 began to develop on the western margin of the Kofi basin at 2125 ± 27 Ma (Boher et al., 1992).

602 4. The Falémé plutonic rocks (including the Boboti, Balangouma and South Falémé plutons) were
603 emplaced into pre-existing volcanic and sedimentary units between 2112 ± 13 Ma and 2080 ±
604 0.9 Ma, coinciding with felsic volcanism at 2099 ± 4 Ma (Hirdes and Davis, 2002). During this
605 period (2103 to 2102 Ma), further granitic plutons intruded the northern MVB (Goujou et al.,
606 2010) and rhyodacite units erupt in the Dialé-Daléma Basin (2098 ± 13 Ma; Delor et al., 2010).
607 Sedimentation in the Kofi basin began at 2093 ± 7 Ma at the latest (Boher et al., 1992). A deltaic
608 deposit began developing at 2125 ± 27 Ma, as reported by (Boher et al., 1992); however it is
609 unclear if this deposit belongs to the Kofi Series or the Falémé Belt. In either case, it provides an
610 argument for syn-volcanic sedimentation.

611 5. The latter stages of magmatism in the FVB and MVB are broadly coincident. The youngest unit of the
612 LKPC (the Kaourou pluton) and the late calc-alkaline series plutons (Tinkoto and Mamakono) in
613 the MVB all crystallised between 2079 ± 6 Ma and 2074 ± 5 Ma (Dia et al., 1997; Hirdes and
614 Davis, 2002; Gueye et al., 2007). A period of felsic volcanism in the FVB between 2082 ± 8 Ma
615 and 2064 ± 30 Ma (Delor et al., 2010) coincided with calc-alkaline volcanism in the MVB at 2067
616 ± 12 Ma (Gueye et al., 2007) . The Tinkoto pluton cooled below 550 °C by 2051 ± 16 Ma (Gueye
617 et al., 2007). The Saraya batholith marks the youngest limit for the Dialé-Daléma basin at 2079 ±
618 2 Ma (Hirdes and Davis, 2002). Metamorphic monazites within the batholith formed at 2064 ± 4
619 Ma and the pluton is interpreted to have cooled below 350 °C by 2021 ± 11 Ma (Gueye et al.,
620 2007).

621 Sedimentation in the Kofi Series is considered to have ceased by 2045 ± 27 Ma; the best-known age of
622 crystallisation of the Gamaye pluton (Bassot and Cean-Vachette, 1984).The data summarised in Figure 18
623 suggest that the development of the volcano-sedimentary belts and sedimentary basins of the KKI occurred
624 broadly synchronously, with a suite of older units within the westernmost MVB likely representing the

earliest development of upper crust in the region (Dia et al., 1997; Geuye et al., 2007). For the older units of the KKI, Gueye et al. (2007) reported prolonged cooling profiles; with K-Ar from amphibole and biotite apparently suggest that the plutons took ~80 Ma to cool from 900 to 550 °C and ~100 Ma to cool from 900 to 300 °C, respectively. Smaller, younger plutons such as the Tinkoto granodiorite yielded K-Ar in amphibole ages within error of the crystallisation age of 2079 ± 6 Ma. Assuming no disturbance of the K-Ar system, this suggests that the western KKI remained hot (~550°C) until ~2100 Ma. The early magmatism in the KKI (represented by the SAG, Badon granodiorite and SLPC) likely corresponds to the Eoeburnean/Eburnean I of Ghana (Allibone et al., 2002; de Kock et al., 2011) and the Tangaean of Burkina Faso (Tshibubudze et al., 2009; Hein, 2010). New inherited zircon data in the Boboti pluton, suggests that magmatism occurred at a similar time in the FVB (~2226 Ma).

Sedimentation coincides with the onset of calc-alkaline volcanism and magmatism in both volcanic belts, supporting derivation from erosion of the arcs (c.f. Roddaz et al., 2007). In general, the more evolved magmatic rocks (the Saraya batholith, Gamaye pluton and the minor felsic stocks in the FVB) post-date the intermediate lithologies, either absolutely (through dating) or based on field relationships. This reflects the temporal evolution of the magmatic systems in the KKI through the arc stage and into the Eburnean orogeny, when crustal thickening increased the amount of assimilation of crustal material during emplacement (Figure 15).

The Boboti pluton contained two zircon grains which were partially (~95 %) concordant at ~3.0 and 3.4 Ga respectively. Very little Archaean material has previously been reported in Birimian terranes. However, the Birimian is bounded by older Archaean domains, which may conceivably have been reworked during arc formation, basin opening and terrane accretion. The Leo-Man Rise, to the south of the KKI contains units between 3540 to 3050 Ma (Thiéblemont et al., 2004). Inherited material from the Boboti pluton fall within this age range. Begg et al., (2009) reported tomographic data which suggested the presence of reworked Archaean crust and subcontinental lithospheric mantle beneath large portions of the West Africa Craton. Such material may be reworked by melts generated in the lower crust or upper mantle. Alternatively, Lebrun

et al. (2015) reported the presence of Archaean derived clasts of banded iron formation within the Birimian aged Kintinian conglomerates of the Siguiri Basin in Southern Mali. Similar detrital material could conceivably have been present in the country rocks in to which the Boboti pluton intruded. This material may then have been incorporated during emplacement. While two zircon grains cannot be considered statistically significant and contamination cannot be wholly ruled out, there may be scope for future investigation into possible crustal contamination from Archaean terranes.

8.3 Temporal constraints on tectonic setting

The igneous rocks of the KKI show some distinct variation in their trace, REE and major element chemistry, which cannot wholly be attributed to the affinity of their host terranes (i.e. belt versus basin-type plutons). As an example, the minor felsic stocks that intruded the Balangouma and Boboti plutons are distinctly more evolved than their hosts, with peraluminous A/CNK, fractionated REE patterns and distinct Eu anomalies. It is therefore necessary to examine these geochemical variations in a temporal rather than spatial context.

In Figure 19 several geochemical parameters have been plotted against absolute ages of plutons from across the KKI. The data show a distinct positive trend in Dy/Yb values with time indicating an increasing control on REE patterns by residual garnet in the magma source (Davidson et al., 2013). This indicates sufficient thickening of the lithosphere to allow garnet to become stable in the magma source region. The trend of decreasing Eu* with time reflects fractional crystallisation of Ca-plagioclase. Higher Nb/Zr and La/Sm reflect increasing HFSE and LREE enrichment, respectively. The positive trend in these two ratios represents increase in the concentration of incompatible elements as the magmas become more evolved and collision begins to take place (c.f. Draut and Clift, 2001). Rb content in magmas is increased by partial crustal melts, combined with further enhancement due to addition of a Rb-rich volatile component (Pearce et al., 1984; Pearce, 1996). Increase in the Rb content of igneous rocks in the KKI over time reflects the transition from volcanic arc to syn-collision magmatism (Figure 17A). The overall positive ε_{Nd}(2.1Ga) values may be explained by the juvenile nature of the newly formed Birimian crust (Abouchami et al., 1990; Boher

et al., 1992; Pawlig et al., 2006; Ngom et al., 2009). However, ε_{Nd}(2.1Ga) data (from Boher et al., 1992; Pawlig et al., 2006) shows a general trend toward lower positive values, indicating a greater contribution of continental derived sediment with time (c.f. Draut and Clift, 2001). In addition, the time difference between Nd model ages (Boher et al., 1992; Pawlig et al., 2006) and absolute ages of crystallisation increases with time, suggesting that more evolved melts began to stall in the thickened crust (Brown and Rushmer, 2006).

While there are some anomalously evolved rocks present in the older Mako sequences, in general Figure 19 shows a trend with time towards more evolved magmas with a greater contribution of sediments. This represents thickening of the newly formed Birimian crust as the volcanic island arc became accreted and collisional magmatism set in.

8.4 Comparisons to other Birimian terranes

The majority of previous research has concluded that the growth of Birimian crust initially took place in an oceanic setting, with immature island arcs evolving to continental arcs through a process of subduction generated magmatism and terrane accretion (Sylvester and Attoh, 1992; Abouchami et al., 1990 and Boher et al., 1992; Salah et al., 1996; Dia et al., 1997; Pawlig et al., 2006; Baratoux et al., 2011; Tshibubudze et al., in press). Granitoid rocks in Cote D'Ivoire (Pouclet et al., 2006), Burkina Faso (Tapsoba et al., 2012), Niger (Salah et al., 1996) and Ghana (Sylvester and Attoh, 1992) all display geochemical characteristics consistent with those described in the KKI (REE fractionation and negative Nb-Ta, P, Ti and Eu anomalies). Many igneous units throughout the Birimian are described as tonalite–trondhjemite–granodiorite series (TTG; e.g. Soumaila et al., 2008; Vidal et al., 2009; de Kock et al., 2011; Baratoux et al., 2011; Tapsoba et al., 2012; Tshibubudze et al., in press). This is not the case for the plutonic rocks in the eastern KKI where tonalitic compositions result from widespread alkali metasomatism (Figure 5). As described in the MVB, the majority of Birimian volcanic belts feature a lower sequence of tholeiitic rocks (Abouchami et al., 1990; Sylvester and Attoh, 1992; Salah et al., 1996; Feybesse et al., 2006). These are entirely lacking in the FVB. The only truly mafic volcanic to sub-volcanic rocks observed in the south-eastern KKI are those of the Daléma suite. There is little to compare the Daléma igneous rocks to in the wider Craton, though Dampare (2008) reported a

700 probable back-arc setting for tholeiitic basaltic andesite in the southern Ashanti Belt. Similarly, back-arc
701 settings have been suggested for Birimian rocks in SW Niger (Soumaila et al., 2008) and in Cote Di'Ivoire
702 (Vidal and Alric, 1994). This suggests that extensional arc settings are likely to have occurred elsewhere in
703 the Baoulé-Mossi domain.

704 Though early volcanism in the KKI is not well constrained, inherited zircons in the MVB and FVB suggest
705 that magmatism took place at ca. 2200 Ma related to coeval volcanism. This agrees with whole rock Sm-Nd
706 ages of volcanic rocks in Ghana (2266 ± 2 to 2132 ± 3 Ma; Taylor et al., 1992; Davis et al., 1994; de Kock et
707 al., 2011) as well as U-Pb zircon data from TTG suites in Burkina Faso (2203 ± 12 Ma and 2207 ± 38 Ma;
708 Tshibubudze et al., in press) and in south western Niger (2174 ± 4 Ma; U-Pb zircon; Soumaila et al., 2008).
709 Alternatively, these inherited zircons may represent basement material. Crystallisation ages of Pre-Birimian
710 gneiss in the Oudalan-Gorouol belt in NE Burkina have been reported by Tshibubudze et al.,(2013) at 2253 ±
711 9 Ma to 2255 ± 26 Ma (U-Pb zircon). In addition, detrital zircons in micaschists from south western Niger
712 indicate the presence of a calc-alkali protolith between 2273 and 2278 Ma (U-Pb ages; Soumaila et al., 2008).

713 In Ghana (Leube et al., 1990; Oberthür et al., 1998; Davis et al., 1994), Burkina Faso (Roddaz et al., 2007;
714 Baratoux et al., 2011; Tshibubudze et al., in press) and the KKI (Hirdes and Davis, 2002), sedimentation and
715 belt magmatism overlap , suggesting that the basins are lateral facies equivalents of the volcanic arcs.
716 Crystallisation of the Badon batholith, SAG and SLPC occurred between 2200 and 2150 Ma, matching the age
717 range of belt-type plutons in Ghana (White et al., 2014 and references therein) and Burkina Faso
718 (Tshibubudze et al., in press). The two-phase Eburnean model applied elsewhere in the Birimian (Allibone et
719 al., 2002; Tshibubudze et al., 2009; Hein, 2010; de Kock et al., 2011) is also applicable in the KKI. Two distinct
720 peaks in magmatic zircon abundance occur at 2150 and 2075 Ma, the majority of age data for the KKI fall
721 between these peaks and likely represent the main phase of Eburnean magmatism. An older peak around
722 2200 Ma may represent the pre-Eburnean event (Eoeburnean, Eburnean I, Tangaean) described in other
723 Birimian terranes (Allibone et al., 2002; Tshibubudze et al., 2009; Hein, 2010; de Kock et al., 2011). With the

724 exception of inherited zircons from the Boboti pluton, material of this age is entirely lacking in the area of
725 the south-eastern KKI studied. In

726 The general trend of increasingly felsic, peraluminous magmatism through time, as a result of crustal
727 thickening, seems common throughout the Birimian (e.g. Ama Salah et al., 1996; Perrouty et al., 2012;
728 Tapsoba et al., 2012).

729 **9 Conclusions**

730 The igneous rocks that define the eastern KKI are dominantly of high-K calc-alkaline affinity. Though in
731 some units, this affinity is masked by albitisation. Nevertheless, use of the Th-Co diagram of Hastie et al.
732 (2007) shows that all igneous units, prior to albitisation, belonged to the high-K calc-alkaline series. Indeed,
733 the Falémé Volcanic Belt altogether lacks the tholeiitic igneous units common to other Birimian belts.

734 Fractionated REE patterns and ubiquitous negative Nb-Ta anomalies suggest a tectonic setting analogous
735 to modern volcanic arcs and active continental margins. Furthermore, changes in trace element ratios, Eu-
736 anomaly and $\varepsilon_{Nd}t$ over ~200 Ma (Figure 19) reveal the tectonic setting in the KKI to have evolved from a
737 volcanic arc environment to an active continental margin, with more peraluminous, granitic melts
738 developing as the crust thickened. The Daléma igneous rocks on the eastern margin of the Dialé-Daléma
739 basin are highly metaluminous and display limited LILE enrichment, with normalised HREE values close to
740 unity. These may have formed in an extensional back arc system.

741 New U-Pb zircon age data show that the Boboti and Balangouma plutons were emplaced at 2088.5 ± 8.5
742 Ma and 2112 ± 13 Ma, respectively. Zircons in the Boboti pluton showed evidence of inherited material from
743 2226 ± 13 Ma, ~3.0 and 3.4 Ga. The Palaeoproterozoic age coincides with the oldest dated units in the
744 Western Mako Belt, whereas the Archaean ages suggest the possible reworking of Archaean material either
745 within the detrital basins or at depth beneath the Birimian crust. The available data suggest that the south-
746 eastern KKI is one of the younger terranes in the wider Birimian, lacking any significant component (bar

747 inherited material) that correlates to earlier Birimian events (>2150 Ma) either in the Mako Belt or in Ghana
748 and Burkina Faso.

749 **Acknowledgements**

750 The Authors wish to thank Randgold Resources for generously funding this research. Additional thanks
751 must go to technical staff at Kingston University and to Andrew Miles and Philip Bird who provided helpful
752 discussion while preparing the manuscript. Constructive reviews by L. Baratoux, K. Hein and the Editor J.
753 Miller are also gratefully acknowledged.

754 **References**

755 Abouchami, W., Boher, M., Michard, A. Albarede, F., 1990. A major 2.1 Ga event of mafic magmatism in
756 West Africa: an early stage of crustal accretion. Journal of Geophysical Research 95, 17605-17629.

757 Allibone, A., Teasdale, J., Cameron, G., Etheridge, M., Uttley, P., Soboh, A., Appiah-Kubi, J., Adanu, A.,
758 Arthur, R., Mamphey, J., Odoom, B., Zuta, J., Tsikata, A., Pataye, F. Famiyeh, S., 2002. Timing and structural
759 controls on gold mineralisation at the Bogoso gold mine, Ghana, West Africa. Economic Geology 97, 949-
760 969.

761 Baier, J., Audétat, A., Keppler, H., 2008. The origin of the negative niobium tantalum anomaly in
762 subduction zone magmas. Earth and Planetary Science Letters 267, 290-300.

763 Baratoux, L., Metelka, V., Naba, S., Jessell, M. W., Grégoire, M., Ganne, J., 2011. Juvenile

764 Paleoproterozoic crust evolution during the Eburnean orogeny (~ 2.2–2.0 Ga), western Burkina Faso.

765 Precambrian Research 191, 18-45.

766 Bassot, J.P. and Caen-Vachette, M., 1984. Données géochronologiques et géochimiques nouvelles sur les
767 granitodes de l'Est du Sénégal: implications sur l'histoire geologique du Birrimien de cette région. In: Klerkx,
768 J. and Michot, J. (Eds.), African Geology. Tervuren, Belgium, pp. 196-209.

769 Bassot, J. P., Dommanget, A., 1986. Mise en évidence d'un accident majeur affectant le Protérozoïque
770 inférieur des confins Sénégalo-Maliens:new data on an important fault in lower Proterozoic on the borders
771 of Senegal and Mali, Comptes Rendus De l'Académie Des Sciences. Série 2, Mécanique, Physique, Chimie,
772 Sciences De l'Univers, Sciences De La Terre 302, 1101-1106.

773 Béziat, D., Bourges, F., Debat, P., Lompo, M., Martin, F. Tollon, F., 2000. A Palaeoproterozoic ultramafic-
774 mafic assemblage and associated volcanic rocks of the Boromo greenstone belt: fractionates originating
775 from island-arc volcanic in the West African Craton. Precambrian Research 101, 25-47.

776 Black, L. P., Gulson, B. L., 1978. The age of the mud tank carbonatite, strangways range, northern
777 territory. BMR Journal of Australian Geology and Geophysics 3, 227-232.

778 Black, L. P., Kamo, S. L., Allen, C. M., Davis, D. W., Aleinikoff, J. N., Valley, J. W., Mundil, R., Campbell, I.
779 H., Korsch, R. J., Williams, I. S. Foudoulis, C., 2004. Improved $^{206}Pb/^{238}U$ microprobe geochronology by the
780 monitoring of a trace-element-related matrix effect; SHRIMP, ID–TIMS, ELA–ICP–MS and oxygen isotope
781 documentation for a series of zircon standards. Chemical Geology 205, 115-140.

782 Boher, M., Abouchami, W., Michard, A., Albarede, F. Arndt, N.T., 1992. Crustal growth in West Africa at
783 2.1 Ga. Journal of Geophysical Research 97, 345-369.

784 Bonhomme, M., 1962. Contribution à l'ètude géochronologique de la plate-forme de l'Ouest africain.
785 Ph.D. Thesis, University of Clermont-Ferrand, France, 62 pp.

786 Brenan, J. M., Shaw, H. F., Phinney, D. L., Ryerson, F. J., 1994. Rutile-aqueous fluid partitioning of Nb, Ta,
787 Hf, Zr, U and Th: implications for high field strength element depletions in island-arc basalts. Earth and
788 Planetary Science Letters 128, 327-339.

789 Brown, M., Rushmer, T., 2006. Evolution and differentiation of the continental crust. Cambridge
790 University Press, 564 p.

791 Dabo, M., Aïfa, T., 2010. Structural styles and tectonic evolution of the Kolia-Boboti sedimentary Basin,
792 Kédougou-Kéniéba inlier, eastern Senegal. Comptes Rendus Geoscience 342, 796-805.

793 Dampare, S. B., Shibata, T., Asiedu, D. K., Osae, S., Banoeng-Yakubo, B., 2008. Geochemistry of
794 Paleoproterozoic metavolcanic rocks from the southern Ashanti volcanic belt, Ghana: petrogenetic and
795 tectonic setting implications. Precambrian Research 162, 403-423.

796 Davidson, J., Turner, S., Plank, T., 2013. Dy/Dy*: variations arising from mantle sources and petrogenetic
797 processes. Journal of Petrology 54, 525-537.

798 Davis, D.W., Hirdes, W., Schaltegger, U. Nunoo, E.A., 1994. U-Pb age constraints on deposition and
799 provenance of Birimian and gold-bearing Tarkwaian sediments in Ghana, West Africa. Precambrian Research
800 67, 89-107.

801 De Kock, G. S., Armstrong, R. A., Siegfried, H. P., Thomas, E. 2011. Geochronology of the Birim
802 Supergroup of the West African craton in the Wa-Bolé region of west-central Ghana: Implications for the
803 stratigraphic framework. Journal of African Earth Sciences 59, 1-40.

804 Debat, P., Diallo, D. P., Ngom, P. M., Rollet, M., Seyler, M., 1984. La série de Mako dans ses parties
805 centrale et méridionale (Sénégal oriental, Afrique de l'Ouest). précisions sur l'évolution de la série
806 volcanosédimentaire et données géochimiques préliminaires sur les formations magmatiques post-
807 tectoniques', Journal of African Earth Sciences 2 , 71-79.

808 Delor, C., Couëffé, R., Goujou, J. C., Diallo, D. P., Théveniaut, H., Fullgraf, T., Ndiaye, P.M., Dioh, E., Blein
809 O., Barry, T.M.M., Le Métour, J., Martelet, G., Sergeev, S., Wemmer, K., 2010. Notice explicative de la carte
810 géologique à 1/200 000 du Sénégal, feuille Saraya-Kédougou Est. Ministère des Mines, de l'Industrie, de
811 l'Agro-Industrie et des PME, Direction des Mines et de la Géologie, Dakar.

812 Dia, A., 1985. Le complexe plutonique de laminia: Un exemple d'associations acide - basique dans le
813 massif de granitoids de Kakadian (Sénégal est), 13th Colloquium of African Geology, Abstracts 13, 64.

814 Dia, A. 1988. Caractères et significations des complexes magmatiques et métamorphiques du secteur de
815 Sandikounda–Laminia (nord de la boutonnière de Kédougou, est Sénégal). un modèle géodynamique du
816 birimien de l'Afrique de l'Ouest, Unpublished PhD Thesis, University of Dakar, Sénégal, .

817 Dia, A., Van Schmus, W.R. Kröner, A., 1997. Isotopic constraints on the age and formation of a
818 Palaeoproterozoic volcanic arc complex in the Kédougou inlier, eastern Senegal, West Africa. Journal of
819 African Earth Sciences 24, 197-213.

820 Diallo, D.P., 2001. Le paléovolcanisme de la bordure occidentale de la boutonnierè de Kédougou,
821 Paléoprotérozoïque du Sénégal oriental: incidences géotectoniques. Journal of African Earth Sciences 32,
822 919-940.

823 Dioh, E., Béziat, D., Debat, P., Grégoire, M. Ngom, P.M., 2006. Diversity of the Palaeoproterozoic
824 granitoids of the Kédougou inlier (eastern Senegal): Petrographical and geochemical constraints. Journal of
825 African Earth Sciences 44, 351-371.

826 Dommanget, A., Milesi, J.P. Diallo, M., 1993. The Loulo gold and tourmaline-bearing deposit. Mineralium
827 Deposita 28, 253-263.

828 Drake, M. J., 1975. The oxidation state of europium as an indicator of oxygen fugacity. Geochimica et
829 Cosmochimica Acta 39, 55-64.

830 Draut, A. E., Clift, P. D. 2001. Geochemical evolution of arc magmatism during arc-continent collision,
831 South Mayo, Ireland. Geology 29, 543-546.

Feybesse, J. Milési, J.P., 1994. The Archaean/Proterozoic contact zone in West Africa: a mountain belt of decollement thrusting and folding on a continental margin related to 2.1 Ga convergence of Archean cratons? Precambrian Research 69, 199-227.

Feybesse, J., Billa, M., Guerrot, C., Duguey, E., Lescuyer, J., Milési, J.P. Bouchot, V., 2006. The Palaeoproterozoic Ghanaian province: Geodynamic model and ore controls, including regional stress modelling. Precambrian Research 149, 149-196.

Ganne, J., De Andrade, V., Weinberg, R. F., Vidal, O., Dubacq, B., Kagambega, N., Naba, S., Baratoux, L., Jessell, M. Allibon, J., 2011. Modern-style plate subduction preserved in the Palaeoproterozoic West African craton. Nature geoscience 5, 60-65.

Goujou, J. C., Buscail, F., Théveniaut, H., Dioh, E., Delor, C., Blein, O., Diallo, D.P., Ndiaye, P.M., Le Métour, J., Fullgraf T., Caby, R., Couëffé, R., Martelet, G., Sergeev, S., Tegyey, M., Villeneuve, M., Wemmer, K., 2010. Notice explicative de la carte géologique à 1/200 000 du Sénégal, feuille Kossanto-Dalafi Est, 2010, Ministère des Mines, de l'Industrie, de l'Agro-Industrie et des PME. Direction des Mines et de la Géologie, Dakar.Gueye, M., Siegesmund, S., Wemmer, K., Pawlig, S., Drobe, M., Nolte, N. Layer, P., 2007. New evidence for an early Birimian evolution in the West African Craton: an example from the Kédougou-Kéniéba inlier, southeast Senegal. South African Journal of Geology 110, 511-534.

Gueye, M., Ngom, P.M., Diene, M., Thiam, Y., Siegesmund, S., Wemmer, K. Pawlig, S., 2008. Intrusive rocks and tectno-metamorphic evolution of the Mako Palaeoproterozoic belt (Eastern Senegal, West Africa). Journal of African Earth Sciences 50, 88-110.

Hastie, A. R., Kerr, A. C., Pearce, J. A., Mitchell, S. F., 2007. Classification of altered volcanic island arc rocks using immobile trace elements: development of the Th–Co discrimination diagram. Journal of Petrology 48, 2341-2357.

854 Hastie, A. R., Mitchell, S. F., Treloar, P. J., Kerr, A. C., Neill, I., Barfod, D. N., 2013. Geochemical
855 components in a Cretaceous island arc: The Th/La–(Ce/Ce*)Nd diagram and implications for subduction
856 initiation in the inter-American region. Lithos 162, 57-69.

857 Hein, K. A., 2010. Succession of structural events in the Goren greenstone belt (Burkina Faso):
858 implications for West African tectonics. Journal of African Earth Sciences 56, 83-94.

859 Hirdes, W. Davis, D.W., 2002. U-Pb Geochronology of Palaeoproterozoic rocks in the southern part of the
860 Kédougou-Kéniéba inlier, Senegal, West Africa: evidence for diachronous accretionary development of the
861 Eburnean Province. Precambrian Research 118, 83-99.

862 Hirdes, W., Davis, D.W. Eisenlohr, B.N., 1992. Reassessment of Proterozoic granitoid ages in Ghana on
863 the basis of U/Pb zircon and monazite dating. Precambrian Research 56, 89-96.

864 Hirdes, W., Davis, D.W., Ludtke, G., Konan, G., 1996. Two generations of Birimian (Paleoproterozoic)
865 volcanic belts in northeastern Cote d'Ivoire (West Africa): consequences for the `Birimian controversy'.
866 Precambrian Research 80, 173-191.

867 Jackson, S.E., Pearson, N.J., Griffin, W.L., Belousova, E.A., 2004. The application of laser ablation-inductively
868 coupled plasma-mass spectrometry to in situ U-Pb zircon geochronology. Chemical Geology 211, 47-69.

869

870 John, T., Klemd, R., Hirdes, W. Loh, G., 1999. The metamorphic evolution of the Palaeoproterozoic
871 (Birimian) volcanic Ashanti belt (Ghana, West Africa). Precambrian Research 98, 11-30.

872 Junner, N.R., 1940. Geology of the Gold Coast and Western Togoland. Gold Coast Geological Survey
873 Bulletin 11, 1-40.

874 Lawrence, D.M., Treloar P.J., Rankin, A.H., Harbidge, P., Holliday, J., 2013a The Geology and Mineralogy
875 of the Loulo Mining District, Mali, West Africa: Evidence for Two Distinct Styles of Orogenic Gold
876 Mineralization. Economic Geology 108, 199-227.

877 Lawrence, D.M., Treloar, P.J., Rankin, A.H., Boyce, A., Harbidge, P., 2013b, A fluid inclusion and stable
878 isotope study at the Loulo mining district, Mali, West Africa: Implications for multifluid sources in the
879 generation of orogenic gold deposits. Economic Geology 107, 229–257.

880 Le Maitre, R. W. 1989. A classification of igneous rocks and glossary of terms.Recommendations of the
881 International Union of Geological Sciences, Sub-commission on the Systematics of Igneous rocks: Oxford,
882 Blackwell.

883 Lebrun, E., Thébaud, N., Miller, J., Bourget, J., Ulrich, S., Terblanche, O., 2015. Geochronology and
884 lithostratigraphy of the Siguiri district: implications for gold mineralisation in the Siguiri Basin (Guinea, West
885 Africa). 13th SGA Biennial Meeting, Nacy, France, 1-4.Ledru, P., Pons, J., Milesi, J. P., Feybesse, J. L. Johan, V.,
886 1991. Transcurrent tectonics and polycyclic evolution in the lower Proterozoic of Senegal-Mali, Precambrian
887 Research 50, 337-354.

888 Leube, A., Hirdes, W., Mauer, R., Kesse, G.O. 1990. The early Proterozoic Birimian Supergroup of Ghana
889 and some aspects of its associated gold mineralisation. Precambrian Research 46, 139-165.

890 Loh, G., Hirdes, W., Anani, C., Davis, D.W., Vetter, U., 1999. Explanatory notes for the geological map of
891 Southwest Ghana 1: 100,000. Geologisches Jahrbuch B 93, 150.

892 Ludwig, K. R., 2003. User's manual for Isoplot 3.00: A geochronological toolkit for Microsoft Excel (No. 4).
893 Kenneth R. Ludwig, 76 .p

894 Maniar, P.D., Piccoli, P.M., 1989. Tectonic discrimination of granitoids. Geological Society of America
895 Bulletin 101, 635-643.

Milési, J.P., Feybesse, J.L., Ledru, P., Dommanget, A., Ouedrago, M., Marcoux, E., Prost, A., Vinchon, C., Sylvain, J.P., Johan, V., Tegyey, M., Calvez, J.Y. Lagny, P., 1989. West African gold deposits in their Lower Proterozoic lithostructural setting. Chronique de la Recherche Miniere 497, 3-98.

Müller, W., Shelley, M., Miller, P., Broude, S., 2009. Initial performance metrics of a new custom-designed ArF excimer LA-ICPMS system coupled to a two-volume laser-ablation cell. Journal of Analytical Atomic Spectrometry 24, 209-214.

Ngom, P. M., Cordani, U. G., Teixeira, W. Janasi, V. A., 2009. Sr and nd isotopic geochemistry of the early ultramafic–mafic rocks of the Mako bimodal volcanic belt of the Kedougou-Kéniéba Inlier (Senegal). Arabian Journal of Geosciences 3 , 49-57.

Oberthür, T., Vetter, U., Davis, D.W. Amanor, J.A., 1998. Age constraints on gold mineralisation and Palaeoproterozoic crustal evolution in the Ashanti belt of southern Ghana. Precambrian Research 89, 129-143.

Parra-Avila, L. A., Belousova, E., Fiorentini, M. L., Baratoux, L., Davis, J., Miller, J., McCuaig, T. C., 2015. Crustal evolution of the Paleoproterozoic Birimian terranes of the Baoulé-Mossi domain, southern West African Craton: U–Pb and Hf-isotope studies of detrital zircons. Precambrian Research. doi:10.1016/j.precamres.2015.09.005.

Paton, C., Woodhead, J. D., Hellstrom, J. C., Hergt, J. M., Greig, A., Maas, R., 2010. Improved laser ablation U-Pb zircon geochronology through robust downhole fractionation correction. Geochemistry, Geophysics, Geosystems 11, Q0AA06, doi:10.1029/2009GC002618.

Pawlig, S., Gueye, M., Klisches, R., Schwarz, S., Wemmer, K. Siegesmund, S., 2006. Geochemical and Sr-Nd isotopic data on the Birimian of the Kédougou-Kéniéba Inlier (Eastern Senegal): Implications on the Palaeoproterozoic evolution of the West African Craton. South African Journal of Geology 109, 411-427.

Pearce, J. A., 1996. Sources and settings of granitic rocks. Episodes 19, 120-125.

Pearce, J. A., 2008. Geochemical fingerprinting of oceanic basalts with applications to ophiolite classification and the search for Archean oceanic crust. Lithos 100, 14-48.

Pearce, J.A., Harris, N.B. Tindle, A.G., 1984. Trace element discrimination diagrams for the tectonic interpretation of granitic rocks. Journal of Petrology 25, 956-983.

Pearce, J. A., Peate, D. W., 1995. Tectonic implications of the composition of volcanic arc magmas. Annual Review of Earth and Planetary Sciences 23, 251-286.

Perrouty, S., Aillères, L., Jessell, M. W., Baratoux, L., Bourassa, Y., Crawford, B., 2012. Revised Eburnean geodynamic evolution of the gold-rich southern Ashanti Belt, Ghana, with new field and geophysical evidence of pre-Tarkwaian deformations. Precambrian Research 204, 12-39.

Plank, T., 2005. Constraints from thorium/lanthanum on sediment recycling at subduction zones and the evolution of the continents. Journal of Petrology 46, 921-944.

Pouclet, A., Doumbia, S. Vial, D.S., 2006. Geodynamic setting of the Birimian volcanism in central Ivory Coast (western Africa) and its place in the Palaeoproterozoic evolution of the Man Shield. Bulletin Societe Geologique de France 177, 105-121.

Rickwood, P.C.,1989. Boundary lines within petrologic diagrams which use oxides of major and minor elements. Lithos 22, 247-263.

Roddaz, M., Debat, P. Nikiéma, S., 2007. Geochemistry of Upper Birimian sediments (major and trace elements and Nd–Sr isotopes) and implications for weathering and tectonic setting of the Late Palaeoproterozoic crust. Precambrian Research 159, 197-211.

Salah, I. A., Liegeois, J. P., Pouclet, A., 1996. Evolution d'un arc insulaire océanique birimien précoce au Liptako nigérien (Sirba): géologie, géochronologie et géochimie. Journal of African Earth Sciences 22, 235-254.

941 Schwartz, M.O. Melcher, F., 2004. The Falémé Iron District, Senegal. Economic Geology 99, 917-939.

942 Sláma, J., Košler, J., Condon, D. J., Crowley, J. L., Gerdes, A., Hanchar, J. M., Horstwood, M. S. A., Morris,
943 G. A., Nasdala, L., Norberg, N., Schaltegger, U., Schoene, B., Tubrett, M. N. Whitehouse, M. J., 2008.
944 Plešovice zircon—a new natural reference material for U–Pb and Hf isotopic microanalysis. Chemical
945 Geology 249, 1-35.

946 Soumaila, A., Henry, P., Garba, Z., Rossi, M., 2008. REE patterns, Nd-Sm and U-Pb ages of the
947 metamorphic rocks of the Diagorou-Darbani greenstone belt (Liptako, SW Niger): implication for Birimian
948 (Palaeoproterozoic) crustal genesis. Geological Society, London, Special Publications 297, 19-32.

949 Sun, S.S. Mcdonough,W. F., 1989. Chemical and isotope systematics of oceanic basalts: implications for
950 mantle composition and processes, in: SAUNDERS, A. D. and NORRY, M. J. (Eds.) Magmatism in the Ocean
951 Basins. Geological Society, London, Special Publications 42, 313-345.

952 Sylvester, P.J. Attoh, K., 1992. Lithostratigraphy and composition of 2.1 Ga greenstone belts of the West
953 African Craton and their bearing on crustal evolution and the Archean-Proterozoic boundary. Journal of
954 Geology 100, 377-393.

955 Tapsoba, B., Lo, C. H., Jahn, B. M., Chung, S. L., Wenmenga, U., Iizuka, Y., 2013. Chemical and Sr–Nd
956 isotopic compositions and zircon U–Pb ages of the Birimian granitoids from NE Burkina Faso, West African
957 Craton: Implications on the geodynamic setting and crustal evolution. Precambrian Research 224, 364-396.

958 Taylor, B., Martinez, F., 2003. Back-arc basin basalt systematics. Earth and Planetary Science Letters 210,
959 481-497.

960 Taylor, P.N., Moorbath, S., Leube, A. Hirdes, W., 1992. Early Proterozoic crustal evolution in the Birimian
961 of Ghana: constraints from geochronology and isotope geochemistry. Precambrian Research 56, 97-111.

962 Thiéblemont, D., Goujou, J. C., Egal, E., Cocherie, A., Delor, C., Lafon, J. M., Fanning, C. M., 2004. Archean
963 evolution of the Leo Rise and its Eburnean reworking. Journal of African Earth Sciences 39, 97-104.

964 Treloar, P. J., Lawrence, D. M., Senghor, D., Boyce, A., Harbidge, P., 2014. The Massawa gold deposit,
965 Eastern Senegal, West Africa: an orogenic gold deposit sourced from magmatically derived fluids? Geological
966 Society, London, Special Publications 393, SP393-12.

967 Tshibubudze, A., Hein, K. A., Marquis, P., 2009. The Markoye Shear Zone in NE Burkina Faso. Journal of
968 African Earth Sciences 55, 245-256.Tshibubudze, A., Hein, K. A. A., Peters, L. F. H., Woolfe, A. J., McCuaig, T.
969 C., 2013. Oldest U-Pb crystallisation age for the West African craton from the Oudalan-Gorouol Belt of
970 Burkina Faso. South African Journal of Geology 116, 169-181.

971 Tshibubudze, A., Hein, K. A., McCuaig, T. C. (In Press). The relative and absolute chronology of strato-tectonic
972 events in the Gorom-Gorom granitoid terrane and Oudalan-Gorouol belt, northeast Burkina Faso. Journal
973 of African Earth Sciences.

974 Vidal, M. Alric, G., 1994. The Palaeoproterozoic (Birimian) of Haute-Comoé in the West African Craton,
975 Ivory Coast: a transtensional back-arc basin. Precambrian Research 65, 207-229.

976 Vidal, M., Gumiaux, C., Cagnard, F., Pouclet, A., Ouattara, G., Pichon, M., 2009. Evolution of a
977 Paleoproterozoic “weak type” orogeny in the West African Craton (Ivory Coast). Tectonophysics 477, 145-
978 159.

979 White, A., Burgess, R., Charnley, N., Selby, D., Whitehouse, M., Robb, L., Waters, D., 2014. Constraints on
980 the timing of late-Eburnean metamorphism, gold mineralisation and regional exhumation at Damang mine,
981 Ghana. Precambrian Research 243, 18-38.

982 Wiedenbeck, M., Hanchar, J. M., Peck, W. H., Sylvester, P., Valley, J., Whitehouse, M., Kronz, A.,
983 Morishita, Y., Nasdala, L., Fiebig, J., Franchi, I., Girard, J.-P., Greenwood, R.C., Hinton, R., Kita, N., Mason,
984 P.R.D., Norman, M., Ogasawara, M., Piccoli, P.M., Rhede, D., Satoh, H., Schulz-Dobrick, B., Skår, O., Spicuzza,

985 Mj., Terada, K., Tindle, A., Togashi, S., Vennemann, T., Xie, Q. Zheng, Y.-F., 2004. Further Characterisation of
986 the 91500 Zircon Crystal. Geostandards and Geoanalytical Research 28, 9–39.

987 Figures

988 Figure 1. Geological map of the Kédougou-Kéniéba Inlier, including units of the Mako belt referred to in
989 the text (modified after Lawrence, 2010).

990 Figure 2. Detailed geology of the Falémé Volcanic Belt and Kofi Series, locations of whole-rock
991 geochemistry samples are indicated.

992 Figure 3. Hand specimen photographs of: A) medium grained diorite (BP31); B) porphyritic basaltic
993 andesite (CLIB08); C) phaneritic gabbroic diorite (CLIB09); D) coarse gabbroic diorite with biotite phenocrysts
994 (CLIB10); E) sheared quartz monzodiorite from near the sheared contact between the FVB and Kofi series
995 (CLIB01); F) a coarse grained quartz monzonite with K-feldspar phenocrysts (CLIB05); G) an aplite dyke
996 (CLIB06) that cross-cuts the Balangouma pluton; H) a coarse porphyritic monzonite (CLIB07).

997 Figure 4. Hand specimen photographs of: A) coarse porphyritic quartz monzodiorite (BOP1A); B)
998 porphyritic monzogranite (BOP2 and 3); C) porphyritic pyroxene-bearing quartz diorite (BOP4); D) hand
999 specimen of coarse grained quartz diorite (BO4); E) hand specimen of medium grained quartz diorite (BO5);
1000 F) pink, medium-grained monzogranite (PTG1); G) equigranular monzogranite (MAD01); H) biotite-quartz-
1001 feldspar porphyry (FDGI01).

1002 Figure 5. A) K_2O versus Silica diagram (Rickwood, 1989) showing the plutonic and volcanic units of the
1003 eastern KKI, note the 'upper trend' represents unaltered samples of high-K calc-alkaline affinity and the
1004 'lower' calc-alkaline to tholeiitic trend represents albitised samples, see text for details; B) Th-Co
1005 discrimination diagram (Hastie et al., 2007) showing albitised and fresh samples plotting in the high-K and
1006 upper calc-alkaline series.

Figure 6. Geochemical samples plotted on total alkali silica (TAS) classification diagram (after Le Maitre et al., 1989) showing lithology names for: A) intrusive-plutonic samples and B) extrusive (volcanic) from the FVB and Kofi Series.

Figure 7. A/NK versus A/CNK diagram (after Maniar and Piccoli, 1989) for igneous rocks from the eastern KKI. Albitised samples are highlighted in red, note that albitisation results in lower A/NK values due to increase in overall N_2O.

Figure 8. N-MORB normalised REE patterns for A) the Daléma Igneous rocks from the eastern margin of the Diale-Dalema Basin; B) the intermediate composition (diorite to granodiorite) igneous rocks of the FVB and Kofi Series (see key); C) the granitic rocks of the FVB and Kofi Series. N-MORB normalised trace element diagrams of for D) the Daléma Igneous rocks from the eastern margin of the Diale-Dalema Basin; E) the intermediate composition (diorite to granodiorite) igneous rocks of the FVB and Kofi Series (see key); F) the granitic rocks of the FVB and Kofi Series, note the consistent depletion of Nb-Ta compared to other HFSE. Albitised samples were excluded from multi-element plots (D, E and F) due to extreme perturbation of the trace element patterns.

Figure 9. Representative SEM-CL images of: A) and B) zircons from sample BOP1A of the Boboti Pluton; C) and D) zircons BOP1A-09 and BOP1A-22 from the Boboti pluton with U-Pb ages indicated inheritance at ~2200 Ma (BOP1A; ages given are from $^{206}Pb/^{238}U$); E) and F) zircons BOP1A-73 and BOP1A-75 with ablation spots marked; G) and H) zircons from sample CLIB01 of the Balangouma Pluton; I) and J) zircons from sample CLIB05 of the Balangouma Pluton K) and L) zircons from sample CLIB07 of the Balangouma Pluton

Figure 10. A) Concordia diagram showing discordia plotted from 70 concordant and discordant grains from sample BOP1A of the Boboti pluton, the discordia trends toward the origin and is likely a result of recent Pb-loss; B) Diagram of the weighted mean $^{206}Pb/^{238}U$ age of 19 concordant grains from BOP1A and; C) the weighted mean $^{207}Pb/^{206}Pb$ age of the same 19 grains from BOP1A.

1030 Figure 11. Evidence for inherited material in the Boboti pluton: A) two partially concordant grains at
1031 ~2230 Ma, corresponding to early volcanic activity in the Falémé Belt; B) two partially concordant Archaean
1032 U-Pb ages from zircons BOP1A-73 and BOP1A-75 in the Boboti pluton.

1033 Figure 12. Diagrams of A) discordia plotted from 43 ablation spots in sample CLIB01 trending toward the
1034 origin indicating recent Pb-loss, age of intercept is indicated; B) weighted mean of $^{206}Pb/^{238}U$ ages from the 7
1035 most concordant grains; C) weighted mean $^{207}Pb/^{206}Pb$ ages for 43 grains from CLIB01. Weighted mean ages
1036 and MSWD values are indicated.

1037 Figure 13. Diagrams of A) discordia plot constructed from 43 concordant and discordant grains from
1038 sample CLIB05, upper intercept age is indicated; B) a weighted average of the 13 most concordant $^{206}Pb/^{238}U$
1039 ages from CLIB05 yielding a younger age than the discordia intercept in A; C) a weighted average of the 13
1040 equivalent $^{207}Pb/^{206}Pb$ ages; D) a weighted average of 57 $^{207}Pb/^{206}Pb$ ages with 9 outliers rejected.

1041 Figure 14. Diagrams of A) discordia plotted from 56 discordant and concordant spots from CLIB07 with
1042 the upper intercept indicated; B) a weighted average $^{207}Pb/^{206}Pb$ age of the same 56 spots with 6 outliers
1043 rejected; C) a weighted average $^{206}Pb/^{238}U$ age calculated from the 9 most concordant spots from CLIB07.

1044 Figure 15. Th/La–(Ce/Ce*)Nd diagram after Hastie et al. (2013) showing the affinity of slab derived
1045 components in the igneous rocks of the FVB and Kofi Series, albitised samples not plotted. Th/La values are
1046 generally inherited from subducting slab sediments, which typically have Th/La > island arc lavas and N-
1047 MORB. $(Ce/Ce^*)_{Nd} = Ce_{CN}/(La_{CN}^{2/3} \times Nd_{CN}^{1/3})$; this reflects enrichment of Ce relative to other REEs, which
1048 relates to different oxidation states in the marine environment. Subducting marine sediment end members:
1049 SSC-HD = slow sediment clay-hydrogenous and SSC-FH = slow sediment clay-fish debris/hydrothermal, as
1050 described in Hastie et al., (2013).

1051 Figure 16. Dy/Dy* vs Dy/Yb diagram of Davidson et al. (2013), this diagram describes the slope (Dy/Yb)
1052 and curvature (Dy/Dy*) of REE patters as a single point for any given sample. MORB field includes N-MORB
1053 and E-MORB data from the East Pacific Rise. Decreasing Dy/Dy* values below the MORB array are largely

controlled by fractionation of clinopyroxene and amphibole, whereas increasing Dy/Yb reflects increasing control of residual garnet on REE patterns. PM, primitive mantle; DM, depleted mantle; GLOSS, average global subducting sediment; see Davidson et al., (2013) for details. Note that data for the Dalema rocks falls within the field for LREE enriched MORB, whereas the majority of the plutonic rocks in the FVB and Kofi plot toward bulk crustal values or along a trend of increasing sediment contamination. The most felsic, peraluminous units display the highest Dy/Yb values.

Figure 17. The A) Rb versus (Y+Nb) and B) Ta versus Nb diagrams of Pearce et al. (1984) for discriminating the tectonic environment of granitic rocks. Albitised samples are highlighted in red.

Figure 18. Summary diagram of published age data for the KKI. Data source is indicated by the numbers below the Belt-Series labels (1) Bassot and Caen-Vachette (1984); (2) Dia (1988); (3) Milesi et al. (1989); (4) Calvez et al. (1990); (5) Boher et al. (1992); (6) Dia et al. (1997); (7) Hirdes and Davis (2002); (8) Gueye et al. (2007); (9) Goujou et al., (2010); (10) Delor et al., (2010).

Figure 19. Tectonic evolution of the KKI defined by the trace element chemistry and isotope geochemistry of plutonic rocks in the FVB, Mako Belt, Saraya Batholith and Kofi Series. $\varepsilon Nd_{(2.1Ga)}$ becomes less positive with time, indicating an increasing influence of continent derived material. Higher Nb/Zr and La/Sm reflect increasing HFSE and LREE enrichment, respectively. Decreasing Eu* reflects fractional crystallisation of Ca-rich plagioclase. Increasing Dy/Yb reflects greater control on REE pattern by residual garnet as a result of slab sediment melting. Error bars for the x-axis are 2σ. Trace element and geochronological data are form this study with the additional geochemical, isotopic and geochronological data compiled from Boher et al., (1992), Pawlig et al., (2006), Dioh et al., (2006) Bassot and Caen-Vachette (1984); Dia et al. (1997); Hirdes and Davis (2002); Gueye et al. (2007).

Tables

Table 1 – A summary of published geochronological data from the Kédougou-Kéniéba Inlier. Published sources are referenced in the table.

1078 Table 2 - LA-ICPMS instrumental parameters.

1079 Table 3 – LA-MC-ICP-MS data for analyses of standard zircon materials GJ-1, Temora-2, 91500, Mud Tank
1080 and Plešovice.

1081 Table 4 – A summary whole rock geochemical data collected from the South-eastern KKI as part of this
1082 study.

1083 Table 5 – A summary whole rock geochemical data collected from the South-eastern KKI as part of this
1084 study.

1085 Table 6 – A summary whole rock geochemical data collected from the South-eastern KKI as part of this
1086 study.

1087 Table 7 – A summary whole rock geochemical data collected from the South-eastern KKI as part of this
1088 study.

1089 Table 8 - LA-MC-ICP-MS data for analyses of sample BOP1A - Boboti pluton, quartz monzodiorite
1090 porphyry.

1091 Table 9 - LA-MC-ICP-MS data for analyses of sample CLIB01 - Balangouma pluton, quartz monzodiorite
1092 porphyry.

1093 Table 10 - LA-MC-ICP-MS data for analyses of sample CLIB05 – Balangouma pluton, quartz monzonite
1094 porphyry.

1095 Table 11 - LA-MC-ICP-MS data for analyses of sample CLIB07 - Balangouma pluton, monzonite porphyry.

1096

1096 Table.1

Terrane	Unit	Method	Date (Ma)	± (Ma)	Event	Reference
Mako volcanic Belt	Badon granodiorite	Ar-Ar (biotite)	2098	20	Cooling below 300 °C	Gueye et al., (2007)
		K-Ar (biotite	2090	9	Cooling below 300 °C	Gueye et al., (2007)
		Pb-Pb (zircon)	2213	3	Inherited core	Gueye et al., (2007)
		Pb-Pb (zircon)	2198	2	Magmatic emplacement (rim)	Gueye et al., (2007)
	SAG dioritic gneiss	Pb-Pb (zircon)	2202	6	Protolith crystallisation	Gueye et al., (2007)
	SAG tonalitic gneiss	Ar-Ar (horneblende)	2112	12	Cooling below 550 °C	Gueye et al., (2007)
		K-Ar (hornblende)	2118	31	Cooling below 550 °C	Gueye et al., (2007)
		Pb-Pb (zircon)	2194	4	Protolith crystallisation	Dia et al., (1997)
		Pb-Pb (zircon)	2194	4	Protolith crystallisation	Gueye et al., (2007)
		U-Pb (zircon)	2205	15	Protolith crystallisation	Gueye et al., (2007)
	SLP complex diorite	Pb-Pb (zircon)	2158	8	Magmatic emplacement	Dia et al., (1997)
	SLP complex migmatite	U-Pb (zircon)	2171	9	Migmatisation	Goujou et al., (2010)
	LKP granodiorite gneiss	Pb-Pb (zircon)	2138	12	Protolith crystallisation	Dia et al., (1997)
	LKP Kaourou Pluton	Pb-Pb (zircon)	2079	6	Magmatic emplacement	Dia et al., (1997)
		Rb-Sr (WR)	2189	23	Possible inheritence	Dia et al., (1997)
	LKP Laminia Pluton	Pb-Pb (zircon)	2105	8	Magmatic emplacement	Dia (1988)
		U-Pb (zircon)	2127	6	Magmatic emplacement	Dia et al., (1997)
	Mamakono rhyolite	Pb-Pb (zircon)	2067	12	Eruption	Gueye et al., (2007)
	Mamakono granodiorite	U-Pb (zircon)	2076	3	Magmatic emplacement	Hirdes and Davis (2002)
	Granite	U-Pb (zircon)	2102	8	Magmatic emplacement	Goujou et al., (2010)
	Granite	U-Pb (zircon)	2103	11	Magmatic emplacement	Goujou et al., (2010)
	Granite	U-Pb (zircon)	2142	7	Magmatic emplacement	Delor et al., (2010)
	Andesite lava	Sm-Nd (WR)	2160	16	Eruption	Boher et al., (1992)
	Tinkoto granodiorite	Ar-Ar (horneblende)	2051	16	Cooling below 550 °C	Gueye et al., (2007)
		K-Ar (biotite	2064	20	Cooling below 300 °C	Gueye et al., (2007)
		Pb-Pb (zircon)	2074	5	Magmatic emplacement	Gueye et al., (2007)
Dialé-Daléma Series	Metasedimentary rocks	U-Pb (zircon)	2164.7	0.9	Upper age of sedimentation	Hirdes and Davis (2002)
	Saraya Batholith	Ar-Ar (muscovite)	2022	12	Cooling below 350 °C	Gueye et al., (2007)
		K-Ar (muscovite)	2021	11	Cooling below 350 °C	Gueye et al., (2007)
		U-Pb (monazite)	2079	2	Magmatic emplacement	Hirdes and Davis (2002)
		U-Pb (monazite)	2064	4	Metamorphic overprint	Hirdes and Davis (2002)
		U-Pb (zircon)	2072	10	Magmatic emplacement	Delor et al., (2010)
		U-Pb (zircon)	2061	15	Magmatic emplacement	Delor et al., (2010)
		U-Pb (zircon)	2075	10	Magmatic emplacement	Goujou et al., (2010)
	Metasedimentary rocks	Pb-Pb (zircon)	2096	8	Upper age of sedimentation	Milesi et al., (1989)
		Pb-Pb (zircon)	2156	10	Upper age of sedimentation	Milesi et al., (1989)
	Andesite dyke	Pb-Pb (zircon)	2070	10	Crystallisation	Milesi et al., (1989)
		Pb-Pb (zircon)	2072	9	Crystallisation	Calvez et al., (1990)
	Rhyodacite	U-Pb (zircon)	2098	13	Eruption or crystallisation	Delor et al., (2010)
Faleme Volcanic Belt	Balangouma pluton	U-Pb (zircon)	2118	16	Magmatic emplacement	This study

	Boboti granodiorite	U-Pb (zircon)	2105	9.8	Magmatic emplacement	This study
		U-Pb (zircon)	2113	15	Magmatic emplacement	This study
		U-Pb (zircon)	2080.2	0.9	Magmatic emplacement	Hirdes and Davis (2002)
		U-Pb (zircon)	2088.5	8.5	Magmatic emplacement	This study
		U-Pb (zircon)	3000	120	Inherited core	This study
		U-Pb (zircon)	3380	160	Inherited core	This study
		U-Pb (zircon)	2218	83	Inherited core	This study
	South Falémé tonalite	U-Pb (zircon)	2081.5	1.1	Magmatic emplacement	Hirdes and Davis (2002)
	Rhyolite lava	U-Pb (zircon)	2099	4	Eruption	Hirdes and Davis (2002)
	Rhyolite lava	U-Pb (zircon)	2155	34	Inheritence	Hirdes and Davis (2002)
	Bofeto rhyolite	U-Pb (zircon)	2082	8	Eruption or crystallisation	Delor et al., (2010)
	Rhyolite lava	U-Pb (zircon)	2064	30	Eruption	Delor et al., (2010)
Kofi Series	Tourmalinised quartz wacke	Pb-Pb (zircon)	2093	7	Upper age of sedimentation	Boher et al., (1992)
	Deltaic deposits	U-Pb (zircon)	2125	27	Upper age of sedimentation	Boher et al., (1992)
	Gara Au deposit	U-Pb (mon-xen)	2028	10	Mineralisation	Vielriecher (2006)
	Gamaye pluton	Rb-Sr (WR)	2045	27	Magmatic emplacement	Bassot and Caen-Vachette (1984)

1097

1098

1098 Table. 2

Laboratory & Sample Preparation	
Laboratory name	Dept. of Earth Science, Royal Holloway University of London (LA-ICPMS analyses)
Sample type/mineral	Igneous zircons
Laser ablation system	
Make, Model & type	Resonetics / ASI RESOlution M-50 with Compex 110
Ablation cell & volume	Laurin two-volume cell (M-50), upper volume ~2 cm^3
Laser wavelength (nm)	193nm
Pulse width (ns)	20 ns
Fluence ($J.cm^{-2}$)	3 J/cm^{-2}
Repetition rate (Hz)	5Hz
Ablation duration (secs)	30 s, 15 s background before and after
Signal smoothing	'Squid' signal smoothing device included
Spot size (□m)	34 □m
Sampling mode	Spot ablation
Carrier gas	He only through LA cell; N_2 & Ar carrier-gas combined before squid
Cell carrier gas flow (l/min)	850 ml/min He
ICPMS Instrument	
Make, Model & type	Agilent 7500ce
Sample introduction	Laser ablation only
RF power (W)	1200W
Carrier gas flow (l/min)	450 ml/min Ar, 6 ml/min N_2
Detection system	Dual-stage detector
Masses measured	m/z = 29, 31, 139, 140, 141, 172, 175, 177, 206, 207, 208, 232, 238
Dwell time per peak (ms)	5 – 60 ms
Total sweep time per reading (ms)	202 ms
Th/ThO, $^{232}Th/^{238}U$	<0.25%, >93 %
Data Processing	See text for details

1099

1100

For all tables: Alb = albitised lithologies; Unalt = unaltered lithologies

Table 4

	Alb	Alb	Unalt	Unalt	Unalt	Unalt	Unalt	Unalt	Unalt	Unalt
Pluton/Area						Balangouma				
Sample	LR4	WP174	CLIB05	CLIB06	CLIB07	LR5	R35	R36	R37	R41
SiO2	64.5	75.7	64.3	73.3	62.3	63.7	64.0	55.7	58.6	62.3
TiO2	0.5	0.1	0.7	0.1	0.7	0.8	0.4	0.6	0.8	0.7
Al2O3	16.2	14.7	15.6	14.9	14.9	15.6	15.6	13.9	16.4	15.4
Fe2O3T	2.2	0.1	5.0	0.6	6.0	5.7	3.8	5.0	6.6	5.3
MnO	0.0	0.0	0.1	0.0	0.1	0.1	0.1	0.1	0.1	0.1
MgO	3.1	0.1	2.2	0.2	3.4	3.1	1.7	2.5	3.5	2.7
CaO	2.8	0.2	3.5	0.8	4.6	4.4	5.1	3.8	5.1	4.2
Na2O	8.5	8.2	4.4	4.4	3.8	4.1	4.1	3.5	4.5	4.1
K2O	0.3	0.2	3.7	4.6	3.2	2.4	2.6	2.7	2.2	3.0
P2O5	0.2	0.1	0.2	0.0	0.2	0.2	0.2	0.2	0.2	0.2
LOI	0.8	0.3	0.6	0.5	0.6	0.9	1.3	11.0	1.0	0.8
Total	99.2	99.6	100.2	99.4	99.6	100.9	99.0	98.9	99.1	98.8
Sample	LR4	WP174	CLIB05	CLIB06	CLIB07	LR5	R35	R36	R37	R41
V	67.2	3.7	67.8	5.9	103.0	87.6	55.3	88.5	124.4	78.0
Cr	88.9	32.8	79.2	16.2	146.2	92.3	42.9	79.4	101.1	78.2
Co	7.2	0.0	7.2	0.0	12.5	16.6	11.7	16.6	21.7	14.5
Ni	11.8	4.1	21.8	4.9	42.0	37.6	10.7	35.2	45.5	34.3
Ga	21.7	20.9	21.8	20.9	20.6	25.0	28.7	29.7	32.7	26.5
Rb	7.1	7.5	228.3	268.3	164.9	142.5	120.6	121.2	108.1	128.0
Sr	205.8	47.2	341.2	213.1	398.7	381.6	453.0	419.0	538.4	377.1
Y	14.0	2.7	17.8	6.6	21.4	11.2	9.6	16.2	16.4	16.5
Zr	149.2	73.0	268.8	79.9	201.5	195.8	131.5	252.9	212.2	190.4
Nb	7.6	7.6	12.5	7.8	10.1	12.1	6.6	12.2	10.6	13.0
Ta	0.9	1.6	0.6	1.9	1.5	1.2	0.9	1.1	1.0	1.1
Mo	1.0	0.0	0.2	1.3	0.3	3.2	2.4	2.1	1.6	5.3
Cs	0.1	0.2	16.9	9.1	9.2	6.8	1.9	5.0	7.9	4.8
Ba	183.2	36.1	534.8	543.1	663.8	359.8	490.7	668.1	590.8	588.8
La	29.3	2.8	32.0	19.7	35.3	24.9	24.7	35.5	35.0	32.2
Ce	52.1	9.0	72.5	39.6	74.9	51.4	47.9	69.0	64.9	62.1
Pr	6.4	1.2	7.8	4.7	8.7	5.8	5.3	7.7	7.3	6.9
Nd	22.3	5.0	26.1	15.4	29.9	21.8	20.9	28.8	29.3	25.9
Sm	4.1	1.2	4.9	3.1	5.8	3.2	3.3	5.0	5.6	4.7
Eu	1.1	0.2	1.1	0.7	1.3	1.1	1.0	1.3	1.5	1.2
Gd	3.5	1.0	4.0	2.3	4.8	3.4	3.1	4.8	5.2	4.2
Tb	0.5	0.1	0.5	0.3	0.6	0.5	0.4	0.6	0.6	0.6
Dy	2.8	0.5	2.9	1.2	3.6	2.2	1.8	3.4	3.4	2.8
Ho	0.5	0.0	0.6	0.2	0.7	0.5	0.4	0.6	0.6	0.5
Er	1.6	0.2	1.5	0.4	1.8	1.2	1.0	1.7	1.7	1.5
Tm	0.0	0.0	0.2	0.1	0.3	0.0	0.0	0.2	0.2	0.2
Yb	1.5	0.2	1.6	0.5	1.7	1.2	1.1	1.5	1.6	1.4
Lu	0.2	0.0	0.3	0.1	0.3	0.2	0.2	0.3	0.2	0.2
Hf	3.9	2.5	7.3	3.1	5.3	5.6	3.6	6.3	5.1	5.0
Th	10.4	9.4	18.1	9.5	13.2	9.4	2.9	11.3	7.7	13.7
U	5.1	2.3	5.8	8.5	3.2	5.1	1.4	3.3	2.3	2.6

Table 5

	Alb	Alb	Unalt	Unalt	Unalt	Unalt	Unalt	Unalt	Unalt	Unalt

Pluton/Area	Baqata		Boboti					Daléma			
Sample	BAQ01	BP08	BOP1A	BOP1B	BOP2	BOP3	BOP4	CLIB08	CLIB09	CLIB10	
SiO2	72.4	65.0	60.9	61.7	74.0	74.8	60.0	51.8	49.9		52.1
TiO2	0.1	0.5	0.8	0.8	0.1	0.1	1.0	2.2	1.2		1.1
Al2O3	16.4	17.5	14.4	14.4	14.2	13.9	15.2	14.3	15.0		14.8
Fe2O3T	0.3	0.9	6.2	6.2	0.8	0.6	8.4	14.6	12.0		9.8
MnO	0.0	0.0	0.1	0.1	0.0	0.0	0.1	0.2	0.1		0.1
MgO	0.3	1.5	3.7	3.7	0.2	0.1	3.7	4.1	6.9		7.5
CaO	0.3	3.0	4.1	4.1	0.7	0.6	5.4	8.0	8.3		7.9
Na2O	8.7	9.8	3.8	3.7	4.1	4.0	3.6	3.1	2.8		3.4
K2O	0.5	0.5	3.8	3.9	4.8	5.1	2.9	1.6	1.6		1.7
P2O5	0.0	0.2	0.2	0.2	0.1	0.0	0.2	0.4	0.4		0.3
LOI	0.5	0.8	0.6	0.5	0.4	0.4	0.3	0.0	1.0		1.1
Total	99.4	99.7	98.5	99.4	99.4	99.5	100.8	100.3	99.3		99.5
Sample	BAQ01	BP08	BOP1A	BOP1B	BOP2	BOP3	BOP4	CLIB08	CLIB09	CLIB10	
V	0.1	28.3	104.8	106.8	0.8	2.8	139.5	241.5	245.1		224.0
Cr	10.1	39.1	206.6	206.2	20.2	11.7	120.9	37.1	224.2		321.1
Co	0.0	0.0	15.6	15.4	0.0	0.0	20.7	37.4	27.9		30.8
Ni	4.1	6.1	74.4	71.8	4.1	4.1	66.3	7.2	40.2		93.1
Ga	13.3	18.5	21.5	21.2	23.8	21.0	20.5	22.1	23.0		21.8
Rb	5.6	9.2	224.4	231.4	304.4	232.2	150.5	51.2	47.0		61.1
Sr	137.3	114.5	317.8	320.2	95.9	107.2	339.9	440.4	495.5		498.7
Y	3.2	16.5	20.2	20.3	5.3	9.5	19.9	33.1	33.8		29.1
Zr	41.3	176.7	241.2	213.8	59.6	53.6	151.8	169.2	99.4		153.0
Nb	0.3	7.5	13.4	13.2	5.6	3.9	9.4	14.9	6.4		4.9
Ta	0.0	0.7	1.3	1.4	1.2	1.2	0.9	0.7	0.0		0.2
Mo	0.0	0.7	3.4	3.7	1.2	0.0	2.3	0.7	0.0		0.0
Cs	0.0	0.1	12.1	13.2	18.4	9.1	8.3	2.0	4.1		32.3
Ba	128.9	258.2	696.8	727.4	301.8	426.0	527.5	636.6	462.6		461.1
La	2.6	30.8	45.7	40.9	16.2	27.0	35.8	27.4	19.6		18.1
Ce	3.3	68.9	103.1	94.1	35.9	54.7	74.9	65.7	53.6		51.9
Pr	0.6	8.2	11.3	10.4	3.8	6.1	8.8	8.3	7.8		7.5
Nd	1.9	28.7	38.8	35.9	12.3	18.7	31.1	32.8	34.0		32.1
Sm	0.4	5.0	6.7	6.6	2.7	3.4	6.0	7.1	7.7		7.6
Eu	0.1	1.3	1.4	1.5	0.4	0.6	1.5	2.3	2.0		1.9
Gd	0.5	3.8	5.4	5.2	1.7	2.6	5.0	6.8	7.1		6.3
Tb	0.0	0.5	0.7	0.7	0.2	0.3	0.7	1.0	1.0		0.9
Dy	0.4	2.8	3.5	3.6	0.8	1.6	3.7	5.7	5.7		5.0
Ho	0.0	0.5	0.7	0.7	0.1	0.2	0.7	1.2	1.2		1.0
Er	0.2	1.4	1.7	1.8	0.4	0.7	1.8	2.9	3.1		2.6
Tm	0.0	0.2	0.3	0.3	0.1	0.1	0.3	0.4	0.5		0.4
Yb	0.1	1.4	1.5	1.6	0.3	0.7	1.6	2.7	2.9		2.6
Lu	0.0	0.2	0.3	0.3	0.0	0.1	0.3	0.4	0.5		0.4
Hf	1.4	4.8	6.7	5.9	2.7	1.9	4.7	4.8	3.2		4.1
Th	0.4	5.6	15.7	15.0	8.2	12.7	14.2	3.7	1.4		1.9
U	0.5	2.3	4.4	4.7	4.1	6.0	4.3	1.2	0.7		0.7

1104

1105 *Table 6*

	Unalt	Alb	Alb	Alb	Unalt	Unalt	Unalt	Unalt	Unalt	Alb
Pluton/Area	Fadougou	Falémé Volcanics				Gamaye		Gara		Kolya
Sample	FDGI01	BP31	BP29	BO8	BP32	MAD01	MOU02	LD23	LD9	BO1
SiO2	71.2	59.8	57.4	63.5	54.8	72.1	70.9	53.1	48.0	74.9
TiO2	0.2	0.7	0.7	0.5	0.8	0.3	0.0	0.8	0.5	0.1
Al2O3	14.9	14.8	13.3	15.4	13.0	15.2	16.9	18.1	8.9	14.2
Fe2O3T	2.4	3.8	5.4	1.5	11.7	1.5	0.1	9.2	8.8	0.2
MnO	0.0	0.0	0.0	0.0	0.0	0.0	0.0	0.0	0.1	0.0

MgO		0.5	6.7	7.7	3.0	8.5	0.5	0.0	6.7	12.5	0.0
CaO		1.6	3.7	5.5	6.1	1.1	0.8	0.3	1.1	6.4	0.1
Na2O		4.0	7.4	6.2	8.9	3.2	4.7	4.6	3.8	0.1	8.0
K2O		4.4	0.3	1.2	0.1	4.4	4.2	4.3	2.1	1.4	0.1
P2O5		0.0	0.3	0.3	0.1	0.3	0.3	1.2	0.3	0.2	0.0
LOI		0.5	1.3	1.1	0.7	1.6	0.4	0.9	4.5	12.6	0.5
Total		99.7	98.7	98.7	99.9	99.3	100.0	99.1	99.8	99.4	98.1
Sample	FDGI01		BP31	BP29	BO8	BP32	MAD01	MOU02	LD23	LD9	BO1
V		13.5	125.5	132.4	88.0	137.7	15.4	31.8	141.2	136.8	3.3
Cr		22.8	331.0	475.0	124.9	438.6	28.9	16.0	224.9	214.8	15.4
Co		0.0	3.5	23.0	0.0	16.7	0.0	214.6	17.6	16.8	0.0
Ni		5.7	119.7	213.3	35.2	328.9	4.1	110.2	14.6	10.3	4.1
Ga		20.8	19.4	19.7	20.1	23.2	26.3	25.4	28.2	28.0	20.4
Rb		188.2	0.9	42.4	0.0	264.8	641.1	269.2	54.3	55.4	0.0
Sr		222.7	155.6	216.1	162.8	103.4	232.1	236.3	451.8	455.1	26.6
Y		10.3	18.2	15.6	13.8	14.7	4.7	8.0	10.2	10.3	15.2
Zr		141.1	167.7	148.5	131.6	131.7	200.4	176.6	136.8	139.3	59.7
Nb		9.6	6.8	5.9	6.0	3.5	13.3	13.2	8.8	11.5	4.9
Ta		0.9	0.4	0.8	0.7	0.2	2.2	1.7	0.6	0.7	1.1
Mo		1.1	0.0	24.9	0.6	0.6	0.0	1.2	2.4	4.7	0.0
Cs		3.0	0.0	1.2	0.0	4.7	484.5	70.3	1.7	1.9	0.0
Ba		622.4	59.8	88.7	38.0	260.4	825.2	745.7	566.3	594.7	23.6
La		30.6	18.0	50.7	12.8	8.8	63.4	49.2	12.1	11.6	19.7
Ce		66.6	46.1	108.8	40.5	22.0	123.5	110.4	25.4	26.1	44.1
Pr		7.6	6.3	11.9	5.3	2.7	12.4	10.2	3.2	3.3	5.3
Nd		26.1	26.5	41.6	20.5	10.4	37.4	30.8	12.6	12.4	19.5
Sm		4.7	5.8	7.2	4.2	2.5	5.1	4.7	2.8	2.9	4.2
Eu		0.9	1.5	2.2	1.2	0.9	0.7	0.9	0.7	0.7	0.5
Gd		3.2	4.7	5.3	3.3	2.5	3.0	3.2	2.5	2.6	3.4
Tb		0.4	0.6	0.6	0.5	0.4	0.2	0.3	0.4	0.4	0.4
Dy		1.8	3.2	3.0	2.5	2.4	1.0	1.5	2.1	1.8	2.5
Ho		0.3	0.6	0.5	0.4	0.5	0.1	0.2	0.4	0.4	0.5
Er		0.8	1.6	1.3	1.2	1.3	0.3	0.6	1.2	1.2	1.3
Tm		0.1	0.2	0.2	0.2	0.2	0.0	0.1	0.0	0.0	0.2
Yb		0.8	1.5	1.2	1.2	1.3	0.3	0.6	1.4	1.5	1.3
Lu		0.1	0.2	0.2	0.2	0.2	0.0	0.1	0.2	0.2	0.2
Hf		4.5	4.6	4.1	3.6	3.9	5.5	5.1	3.7	3.9	2.3
Th		9.3	5.5	5.2	3.8	4.4	35.4	23.6	4.6	4.8	10.1
U		4.1	1.9	1.5	1.8	1.7	6.3	5.4	1.8	1.7	3.6

1106

1107 *Table 7*

	Alb	Alb	Alb	Alb	Alb	Unalt	Unalt	Unalt	Alb	Unalt
Pluton/Area		Kabe West		Karekeane		North Gara		South Falémé	Yalea	Yatea
Sample	BO4	BO5	BP21	R21	R25	R42	R43	FDGI02	UYP1	PTG1
SiO2	52.4	53.9	59.3	61.1	58.8	76.2	74.3	65.1	60.0	69.5
TiO2	1.0	0.8	0.6	0.5	0.6	0.0	0.0	0.5	0.7	0.3
Al2O3	15.4	16.4	15.5	15.5	16.2	13.7	13.8	14.7	14.6	15.4
Fe2O3T	5.4	8.8	2.9	3.0	3.4	0.4	0.5	4.2	4.6	1.9
MnO	0.0	0.0	0.0	0.0	0.0	0.0	0.0	0.0	0.0	0.0
MgO	4.1	4.6	2.8	2.6	3.2	0.1	0.1	3.5	3.1	0.8
CaO	5.7	4.6	5.9	5.3	6.2	0.3	0.4	2.7	2.7	1.5
Na2O	5.2	6.1	8.5	8.8	7.8	3.5	4.2	4.3	7.5	5.2
K2O	2.0	1.3	0.1	0.1	0.6	5.4	4.9	3.4	0.7	3.1
P2O5	0.1	0.1	0.2	0.1	0.3	0.0	0.0	0.2	0.2	0.1
LOI	8.6	2.7	3.6	3.2	3.6	0.8	0.7	0.7	4.8	0.9
Total	100.0	99.4	99.5	100.3	100.7	100.3	98.9	99.3	99.0	98.7

Sample	BO4	BO5	BP21	R21	R25	R42	R43	FDGI02	UYP1	PTG1
V	196.4	168.4	94.3	59.3	84.5	1.9	2.7	68.7	96.9	25.9
Cr	18.0	74.3	48.0	39.4	59.5	11.3	15.8	198.2	123.1	18.8
Co	0.0	18.8	36.7	11.7	11.9	1.8	2.0	9.1	14.3	4.2
Ni	25.7	44.5	38.1	16.7	33.1	5.4	3.7	75.3	54.3	8.0
Ga	18.1	20.3	19.8	16.6	15.9	21.6	23.7	20.5	18.4	34.4
Rb	38.1	30.0	4.7	2.0	26.3	265.8	270.8	133.4	10.1	79.1
Sr	105.8	151.7	140.0	93.4	234.0	53.4	74.6	496.9	104.0	691.5
Y	21.7	23.9	15.4	12.2	21.2	7.8	4.4	14.6	13.4	5.8
Zr	115.8	92.5	133.7	107.6	146.0	38.4	28.4	187.3	143.3	120.4
Nb	6.4	2.9	5.4	6.0	6.4	8.3	8.6	8.4	8.4	6.0
Ta	0.4	0.0	0.7	0.6	0.5	1.4	1.7	0.9	0.7	0.5
Mo	0.0	0.0	1.9	26.4	0.0	1.5	3.0	2.2	0.8	1.2
Cs	0.1	0.0	0.1	0.3	2.2	3.3	13.6	2.9	0.6	2.6
Ba	226.8	221.3	23.4	14.5	80.7	133.2	164.0	807.5	31.3	954.9
La	17.9	19.2	12.6	6.1	15.9	20.6	7.3	43.1	32.7	25.1
Ce	35.5	36.9	34.2	15.9	50.7	30.0	13.6	95.0	77.7	49.6
Pr	4.7	4.9	4.3	2.8	8.0	4.1	1.7	10.4	10.1	5.8
Nd	18.4	19.0	17.9	14.0	36.0	14.6	6.5	35.5	40.2	22.8
Sm	4.0	4.2	4.3	3.7	7.9	2.5	1.7	5.7	7.8	4.1
Eu	1.2	1.3	1.1	1.0	2.4	0.4	0.3	1.4	2.1	1.0
Gd	4.1	4.3	3.6	3.1	6.5	2.5	1.4	4.2	6.3	3.1
Tb	0.7	0.6	0.5	0.4	0.9	0.3	0.2	0.5	0.7	0.3
Dy	3.8	3.9	2.8	2.4	4.9	1.5	0.8	2.6	3.6	1.4
Ho	0.8	0.8	0.5	0.5	0.8	0.2	0.2	0.5	0.5	0.2
Er	2.0	2.1	1.3	1.3	2.2	0.6	0.4	1.2	1.2	0.6
Tm	0.3	0.3	0.2	0.2	0.3	0.0	0.0	0.2	0.0	0.0
Yb	2.0	1.9	1.2	1.2	1.9	0.5	0.4	1.3	1.0	0.5
Lu	0.3	0.3	0.2	0.2	0.2	0.1	0.1	0.2	0.2	0.1
Hf	3.5	2.4	3.8	3.2	3.6	1.8	1.8	5.3	3.6	3.1
Th	3.5	3.8	4.2	4.8	4.4	6.4	15.4	13.4	3.8	4.8
U	1.1	0.9	1.2	1.9	2.1	2.7	2.8	4.4	1.2	1.7

1108

1109

	Ratios											Ages									Concentrations (calculated from 91500)								
Standard -	207Pb/235	Propagatec	206Pb/238	Propagatec	Error Corre	207Pb/206	Propagatec	Error Corre	208Pb/232	Propagatec	207Pb/235	Propagatec	206Pb/238	Propagatec	208Pb/232	Propagatec	207Pb/206	Propagatec	U (ppm)	Internal 2 S	Th (ppm)	Internal 2 S	Pb (ppm)	Internal 2 S	U/Th	Internal 2 SE		
GJ1 - 1	0.807	0.042	0.09713	0.0037	0.021621	0.0605	0.0014	0.33647	0.0303	0.0023	599	24	597.5	22	602	45	603	52	419.5	9.3	13.28	0.35	11.09	0.84	33.35	0.53		
GJ1 - 10	0.819	0.042	0.09816	0.0038	0.2019	0.0605	0.0013	0.2541	0.0308	0.0024	606	24	603.5	22	611	47	599	48	373.8	8.4	11.69	0.34	10.96	0.86	31.19	0.66		
GJ1 - 11	0.842	0.044	0.1003	0.0039	0.39482	0.0608	0.0013	0.067381	0.0299	0.0022	618.5	24	616.1	23	593	42	613	45	350.7	7.2	11.23	0.3	10.16	0.76	31	0.65		
GJ1 - 12	0.774	0.04	0.09479	0.0037	0.20309	0.0593	0.0014	0.24233	0.0308	0.0027	580.7	23	583.7	22	610	53	555	50	325.5	7.7	10.48	0.33	9.37	0.79	31.14	0.66		
GJ1 - 13	0.817	0.042	0.09895	0.0039	0.22596	0.06	0.0013	0.21116	0.0293	0.0023	606.2	24	608.1	23	583	44	587	48	304.7	6.5	10.03	0.29	8.51	0.61	30.81	0.74		
GJ1 - 14	0.788	0.042	0.09648	0.0038	0.35928	0.0594	0.0014	0.039334	0.029	0.0023	590	24	593.7	22	576	45	559	51	321.3	7.6	10.65	0.36	9.08	0.69	30.59	0.68		
GJ1 - 15	0.797	0.042	0.0951	0.0038	0.39748	0.0608	0.0013	0.12953	0.0307	0.0023	593	24	585.5	22	609	46	610	48	382.8	7.2	12.34	0.3	11.03	0.84	31.06	0.74		
GJ1 - 16	0.813	0.043	0.0977	0.0039	0.38528	0.06	0.0013	0.16734	0.0292	0.0026	602	24	601	23	580	51	593	48	385.9	9.4	12.37	0.39	10.38	0.88	31.43	0.82		
GJ1 - 17	0.812	0.042	0.0974	0.0039	0.3071	0.0602	0.0013	0.28943	0.0311	0.0024	602	24	599	23	618	47	595	49	315.9	6.9	10.6	0.33	9.49	0.67	31.52	0.89		
GJ1 - 18	0.823	0.044	0.0982	0.004	0.44961	0.0606	0.0014	0.053348	0.0299	0.0027	609	25	603.7	23	594	54	602	51	274.9	5.4	9.22	0.23	7.92	0.69	32.76	0.82		
GJ1 - 19	0.81	0.043	0.0971	0.0037	0.34257	0.0599	0.0014	0.16601	0.0301	0.0026	600	24	598.1	23	598	51	581	53	320.1	5	10.17	0.25	8.59	0.71	33.61	0.81		
GJ1 - 2	0.816	0.042	0.09852	0.0039	0.058626	0.0598	0.0014	0.27379	0.0296	0.0025	604.1	24	605.7	23	589	48	581	48	402.1	8.4	12.96	0.34	10.96	0.88	31.88	0.51		
GJ1 - 3	0.809	0.041	0.09768	0.0038	0.081061	0.0597	0.0012	0.25257	0.0315	0.0024	600.9	23	600.8	22	624	48	581	44	384.4	9.7	12.22	0.35	11.29	0.87	31.39	0.52		
GJ1 - 4	0.822	0.042	0.0978	0.0038	0.17192	0.0608	0.0012	0.23138	0.0289	0.0024	607.6	23	601.4	22	573	47	618	43	351.2	7.5	11.13	0.29	9.63	0.77	31.09	0.59		
GJ1 - 5	0.789	0.041	0.09663	0.0037	0.15777	0.0593	0.0013	0.22416	0.0298	0.0022	589.4	23	594.6	22	593	43	563	48	342.8	8.2	10.98	0.32	10.14	0.76	30.42	0.46		
GJ1 - 6	0.822	0.043	0.09778	0.0038	0.25927	0.061	0.0013	0.10714	0.0301	0.0024	607.9	24	601.3	22	598	47	632	44	342.5	7.7	11.01	0.29	10.19	0.83	30.65	0.5		
GJ1 - 7	0.812	0.042	0.09839	0.0038	0.098229	0.06	0.0013	0.31226	0.03	0.0024	601.9	24	604.9	22	596	47	582	49	343.5	6.3	11.24	0.3	10.11	0.78	30.78	0.62		
GJ1 - 8	0.813	0.043	0.09696	0.0037	0.15783	0.061	0.0014	0.21275	0.0313	0.0025	602.5	24	596.5	22	622	48	620	48	353.7	9.1	11.75	0.35	10.87	0.81	30.53	0.61		
GJ1 - 9	0.784	0.04	0.09634	0.0037	0.33215	0.0594	0.0012	0.17806	0.0296	0.0023	588.4	23	592.8	22	588	46	568	44	365.9	8.6	11.77	0.34	10.53	0.8	30.91	0.59		
Mudtank -	0.9	0.13	0.1167	0.0062	0.10749	0.0569	0.0081	0.16927	0.0325	0.0046	582	81	710	35	639	90	230	250	9	0.19	3.41	0.11	3.04	0.43	2.815	0.091		
Mudtank -	1.13	0.16	0.1158	0.007	0.072216	0.0721	0.0098	0.26493	0.0373	0.0059	676	83	703	40	730	110	550	270	8.01	0.2	2.96	0.11	3.19	0.49	2.73	0.11		
Mudtank -	1.01	0.16	0.1164	0.0069	0.206	0.068	0.011	0.15434	0.035	0.0057	641	87	707	40	680	110	390	270	7.21	0.34	2.82	0.15	2.89	0.45	2.69	0.14		
Mudtank -	1.12	0.17	0.1208	0.0073	0.30237	0.0671	0.0094	0.27275	0.0418	0.0067	659	90	732	42	810	130	450	270	7.75	0.3	2.83	0.13	3.2	0.49	2.86	0.17		
Mudtank -	1.05	0.19	0.1265	0.0084	0.21129	0.061	0.011	0.1029	0.0458	0.009	614	97	770	49	880	170	250	300	6.32	0.26	2.54	0.11	3.02	0.49	2.84	0.18		
91500 - 1	1.831	0.06	0.1762	0.0033	0.15467	0.0749	0.0022	0.19021	0.0535	0.0035	1050	22	1045.8	18	1053	67	1040	60	84.1	1.7	31.52	0.69	16	0.58	2.665	0.025		
91500 - 1	1.86	0.049	0.1769	0.0029	0.11441	0.0766	0.0021	0.25292	0.0528	0.0023	1064	18	1049.6	16	1040	44	1075	57	80	1.5	29.99	0.61	15	0.52	2.666	0.024		
91500 - 1	1.86	0.049	0.1769	0.0029	0.11441	0.0766	0.0021	0.25292	0.0528	0.0023	1064	18	1049.6	16	1040	44	1075	57	80	1.5	29.99	0.61	15	0.52	2.666	0.024		
91500 - 1	1.814	0.095	0.1766	0.0083	0.24674	0.0757	0.002	0.16418	0.0542	0.0034	1048	33	1048	46	1067	65	1059	55	115	2.8	33.91	0.78	15.11	0.42	2.709	0.028		
91500 - 10	1.835	0.1	0.1807	0.0086	0.30755	0.0736	0.0023	0.18936	0.0547	0.0038	1051	36	1070	47	1074	72	997	65	78.9	1.9	29.17	0.75	15.1	0.49	2.652	0.055		
91500 - 11	1.871	0.1	0.1835	0.0088	0.29466	0.0742	0.0022	0.24041	0.0537	0.0038	1067	37	1085	48	1057	72	1014	64	80.4	2.1	30.12	0.78	14.99	0.57	2.662	0.056		
91500 - 12	1.863	0.1	0.1785	0.0086	0.40286	0.0764	0.0024	0.12401	0.0546	0.0037	1066	37	1058	47	1074	70	1073	64	83.7	2.3	31.3	0.81	15.15	0.51	2.673	0.058		
91500 - 13	1.824	0.1	0.1804	0.0088	0.40853	0.074	0.0023	0.14622	0.055	0.0038	1046	37	1068	48	1081	72	1008	67	79.6	2.1	29.84	0.85	14.85	0.55	2.67	0.058		
91500 - 14	1.849	0.11	0.1799	0.0087	0.32559	0.0755	0.0027	0.17478	0.0539	0.0038	1060	38	1066	48	1061	72	1048	68	79.5	1.7	30.02	0.73	15.05	0.59	2.651	0.06		
91500 - 15	1.787	0.099	0.1787	0.0087	0.42569	0.072	0.0021	0.15027	0.0546	0.004	1036	36	1061	49	1072	76	958	61	80.4	1.8	30.04	0.86	14.99	0.58	2.682	0.071		
91500 - 2	1.891	0.058	0.1801	0.0034	0.044247	0.0764	0.0022	0.29991	0.0535	0.0035	1072	21	1067.3	18	1053	66	1066	58	80.4	1.8	30.37	0.72	15.63	0.54	2.646	0.025		
91500 - 2	1.774	0.051	0.1769	0.0029	0.00405	0.0731	0.0022	0.33314	0.0544	0.0025	1032	19	1049.5	16	1070	48	970	65	80	1.8	30.05	0.7	15	0.56	2.665	0.026		
91500 - 2	1.774	0.051	0.1769	0.0029	0.00405	0.0731	0.0022	0.33314	0.0544	0.0025	1032	19	1049.5	16	1070	48	970	65	80	1.8	30.05	0.7	15	0.56	2.665	0.026		
91500 - 2	1.775	0.092	0.1743	0.0082	0.11613	0.0735	0.0021	0.32952	0.0517	0.0034	1036	34	1035	45	1018	66	1009	58	80.4	1.8	29.42	0.73	15.21	0.49	2.634	0.036		
91500 - 3	1.856	0.058	0.1779	0.0035	0.18963	0.0754	0.0021	0.2349	0.0514	0.0033	1062	21	1055	19	1012	64	1056	59	81.2	1.8	30.39	0.65	15.41	0.54	2.683	0.027		
91500 - 3	1.803	0.049	0.174	0.0028	-0.11593	0.0755	0.0021	0.4418	0.0509	0.0025	1046	17	1034.1	15	1002	48	1053	59	80	1.7	29.95	0.65	15	0.62	2.671	0.026		
91500 - 3	1.803	0.049	0.174	0.0028	-0.11593	0.0755	0.0021	0.4418	0.0509	0.0025	1046	17	1034.1	15	1002	48	1053	59	80	1.7	29.95	0.65	15	0.62	2.671	0.026		
91500 - 3	1.841	0.096	0.1733	0.008	0.27661	0.0765	0.002	0.12063	0.0487	0.0032	1055	34	1030	44	960	62	1087	52	80.5	2	29.45	0.68	14.6	0.47	2.658	0.033		
91500 - 4	1.829	0.063	0.1797	0.0034	0.17195	0.0745	0.0023	0.12546	0.0526	0.0034	1051	22	1065.3	19	1035	65	1025	62	80.4	1.8	30.18	0.73	15.31	0.59	2.674	0.027		
91500 - 4	1.848	0.054	0.1783	0.003	0.13286	0.0754	0.0022	0.25781	0.0556	0.0023	1056	19	1058	16	1093	44	1043	61	80	1.6	29.99	0.65	15	0.5	2.678	0.03		
91500 - 4	1.848	0.054	0.1783	0.003	0.13286	0.0754	0.0022	0.25781	0.0556	0.0023	1056	19	1058	16	1093	44	1043	61	80	1.6	29.99	0.65	15	0.5	2.678	0.03		
91500 - 4	1.807	0.096	0.1754	0.0082	0.0898	0.0744	0.0023	0.31033	0.05	0.0035	1042	35	1042	45	985	67	1013	63	76.9	1.9	29.05	0.73	14.81	0.58	2.613	0.035		
91500 - 5	1.779	0.056	0.1807	0.0035	0.05125	0.0725	0.0021	0.31954	0.055	0.0035	1037	20	1071	19	1082	67	974	61	84.2	2	31.38	0.77	15.8	0.53	2.667	0.029		
91500 - 5	1.913	0.051	0.1787	0.0029	0.23908	0.0773	0.0021	0.12412	0.052	0.0023	1080	18	1061.1	16	1023	44	1117	53	80.4	1.8	30.41	0.74	15.1	0.5	2.628	0.029		
91500 - 5	1.913	0.051	0.1787	0.0029	0.23908	0.0773	0.0021	0.12412	0.052	0.0023	1080	18	1061.1	16	1023	44	1117	53	80.4	1.8	30.41	0.74	15.1	0.5	2.628	0.029		
91500 - 5	1.702	0.091	0.1698	0.008	0.30333	0.0734	0.0022	0.15768	0.0522	0.0033	1004	34	1011	44	1027	64	990	60	77.2	1.6	29.67	0.62	15.19	0.47	2.714	0.039		
91500 - 6	1.829	0.058	0.1778	0.0034	0.29015	0.0746	0.0022	0.1096	0.0558	0.0036	1053	20	1056	19	1100	69	1034	58	85.4	2.1	31.76	0.81	16.57	0.59	2.676	0.027		
91500 - 6	1.876	0.054	0.1786	0.003	0.0236	0.0765	0.0023	0.33294	0.0518	0.0024	1069	19	1059	17	1020	45	1082	60	79.3	1.8	29.6	0.7	14.82	0.54	2.661	0.027		
91500 - 6	1.876	0.054	0.1786	0.003	0.0236	0.0765	0.0023	0.33294	0.0518	0.0024	1069	19	1059	17	1020	45	1082	60	79.3	1.8	29.6	0.7	14.82	0.54	2.661	0.027		
91500 - 6	1.796	0.096	0.1739	0.0083	0.28309	0.0741	0.0021	0.17231	0.0515	0.0034	1040	36	1033	45	1014	65	1022	62	76.3	1.4	29.83	0.6	15.05	0.42	2.664	0.041		
91500 - 7	1.877	0.055	0.1778	0.0034	0.031307	0.0762	0.0019	0.26401	0.0536	0.0035	1068	20	1054.8	18	1054	68	1076	51	87.3	1.8	32.94	0.68	16.48	0.56	2.626	0.025		
91500 - 7	1.846	0.056	0.1802	0.0029	-0.02009	0.0746	0.0024	0.3389	0.0513	0.0023	1054	21	1068	16	1011	44	1004	72	80.2	1.6	30.05	0.64	15.07	0.53	2.696	0.028		
91500 - 7	1.846	0.056	0.1802	0.0029	-0.02009	0.0746	0.0024	0.3389	0.0513	0.0023	1054	21	1068	16	1011	44	1004	72	80.2	1.6	30.05	0.64	15.07	0.53	2.696	0.028		
91500 - 7	1.849	0.099	0.1805	0.0086	0.43065	0.0748	0.0022	0.085427	0.0529	0.0035	1057	36	1069	47	1041	67	1031	58	77.4	2.1	29.86	0.8	14.89	0.5	2.675	0.045		
91500 - 8	1.847	0.063	0.1799	0.0035	0.16401	0.0738	0.0022	0.20618	0.0546	0.0037	1055	22	1066	19	1073	71	996	65	74	1.6	27.27	0.64	14.07	0.57	2.7	0.032		
91500 - 8	1.857	0.099	0.1746	0.0082	0.29002	0.0764	0.0022	0.18854	0.0506	0.0035	1060	36	1037	45	997	66	1076	61	81.4	1.9	31.1	0.74	15.28	0.52	2.644	0.045		
91500 - 9	1.78	0.099	0.1689	0.0082	0.34652	0.0765	0.0025	0.22879	0.0542	0.0037	1031	36	1005	45	1066	70	1080	63	79.3	2.3	28.28	0.79	14.6	0.55	2.717	0.062		
GJ1 - 1	0.814	0.02	0.0976	0.0017	0.009488	0.0602	0.0012	0.35556	0.0293	0.003	604.3	11	600.3	10	582	58	591	43	318.9	7.5	9.9	0.26	2.71	0.22	32.2	0.48		
GJ1 - 1	0.814	0.014	0.09761	0.0014	0.14574	0.0606	0.0011	0.28686	0.0303	0.0026	603.8	8	600.3	8.3	602	51	608	39	321	6.1	9.9	0.23	2.81	0.22	32.59	0.54		
GJ1 - 1	0.807	0.04	0.09757	0.0043	0.03884	0.0617	0.0014	0.27618	0.0307	0.003	599.3	23	600.1	25	609	59	642	50	473.6	9.2	11.19	0.27	2.79	0.22	33.44	0.5		
GJ1 - 10	0.797	0.021	0.0975	0.0018	0.10902	0.0599	0.0013	0.23973	0.0304	0.0031	593.7	12	599.7	11	602	60	575	49	314	7.1	9.88	0.26	2.86	0.23	32.06	0.52		
GJ1 - 10	0.812	0.015	0.09811	0.0015	0.094649	0.06	0.0012	0.25911	0.0291	0.0027	603.3	8.8	603.3	8.6	578	53	596	44	341.2	7	11.03	0.27	3.02	0.27	31.14	0.47		
GJ1 - 10	0.796	0.04	0.09751	0.0045	0.30461	0.0593	0.0014	0.14787	0.0298	0.0029	592.8	22	599.7	26	591	56	555	50	311.4	7.6	9.93	0.31	2.81	0.22	32.1	0.69		
GJ1 - 11	0.804	0.022	0.09802	0.0018	0.16965	0.0598	0.0014	0.14968	0.0297	0.0029	599	12	602.7	11	590	56	567	51	312.7	7	9.95	0.28	2.83	0.23	31.57	0.47		
GJ1 - 11	0.809	0.016	0.09688	0.0014	0.10868	0.0606	0.0012	0.22765	0.0304	0.0031	601.7	9.3	596.1	8.2	602	60	616	45	353.1	7.1	11.26	0.28	3.25	0.3	31.49	0.45		
GJ1 - 11	0.82	0.043	0.0977	0.0046	0.31996	0.0602	0.0014	0.205	0.0308	0.0032	608	24	600.7	27	611	63	603	51	312.1	7.5	9.9	0.34	2.98	0.24	32.11	0.84		
GJ1 - 12	0.819	0.02	0.09778	0.0018	0.22393	0.0604	0.0012	0.17634	0.0298	0.0029	607.3	12	601.3	10	597	58	602	44	301.5	7	9.49	0.28	2.62	0.21	32.08	0.53		
GJ1 - 12	0.798	0.018	0.09654	0.0014	0.23079	0.06	0.0013	0.084028	0.0301	0.0026	594	10	594	8.5	596	52	584	46	351.6	8.5	11.44	0.32	3.29	0.26	30.91	0.49		
GJ1 - 12	0.814	0.041	0.098	0.0046	0.33922	0.0596	0.0015	0.14463	0.0299	0.0029	604	22	602.5	27	594	56	564	53	316.3	8.5	10.12	0.32	2.91	0.22	30.95	0.69		

GJ1 - 13	0.811	0.022	0.09687	0.0018	0.042152	0.06	0.0015	0.33675	0.0291	0.003	601	12	596	11	577	58	575	54	305.7	6	9.62	0.24	2.63	0.23	31.96	0.48
GJ1 - 13	0.811	0.018	0.09775	0.0014	0.062712	0.0602	0.0013	0.27739	0.0301	0.0028	602	10	601.2	8.2	597	56	586	49	347.8	7.6	11.37	0.29	3.34	0.28	30.59	0.45
GJ1 - 13	0.806	0.04	0.0971	0.0046	0.41503	0.0603	0.0013	0.15521	0.0303	0.0033	598.8	22	597.5	27	601	65	602	46	314.9	8.4	9.66	0.34	2.76	0.25	31.91	0.81
GJ1 - 14	0.829	0.02	0.09859	0.0018	0.049349	0.0605	0.0013	0.29254	0.0316	0.0031	611.9	11	606.1	10	626	61	597	47	297.5	6.9	9.47	0.24	2.75	0.24	31.43	0.48
GJ1 - 14	0.804	0.016	0.0976	0.0015	0.19107	0.0602	0.0012	0.21021	0.03	0.0024	599.8	9	600.3	8.9	596	48	591	43	348.9	7.3	11.5	0.3	3.43	0.25	30.48	0.45
GJ1 - 14	0.806	0.041	0.0977	0.0046	0.36549	0.06	0.0015	0.083396	0.0294	0.0031	598	23	600.6	27	583	62	582	54	322.1	7.3	10.06	0.3	2.76	0.24	31.35	0.76
GJ1 - 15	0.798	0.02	0.09712	0.0018	0.22069	0.0599	0.0012	0.16277	0.0303	0.0029	594.3	11	597.4	11	602	57	577	45	308.8	6.4	9.64	0.27	2.67	0.21	32.14	0.46
GJ1 - 15	0.812	0.017	0.09701	0.0014	0.016686	0.0608	0.0013	0.32076	0.0311	0.0026	602.1	9.6	596.8	8.3	618	52	607	48	349.1	7.7	11.22	0.3	3.41	0.26	31.22	0.46
GJ1 - 15	0.816	0.042	0.0977	0.0046	0.40421	0.0606	0.0016	0.078582	0.0306	0.0033	604	24	600.8	27	607	65	604	55	314.2	8.1	9.48	0.35	2.73	0.22	33.25	0.96
GJ1 - 16	0.795	0.02	0.09748	0.0017	0.15657	0.0599	0.0012	0.22122	0.0331	0.0032	592.2	12	599.6	9.9	655	62	585	46	312.8	7.2	9.73	0.27	2.89	0.22	32.16	0.47
GJ1 - 16	0.809	0.019	0.09728	0.0015	0.17176	0.0603	0.0014	0.13837	0.0291	0.0022	600	11	598.4	8.6	583	45	595	50	346.4	7.2	11.23	0.28	3.12	0.21	31.04	0.49
GJ1 - 16	0.81	0.042	0.0977	0.0046	0.32548	0.0599	0.0015	0.14322	0.0306	0.0035	600	23	600.6	27	607	69	579	57	333.5	7.1	10.48	0.36	2.99	0.25	32.09	0.9
GJ1 - 17	0.806	0.02	0.09759	0.0017	0.028225	0.0605	0.0013	0.32987	0.0269	0.0028	599.1	11	600.2	10	535	54	605	45	305	6.6	9.53	0.24	2.35	0.2	32.09	0.51
GJ1 - 17	0.804	0.017	0.09868	0.0015	0.10991	0.0592	0.0013	0.25662	0.0307	0.0028	597.5	9.6	606.6	8.6	609	54	555	49	339.2	7.9	10.97	0.31	3.16	0.26	31.03	0.47
GJ1 - 17	0.81	0.042	0.0975	0.0046	0.42166	0.0601	0.0014	0.11831	0.0293	0.0033	602	24	599.5	27	581	64	598	54	337.2	8.7	10.64	0.35	2.76	0.25	31.95	0.8
GJ1 - 18	0.799	0.021	0.09761	0.0018	0.14883	0.0598	0.0013	0.20325	0.0303	0.003	594	12	600.3	11	601	59	569	50	310.5	6.7	9.78	0.23	2.72	0.22	31.67	0.49
GJ1 - 18	0.801	0.018	0.097	0.0014	0.033422	0.0598	0.0014	0.24568	0.0308	0.0026	597	10	596.7	8.1	610	50	575	52	339.3	7.1	10.92	0.25	3.13	0.24	31.25	0.51
GJ1 - 18	0.807	0.041	0.0977	0.0046	0.39819	0.0602	0.0014	0.067988	0.0305	0.003	599	23	600.7	27	606	58	586	53	336.2	8.6	10.52	0.35	2.84	0.23	32.53	0.97
GJ1 - 19	0.816	0.021	0.09785	0.0018	0.062314	0.0604	0.0013	0.32402	0.0295	0.003	604.4	12	601.8	10	585	58	594	48	315.9	7	9.99	0.27	2.73	0.23	31.58	0.45
GJ1 - 19	0.8	0.017	0.09726	0.0014	0.097823	0.0598	0.0014	0.35465	0.0301	0.0027	595.4	9.7	598.3	8.3	598	53	570	50	334.7	6.3	10.67	0.25	2.95	0.25	31.63	0.49
GJ1 - 19	0.812	0.042	0.0979	0.0046	0.44836	0.0608	0.0015	0.12913	0.0299	0.0032	602	23	601.8	27	607	67	610	51	331.2	8.3	10.06	0.39	2.65	0.24	33.7	1.1
GJ1 - 2	0.809	0.021	0.09756	0.0017	0.096566	0.0601	0.0013	0.23542	0.0294	0.0029	600.2	12	600.1	10	584	56	588	48	302.8	6.7	9.48	0.25	2.65	0.2	32.14	0.58
GJ1 - 2	0.81	0.019	0.09829	0.0015	0.12019	0.0596	0.0014	0.17347	0.0293	0.0027	600	11	604.3	8.6	582	54	566	52	327.8	6.5	10.22	0.24	2.83	0.24	32.13	0.47
GJ1 - 2	0.809	0.04	0.09762	0.0047	0.19934	0.0598	0.0014	0.14305	0.0291	0.0028	600.7	22	600.4	27	578	55	577	48	389.3	8.7	10.37	0.28	2.55	0.21	31.4	0.57
GJ1 - 20	0.81	0.02	0.09739	0.0018	0.13462	0.0601	0.0012	0.24835	0.031	0.0031	601.2	11	599	11	614	61	592	45	315.3	7	10.07	0.29	2.88	0.24	31.22	0.49
GJ1 - 20	0.819	0.017	0.09881	0.0015	0.010659	0.06	0.0012	0.34871	0.0294	0.0026	605.9	9.3	607.4	8.6	583	51	593	48	324.3	7.3	10.45	0.29	2.74	0.24	31.23	0.49
GJ1 - 20	0.806	0.041	0.0968	0.0045	0.35369	0.0612	0.0015	0.16072	0.03	0.0031	598	23	595.6	27	595	61	622	54	335.8	8.7	10.31	0.37	2.79	0.25	32.94	0.82
GJ1 - 21	0.817	0.02	0.09768	0.0017	0.01611	0.0601	0.0013	0.34732	0.0305	0.003	604.8	11	600.7	10	605	59	583	47	326.1	8	10.25	0.31	2.98	0.24	31.66	0.54
GJ1 - 21	0.82	0.015	0.09793	0.0014	0.14025	0.061	0.0011	0.20445	0.0293	0.0028	607.9	8.2	602.2	8.1	582	56	621	40	329.7	6.8	10.39	0.26	2.76	0.26	32.03	0.56
GJ1 - 21	0.809	0.042	0.0993	0.0047	0.55317	0.0595	0.0014	0.036829	0.0304	0.0032	600	24	610.1	28	602	63	561	52	312.2	8.5	9.91	0.33	2.78	0.24	31.55	0.95
GJ1 - 22	0.805	0.018	0.09692	0.0014	0.082758	0.0604	0.0014	0.24201	0.0312	0.0027	599	9.9	596.3	8.2	619	54	599	49	323.6	6.3	10.1	0.26	2.96	0.24	32.17	0.55
GJ1 - 22	0.793	0.043	0.096	0.0046	0.55307	0.0601	0.0016	-0.09997	0.0298	0.0034	590	24	590.7	27	591	66	579	57	320.4	8.4	9.75	0.33	2.63	0.24	33	1.1
GJ1 - 23	0.815	0.015	0.09895	0.0015	0.040211	0.0597	0.0012	0.33761	0.0299	0.0025	604	8.6	608.2	8.5	600	49	584	42	311.9	6.9	9.63	0.25	2.77	0.2	32.63	0.5
GJ1 - 23	0.8	0.041	0.0972	0.0046	0.31888	0.0595	0.0015	0.20166	0.0306	0.0031	596	24	597.8	27	607	61	572	55	305.5	7.1	9.48	0.33	2.64	0.21	32.61	0.97
GJ1 - 24	0.831	0.042	0.0992	0.0047	0.47511	0.0604	0.0014	0.22677	0.0298	0.003	612	23	609.2	28	592	60	596	50	300.9	8	9.39	0.32	2.57	0.21	32.02	0.98
GJ1 - 3	0.808	0.021	0.09766	0.0018	0.071119	0.0602	0.0014	0.35388	0.0307	0.003	599.5	12	600.6	10	615	58	592	51	308.7	6.6	9.76	0.27	2.88	0.22	31.88	0.55
GJ1 - 3	0.811	0.018	0.09743	0.0015	0.12504	0.0603	0.0013	0.23475	0.03	0.0027	601	10	599.3	8.8	596	52	599	47	317.8	6.3	9.88	0.24	2.88	0.22	32.2	0.45
GJ1 - 3	0.813	0.04	0.09758	0.0046	0.22833	0.0599	0.0014	0.16763	0.0307	0.0029	603	23	600.2	27	609	58	583	50	336.1	7.3	9.92	0.29	2.91	0.23	31.18	0.59
GJ1 - 4	0.802	0.02	0.0978	0.0018	0.12971	0.0598	0.0013	0.25143	0.0305	0.0029	596.2	12	601.5	10	606	57	570	48	300.6	6	9.51	0.25	2.81	0.21	31.92	0.49
GJ1 - 4	0.802	0.017	0.09833	0.0015	0.013864	0.0592	0.0013	0.34459	0.031	0.0027	596.6	9.6	604.6	8.8	615	52	550	50	323.8	6.8	10.06	0.25	3.05	0.22	32.4	0.48
GJ1 - 4	0.813	0.04	0.09763	0.0045	-0.10892	0.0601	0.0013	0.45376	0.03	0.0029	602.9	22	600.5	27	596	57	592	50	290.2	6.2	9.18	0.25	2.83	0.21	32.14	0.63
GJ1 - 5	0.813	0.022	0.09744	0.0018	0.032938	0.0607	0.0014	0.25036	0.0305	0.003	602	12	599.3	10	606	59	600	53	312.7	7	9.7	0.27	2.9	0.23	32.55	0.56
GJ1 - 5	0.812	0.017	0.09803	0.0014	0.015862	0.06	0.0013	0.33293	0.0305	0.0027	601.7	9.5	602.8	8.4	606	53	580	48	332.8	6.3	10.53	0.27	3.09	0.24	31.87	0.57
GJ1 - 5	0.802	0.041	0.09766	0.0045	0.27919	0.0594	0.0014	0.11176	0.0305	0.0029	596	23	600.6	26	606	58	559	52	291	6.5	9.34	0.24	2.88	0.22	32.56	0.59
GJ1 - 6	0.807	0.022	0.09755	0.0018	0.27755	0.06	0.0013	0.056463	0.0309	0.0032	599	12	600	10	613	63	581	48	310.6	7	9.67	0.24	2.94	0.25	32.21	0.44
GJ1 - 6	0.81	0.019	0.09708	0.0015	0.1191	0.0603	0.0014	0.20049	0.0296	0.0025	602	11	597.2	8.7	589	49	600	52	329.5	6.9	10.52	0.25	2.91	0.22	31.36	0.46
GJ1 - 6	0.811	0.041	0.0974	0.0045	0.072265	0.0609	0.0015	0.38481	0.0294	0.003	601.6	23	599.1	26	583	59	610	52	282	5.3	9.15	0.26	2.51	0.22	32.5	0.66
GJ1 - 7	0.81	0.02	0.09769	0.0017	0.029711	0.0599	0.0012	0.30324	0.0313	0.003	601.3	11	600.8	9.9	620	60	586	45	309.5	6.7	9.75	0.27	2.9	0.22	32.2	0.58
GJ1 - 7	0.826	0.019	0.09793	0.0015	0.18154	0.0612	0.0013	0.15814	0.0296	0.003	610	10	602.2	8.5	587	59	624	47	329.1	8.1	10.55	0.31	2.77	0.26	31.44	0.49
GJ1 - 7	0.81	0.039	0.09782	0.0045	0.25743	0.0594	0.0013	0.1978	0.0302	0.0031	601	22	601.6	26	600	61	573	48	283.1	5.8	9.4	0.27	2.73	0.23	31.72	0.67
GJ1 - 8	0.819	0.02	0.09813	0.0018	0.16882	0.0602	0.0012	0.2075	0.0302	0.0029	605.8	11	603.4	11	600	57	591	43	312.6	7.1	9.96	0.27	2.96	0.24	31.71	0.48
GJ1 - 8	0.796	0.018	0.09747	0.0014	0.13257	0.0592	0.0013	0.17403	0.0294	0.0025	592.8	9.9	599.5	8.4	583	50	550	48	339.7	7	10.87	0.29	2.93	0.24	31.49	0.45
GJ1 - 8	0.808	0.041	0.09754	0.0045	0.31698	0.0599	0.0014	0.11964	0.0307	0.0031	599	23	599.9	27	608	61	583	52	291.6	6.1	9.16	0.26	2.8	0.22	33.32	0.78
GJ1 - 9	0.807	0.021	0.09708	0.0018	0.064812	0.0606	0.0014	0.26057	0.0284	0.003	599	12	597.3	10	564	58	599	49	314.2	7.3	9.92	0.25	2.7	0.24	31.87	0.48
GJ1 - 9	0.807	0.02	0.09685	0.0014	0.20869	0.0604	0.0014	0.094977	0.0322	0.0029	600	11	595.9	8.5	638	56	595	53	343.6	6.9	10.83	0.27	3.19	0.26	31.95	0.49
GJ1 - 9	0.815	0.041	0.0976	0.0045	0.37826	0.0612	0.0014	0.11592	0.0298	0.003	605	22	600	27	592	59	624	50	301.1	6.9	9.59	0.26	2.67	0.21	32.41	0.67
Mudtank -	1.16	0.17	0.1161	0.0056	0.089146	0.077	0.012	0.28148	0.0409	0.0071	702	80	706	32	790	130	560	280	6.77	0.11	2.533	0.075	0.92	0.15	2.729	0.091
Mudtank -	1.06	0.15	0.118	0.0069	0.096207	0.064	0.0089	0.17972	0.0374	0.0064	642	86	717	40	730	120	420	260	7.76	0.17	2.531	0.081	0.81	0.13	2.72	0.098
Mudtank -	0.82	0.16	0.1154	0.0048	-0.01478	0.054	0.011	0.25387	0.0312	0.0066	460	110	702	28	610	130	0	310	7.29	0.15	2.723	0.084	0.82	0.17	2.744	0.083
Mudtank -	1.02	0.16	0.1196	0.0074	0.055093	0.0605	0.0097	-0.01961	0.0385	0.007	605	85	726	42	750	130	230	270	6.48	0.17	2.251	0.087	0.8	0.13	2.8	0.12
Mudtank -	1.01	0.18	0.1164	0.0053	0.088091	0.066	0.011	0.2643	0.0363	0.007	560	100	712	31	710	130	230	300	7.24	0.19	2.752	0.099	0.95	0.16	2.691	0.091
Mudtank -	0.99	0.14	0.1149	0.0069	0.10536	0.0641	0.0087	0.19838	0.0391	0.0059	624	76	699	40	770	110	360	240	6.48	0.15	2.417	0.084	0.95	0.13	2.78	0.11
Mudtank -	1.17	0.16	0.1181	0.007	0.12271	0.0718	0.0092	0.18105	0.0349	0.0063	712	82	718	40	680	120	600	250	6.9	0.33	2.66	0.14	0.86	0.14	2.81	0.15
Plesovice -	0.3939	0.0092	0.05335	0.00097	0.18855	0.05301	0.00098	0.2364	0.01771	0.0012	336.8	6.7	335	5.9	355	24	319	41	705	17	70.2	1.8	11.79	0.48	10.04	0.11
Plesovice -	0.3858	0.0093	0.05347	0.00079	0.11909	0.0521	0.0012	0.18782	0.01671	0.00085	330.5	6.9	335.8	4.9	335	17	282	52	579	11	53.04	0.98	8.38	0.36	10.891	0.091
Plesovice -	0.3889	0.02	0.05376	0.0026	0.11332	0.0525	0.0012	0.24071	0.01696	0.0011	333.7	14	337.6	16	340	22	297	51	904	22	73.9	2	10.42	0.42	9.974	0.087
Plesovice -	0.4042	0.021	0.05375	0.0021	0.19472	0.0545	0.0012	0.11618	0.01765	0.00069	344	15	337.5	13	353	14	371	50	755	12	78	1.2	39	1.6	10.008	0.086
Plesovice -	0.3909	0.02	0.05417	0.0025	0.43243	0.0525	0.0013	0.10223	0.01722	0.0013	334.3	15	340	16	345	25	289	52	642	13	61.1	1.2	9.46	0.43	10.51	0.15
Plesovice -	0.3991	0.02	0.0552	0.0026	0.32494	0.0532	0.0012	0.25567	0.01661	0.0012	340.3	15	346.3	16	333	24	321	51	703	15	70.3	1.6	10.48	0.47	9.96	0.16
Plesovice -	0.406	0.021	0.05577	0.0027	0.46502	0.0533	0.0014	0.11416	0.01628	0.0012	344.8	15	349.8	16	326	24	320	56	672	16	71	1.7	10.73	0.48	9.49	0.18
Plesovice -	0.4074	0.011	0.0535	0.00095	0.12576	0.0556	0.0012	0.21936	0.01637	0.0011	346.3	7.7	336	5.8	328	23	412	49	533.2	7.8	52.16	0.54	8.42	0.37	10.26	0.1
Plesovice -	0.4386	0.01	0.05384	0.00078	-0.03978	0.0588	0.0013	0.35599	0.0227	0.0013	368.4	7	338.1	4.8	453	27	545	50	706	16	69.2	1.5	15.21	0.66	10.219	0.087
Plesovice -	0.4021	0.02	0.05425	0.0026	0.30911	0.053	0.0012	0.079703	0.01769	0.0012	342.6	15	340.5	16	354	24	317	49	763	19	70.6	2	11.21	0.45	9.55	0.11
Plesovice -	0.3859	0.02	0.05315	0.0021	0.18286	0.0526	0.0011	0.18773	0.01622	0.00056	330.8	15	333.8	13	325	11	306	47	755	21	78.1	2.2	39	1.5	9.374	0.095
Plesovice -	0.3895	0.0095	0.05377	0.00093	0.001402	0.0524	0.0011	0.32151	0.01631	0.0011	333.5	6.9	337.6	5.7	327	22	287	45	680	17	67.2	1.6	10.8	0.47	10.155	0.091
Plesovice -	0.3957	0.0085	0.054	0.00081	-0.02999	0.0531	0.0012	0.37872	0.01664	0.00093	337.9	6.1	339	4.9	333	18	318	48	579.1	9.9	57.55	0.79	9.14	0.41	10.03	0.1

Plesovice -	0.3914	0.02	0.05334	0.0024	0.17504	0.0526	0.0012	0.16436	0.01573	0.0011	335.6	14	335	15	315	21	305	50	724	18	70.6	1.9	10.92	0.42	9.689	0.088
Plesovice -	0.3906	0.02	0.05343	0.0021	0.18433	0.053	0.0011	0.25569	0.01687	0.00064	334.3	15	335.5	13	338	13	322	46	757	23	77.9	2.9	39.1	1.9	9.82	0.12
Plesovice -	0.3866	0.011	0.0541	0.00097	0.22063	0.0521	0.0012	0.098467	0.01631	0.0012	331.1	7.7	339.6	5.9	327	24	276	49	636	15	60.8	1.5	9.57	0.5	10.478	0.082
Plesovice -	0.4005	0.0095	0.05354	0.0008	0.089796	0.0543	0.0013	0.25188	0.017	0.00089	341.2	6.8	336.2	4.9	341	18	367	52	644	17	65.2	1.8	10.9	0.47	9.869	0.079
Plesovice -	0.3876	0.019	0.05235	0.0024	0.10911	0.0533	0.0012	0.27444	0.01585	0.0011	332.1	14	328.9	15	318	21	326	51	672	18	68.5	2	11.35	0.44	9.971	0.093
Plesovice -	0.3977	0.021	0.0526	0.0021	0.30331	0.0548	0.0012	0.14264	0.01637	0.00065	339.4	15	330.5	13	328	13	386	47	752	19	78.1	2.2	38.9	1.8	9.33	0.1
Plesovice -	0.3913	0.011	0.05331	0.00094	0.1347	0.0523	0.0012	0.18907	0.01738	0.0012	334.6	7.8	334.8	5.8	348	24	288	50	635	15	60.8	1.4	9.85	0.44	10.423	0.082
Plesovice -	0.3928	0.0073	0.05311	0.00076	-0.02977	0.0538	0.0011	0.3613	0.01601	0.00074	335.9	5.3	333.6	4.7	321	15	347	44	803	21	83.9	2.3	13.03	0.53	9.574	0.088
Plesovice -	0.3862	0.019	0.05241	0.0024	0.26645	0.0536	0.0013	0.11671	0.01706	0.0012	330.9	14	329.3	15	342	23	336	51	627	17	64.8	1.9	10.29	0.45	10.09	0.11
Plesovice -	0.3865	0.02	0.05211	0.0021	0.36639	0.0537	0.0012	0.088697	0.01677	0.00063	331.1	15	327.4	13	336	12	343	47	755	17	77.7	2.1	38.9	1.7	9.64	0.12
Plesovice -	0.3867	0.011	0.0533	0.00092	0.067492	0.0534	0.0013	0.3224	0.01581	0.0011	332	7.8	334.7	5.6	317	22	326	54	629	11	59.6	1	8.64	0.35	10.484	0.082
Plesovice -	0.394	0.0083	0.05378	0.00081	0.25592	0.0532	0.0011	0.095517	0.01615	0.00083	336.6	6.2	337.7	4.9	324	17	317	46	706	21	70.3	2.4	10.78	0.47	10.03	0.1
Plesovice -	0.3998	0.02	0.05341	0.0025	0.19658	0.0547	0.0013	0.26002	0.01552	0.0011	340.8	15	335.4	15	311	22	379	53	642	15	64.4	1.5	9.81	0.39	10.25	0.12
Plesovice -	0.3922	0.02	0.0527	0.0021	0.31995	0.0539	0.0011	0.10268	0.01676	0.00064	335.4	15	331	13	336	13	352	47	757	21	78.4	2.3	39.2	1.7	9.67	0.13
Plesovice -	0.3922	0.011	0.05408	0.00096	0.080774	0.0527	0.0012	0.24153	0.0174	0.0012	335.2	7.9	339.5	5.9	349	25	302	51	625.9	8.7	60.34	0.85	9.61	0.41	10.311	0.083
Plesovice -	0.4038	0.0092	0.05401	0.00081	0.24021	0.0542	0.0012	0.092503	0.01676	0.00097	343.6	6.7	339.1	4.9	336	19	358	50	544	15	54.4	2.1	8.76	0.48	10.28	0.13
Plesovice -	0.3843	0.019	0.05117	0.0024	0.2795	0.054	0.0013	0.15801	0.01643	0.0012	330.3	14	321.7	14	329	24	358	53	684	16	65.6	1.7	10.38	0.44	10.58	0.13
Plesovice -	0.3871	0.02	0.05248	0.002	0.25541	0.0535	0.0011	0.18269	0.01688	0.00062	331.8	15	329.7	12	338	12	334	45	758	21	78.2	2.3	39.2	1.7	9.77	0.11
Plesovice -	0.3991	0.011	0.05375	0.00094	0.053076	0.0537	0.0012	0.2531	0.01731	0.0012	340.3	7.7	337.5	5.8	347	24	335	50	629	15	58.7	1.4	9.52	0.43	10.663	0.091
Plesovice -	0.3877	0.02	0.05214	0.0024	0.35753	0.0539	0.0013	0.13344	0.01677	0.0012	332	14	327.6	15	336	23	350	52	690	15	65.8	1.5	10.53	0.45	10.11	0.14
Plesovice -	0.3862	0.02	0.05225	0.002	0.33507	0.0534	0.0012	0.12151	0.017	0.0007	330.9	15	328.3	12	341	14	331	48	752	18	77.7	1.7	38.6	1.6	9.56	0.11
Plesovice -	0.394	0.0099	0.05358	0.00094	0.17107	0.0531	0.0011	0.15029	0.01764	0.0013	337.4	7.4	336.5	5.7	353	26	317	45	671	22	63.2	2.2	10.64	0.58	10.569	0.091
Plesovice -	0.4005	0.02	0.0539	0.0025	0.25601	0.0537	0.0013	0.21714	0.01566	0.0011	342.1	14	338.4	15	314	22	346	54	732	16	73.2	1.8	11.01	0.44	9.84	0.14
Plesovice -	0.3932	0.021	0.05345	0.0021	0.49695	0.0531	0.0011	-0.03749	0.01731	0.00072	336	15	335.7	13	347	14	319	47	757	18	78.2	2.1	39.2	1.8	10.07	0.14
Temora - 1	0.488	0.024	0.06549	0.0014	0.11303	0.0539	0.0026	0.19008	0.01985	0.0014	400	16	408.8	8.6	397	27	317	95	93.6	2.4	47.5	1.2	8.98	0.4	1.964	0.018
Temora - 1	0.516	0.032	0.0647	0.0014	-0.05654	0.0579	0.0037	0.33478	0.0211	0.0015	414	21	403.9	8.3	422	31	430	130	65.1	1.1	24.21	0.49	4.78	0.32	2.682	0.03
Temora - 1	0.531	0.031	0.0705	0.0015	0.010366	0.0546	0.0032	0.24567	0.0227	0.0018	425	21	439	9.3	453	36	310	110	84.2	2.5	28.53	0.97	6.16	0.39	2.943	0.038
Temora - 2	0.525	0.023	0.06615	0.0013	0.025602	0.058	0.0024	0.23737	0.02053	0.0013	427	15	412.8	8.1	411	27	482	89	123.1	3.6	73.2	2.3	14.5	0.57	1.686	0.014
Temora - 2	0.529	0.038	0.0668	0.0015	0.173	0.057	0.0039	0.059225	0.0183	0.0015	420	25	416.8	9.1	366	29	400	140	54.8	1.2	19.63	0.47	3.57	0.25	2.805	0.037
Temora - 3	0.483	0.025	0.06699	0.0014	0.17967	0.0526	0.0026	0.081402	0.02064	0.0014	398	17	417.9	8.6	413	28	261	96	95.7	1.9	48.63	0.97	9.85	0.4	1.973	0.016
Temora - 3	0.508	0.02	0.06579	0.0011	0.063224	0.0558	0.0021	0.2186	0.02029	0.0011	414	13	410.7	6.7	406	21	412	79	192.2	7.6	62.8	2.5	11.67	0.61	3.068	0.028
Temora - 4	0.521	0.02	0.06586	0.0013	0.17114	0.0579	0.0021	0.10191	0.02041	0.0013	423	13	411.1	7.8	408	25	477	75	140.9	2.6	90.6	1.6	17.83	0.58	1.557	0.011
Temora - 4	0.528	0.018	0.06939	0.0012	0.16532	0.0552	0.0018	0.15519	0.01986	0.00087	428	12	432.4	6.9	397	17	385	70	200.3	2.4	105	2.2	19.92	0.58	1.919	0.022
Temora - 5	0.521	0.028	0.06565	0.0014	0.08197	0.0579	0.0031	0.34019	0.0207	0.0014	420	19	409.8	8.7	414	26	430	110	101.4	2.1	56.9	1.1	11.05	0.41	1.783	0.015
Temora - 5	11.38	0.59	0.1629	0.0077	0.37924	0.513	0.026	0.51711	0.1088	0.0068	2520	49	968	43	2080	120	4228	86	4.9	0.23	12.02	0.7	12.1	0.55	0.443	0.018
Temora - 6	0.491	0.029	0.0661	0.0015	0.036738	0.0531	0.0031	0.3068	0.0221	0.0017	399	20	412.4	8.8	441	33	280	110	80.3	1.6	29.72	0.68	6.06	0.32	2.705	0.028
Temora - 6	0.492	0.029	0.0643	0.0013	-0.0053	0.0558	0.0033	0.20239	0.0199	0.0012	399	20	401.6	8	397	23	370	120	92.1	2.5	35.65	0.92	6.85	0.37	2.577	0.028
Temora - 7	0.522	0.029	0.0702	0.0016	0.065496	0.0549	0.0031	0.18761	0.0223	0.0018	420	19	436.9	9.7	446	35	350	110	77.4	2.6	24.91	0.95	5.04	0.29	3.116	0.04
Temora - 7	0.5	0.02	0.06636	0.0012	-0.05741	0.055	0.0023	0.34877	0.022	0.0012	410	14	414.1	7.1	439	24	372	89	128.3	2.7	41.62	0.98	8.46	0.42	3.092	0.03
Temora - 8	0.565	0.036	0.0719	0.0018	0.22379	0.0569	0.0034	0.12033	0.0213	0.0022	452	24	447.2	11	426	44	410	120	55.8	1.9	15.99	0.55	3.15	0.27	3.46	0.052
Temora - 8	0.515	0.021	0.06652	0.0011	-0.00492	0.0565	0.0024	0.2727	0.02047	0.0011	418	14	415.1	6.8	409	21	415	88	151.4	2.8	55.67	0.96	11.05	0.45	2.71	0.025
Temora - 9	0.526	0.027	0.0709	0.0016	0.080047	0.054	0.0028	0.34941	0.02202	0.0016	424	18	441.5	9.4	440	31	320	100	83	1.4	48.95	0.76	10.14	0.44	1.686	0.015
Temora2 -	0.496	0.031	0.06555	0.0032	0.15333	0.0543	0.0025	0.009433	0.02076	0.0013	405	21	409.2	19	415	27	342	96	129.9	2.8	59.6	1.8	10.61	0.44	1.864	0.025
Temora2 -	no value		no value		NaN	no value		NaN	no value		no value		no value		no value		no value		0.0036	0.0042	0.0049	0.0042	0.05	0.28	no value	NAN
Temora2 -	0.504	0.027	0.06522	0.0031	0.11145	0.0558	0.0018	0.263	0.01907	0.0012	412	19	407.3	19	381.7	24	409	69	185	5.5	124.2	4.3	24.77	0.94	1.53	0.015
Temora2 -	0.468	0.029	0.06061	0.0024	0.22871	0.0558	0.0022	0.10987	0.02031	0.00082	387	20	379.3	15	406	16	396	82	178.9	1.9	63.83	0.71	39.4	1.5	2.716	0.031
Temora2 -	0.496	0.029	0.06547	0.0026	0.27776	0.0549	0.0018	0.079771	0.02079	0.00057	408	20	408.7	16	416	11	379	71	227.9	2.9	141.4	1.5	87.3	2.3	1.594	0.017
Temora2 -	0.499	0.031	0.06411	0.0026	0.18527	0.0566	0.0023	0.16804	0.02017	0.00073	408	21	400.5	16	403	14	422	85	143.2	4.4	70.3	2.7	42.4	1.9	2.068	0.034
Temora2 -	0.469	0.031	0.0618	0.0026	0.14181	0.0554	0.0026	0.20139	0.02062	0.00078	386	22	386.2	16	412	15	369	97	148	3.4	76.8	2.1	47.1	2	1.923	0.026
Temora2 -	0.525	0.039	0.0695	0.0035	0.12973	0.055	0.0032	0.20942	0.0238	0.0022	421	26	432.6	21	474	43	350	120	76.1	2.2	21.64	0.73	4.68	0.31	3.506	0.082
Temora2 -	no value		no value		NaN	no value		NaN	no value		no value		no value		no value		no value		0.006	0.014	0.0036	0.007	0.39	0.35	no value	NAN
Temora2 -	0.51	0.032	0.0638	0.0027	0.4067	0.0576	0.0023	0.050255	0.02105	0.00083	417	22	398.7	16	421	16	464	82	191.3	2.7	77.6	1.5	46.1	1.7	2.674	0.052

	Ratios								Ages								Concentrations (calculated from 91500)									
Sample - ar	207Pb/235	Propagatec	206Pb/238	Propagatec	Error Corre	207Pb/206	Propagatec	Error Corre	208Pb/232	Propagatec	207Pb/235	Propagatec	206Pb/238	Propagatec	208Pb/232	Propagatec	207Pb/206	Propagatec	U (ppm)	Internal 2 S	Th (ppm)	Internal 2 S	Pb (ppm)	Internal 2 S	U/Th	Internal 2 SE
BOP1A - 1	6.965	0.13	0.3827	0.0068	0.27623	0.1318	0.0015	0.3076	0.1106	0.0064	2106	17	2089	31	2124	120	2117	21	131.3	2.6	78	1.5	82.4	1.5	1.679	0.015
BOP1A - 2	6.95	0.15	0.3866	0.007	0.23096	0.1293	0.0023	0.29057	0.1086	0.0064	2103	19	2107	33	2083	120	2083	31	173.6	5.2	117	3.6	120.2	3.2	1.4812	0.0099
BOP1A - 3	7.122	0.13	0.3939	0.0068	0.33797	0.131	0.0013	0.30045	0.1111	0.0064	2125.3	16	2140	32	2129	120	2108	18	199.4	4.8	113.8	2.7	121.4	2.4	1.749	0.012
BOP1A - 4	7.043	0.14	0.3889	0.0068	0.27322	0.1316	0.0018	0.21181	0.1096	0.0063	2116	18	2117	31	2101	120	2112	24	114.7	3.7	64.5	2.2	67.4	2.1	1.782	0.014
BOP1A - 5	7.274	0.14	0.3961	0.0069	0.29231	0.1333	0.0015	0.2765	0.1159	0.0066	2145	16	2151	32	2215	120	2136	20	146.7	4.2	109.5	3	121.7	2.7	1.337	0.01
BOP1A - 6	5.55	0.13	0.3066	0.0073	0.93438	0.13152	0.0009	0.16882	0.1007	0.0063	1904	21	1722	36	1937	120	2117	12	553	22	284	11	266.7	4.7	1.952	0.011
BOP1A - 7	7.063	0.13	0.3893	0.0067	0.27167	0.1319	0.0015	0.29472	0.1098	0.0064	2118	16	2119	31	2105	120	2122	20	163.3	4.5	88.3	2.6	93.1	2.2	1.853	0.014
BOP1A - 8	6.91	0.12	0.3848	0.0066	0.23499	0.1308	0.0013	0.32826	0.1071	0.0061	2098.7	15	2098	31	2056	110	2107	18	207.5	9.5	141.8	7.4	146.5	7	1.485	0.017
BOP1A - 9	7.95	0.18	0.4088	0.0075	0.66692	0.1418	0.0019	-0.16324	0.1626	0.011	2221	21	2209	34	3040	200	2243	23	155.1	5.6	102.5	4.8	153.6	2.9	1.54	0.019
BOP1A - 10	6.946	0.13	0.3854	0.0067	0.47879	0.1315	0.0013	0.17375	0.1106	0.0064	2103	16	2104	31	2120	120	2117	17	211	9.7	167.5	8	177.5	6.6	1.265	0.012
BOP1A - 11	7.104	0.13	0.3916	0.0067	0.21887	0.1325	0.0014	0.36345	0.1136	0.0066	2125.6	16	2130	31	2175	120	2131	19	179.9	7.9	86.2	4	94.5	3.6	2.096	0.016
BOP1A - 12	7.465	0.14	0.4075	0.0071	0.5236	0.1337	0.0014	0.10734	0.12	0.007	2167	17	2203	33	2289	130	2144	18	180.1	5.8	97.2	3	112.9	2.4	1.851	0.012
BOP1A - 13	9.08	0.45	0.4177	0.0092	0.80389	0.1561	0.0054	-0.60343	0.191	0.018	2316	42	2248	42	3490	300	2375	55	86	5.1	53.8	3.5	91.2	5	1.613	0.018
BOP1A - 14	7.394	0.14	0.4037	0.0072	0.43723	0.1335	0.0014	0.29128	0.1205	0.0071	2158	17	2185	33	2299	130	2140	19	202	9.6	160.2	8.6	136.6	9.8	1.279	0.017
BOP1A - 16	7.111	0.13	0.3939	0.0071	0.40345	0.1318	0.0014	0.30268	0.11	0.0063	2125	17	2140	33	2108	120	2120	19	138.6	4.4	99.9	3.5	107.2	3.4	1.398	0.014
BOP1A - 17	7.13	0.16	0.3959	0.0072	0.29812	0.131	0.002	0.22402	0.1092	0.0065	2126	19	2150	33	2093	120	2106	28	90.4	2.6	47.8	1.3	53.4	1.3	1.891	0.017
BOP1A - 19	5.093	0.098	0.2846	0.0054	0.80644	0.1301	0.001	0.12979	0.0877	0.0051	1833	17	1614	27	1699	94	2097	14	210	12	149.2	7.9	126.1	5.6	1.407	0.012
BOP1A - 21	5.971	0.13	0.3298	0.0075	0.82157	0.1314	0.0012	0.12659	0.1053	0.006	1968	19	1836	36	2022	110	2116	16	311.1	4.8	171.4	3.8	177.5	3.7	1.831	0.018
BOP1A - 22	8.04	0.19	0.4104	0.0077	0.78757	0.1425	0.0018	-0.33434	0.145	0.0097	2231	20	2215	35	2731	170	2252	21	152	6.8	97.8	4.7	134.1	4	1.573	0.016
BOP1A - 23	6.854	0.12	0.3842	0.0066	0.26622	0.1294	0.0013	0.31001	0.1084	0.0062	2091.4	15	2096	30	2079	110	2087	17	238	12	166.3	8.7	175.1	7.9	1.4441	0.0095
BOP1A - 24	7.114	0.13	0.3865	0.0067	0.26175	0.1336	0.0016	0.33058	0.1138	0.0066	2124	17	2106	31	2177	120	2140	21	134.6	2.3	76.15	0.9	85.1	1.2	1.773	0.018
BOP1A - 25	7.033	0.13	0.3917	0.0068	0.36904	0.1301	0.0013	0.30328	0.1115	0.0064	2114	16	2130	32	2135	120	2098	19	198.2	9.5	145.8	7.7	157.6	7.1	1.381	0.016
BOP1A - 26	2.99	0.23	0.169	0.012	0.98314	0.1247	0.002	-0.62953	0.0576	0.0047	1333	68	996	68	1128	90	2017	29	472	47	348	32	164.8	2.4	1.34	0.011
BOP1A - 27	6.824	0.12	0.3804	0.0066	0.28122	0.1298	0.0014	0.27365	0.1051	0.006	2087.3	16	2078	31	2020	110	2091	19	273	37	80.1	2.8	120.1	6.5	3.24	0.29
BOP1A - 29	6.747	0.13	0.3813	0.0068	0.36871	0.1281	0.0016	0.17894	0.104	0.0061	2076	17	2082	32	1999	110	2066	22	147.2	5.7	67.6	2.3	68.2	2.2	2.17	0.02
BOP1A - 30	6.846	0.13	0.3875	0.0067	0.39073	0.1278	0.0014	0.23665	0.1078	0.0062	2091	17	2111	32	2068	110	2063	20	156.4	4.3	124	4	129.7	3.4	1.272	0.011
BOP1A - 31	6.704	0.13	0.3799	0.0068	0.40688	0.1278	0.0015	0.26002	0.1057	0.0061	2073	17	2075	32	2031	110	2062	20	180.5	4.7	125.6	2.9	129.6	2.7	1.44	0.015
BOP1A - 32	6.728	0.13	0.3835	0.0067	0.43676	0.127	0.0014	0.20627	0.1097	0.0063	2074	16	2092	31	2104	120	2055	19	156.7	4.4	111.1	3.6	118	3.3	1.42	0.011
BOP1A - 33	6.846	0.13	0.387	0.0068	0.2491	0.128	0.0015	0.34127	0.1115	0.0064	2090	17	2109	32	2136	120	2066	21	164.3	5.6	107.2	3.7	116.1	3.6	1.538	0.01
BOP1A - 34	6.898	0.13	0.391	0.0068	0.35283	0.1281	0.0015	0.23011	0.109	0.0063	2098	17	2127	32	2091	110	2066	21	157.6	4.8	117.3	4.5	123.3	3.9	1.361	0.014
BOP1A - 35	6.909	0.13	0.3915	0.0068	0.32367	0.1282	0.0015	0.24829	0.1097	0.0064	2099	17	2129	32	2103	120	2069	21	159.3	3.7	95.9	2.8	101.6	2.3	1.674	0.016
BOP1A - 36	7.056	0.13	0.4017	0.0071	0.29757	0.1278	0.0015	0.33037	0.1152	0.0068	2118	17	2176	32	2203	120	2062	21	131.9	4.5	75.5	3	83	2.7	1.768	0.018
BOP1A - 37	9.29	0.22	0.4238	0.0082	0.68865	0.1599	0.0023	-0.09408	0.2211	0.016	2362	21	2276	37	4020	250	2450	25	126	6.2	75.2	4.2	155.3	6.3	1.699	0.018
BOP1A - 38	6.796	0.12	0.3891	0.0068	0.19544	0.1282	0.0014	0.43247	0.1085	0.0063	2083.6	16	2118	32	2081	110	2069	19	168.2	6.3	134	5.7	138.3	4.7	1.267	0.01
BOP1A - 41	6.85	0.15	0.3889	0.0073	0.30959	0.1291	0.0021	0.26558	0.11	0.0063	2090	20	2117	34	2110	110	2081	29	257	11	128.2	6	142	4.8	2.36	0.22
BOP1A - 42	6.841	0.12	0.391	0.0068	0.39009	0.1277	0.0013	0.28891	0.1109	0.0063	2089.6	16	2127	32	2126	120	2063	17	171.8	1.8	121.5	1	128.8	1.8	1.413	0.017
BOP1A - 43	7.107	0.13	0.3974	0.0069	0.35649	0.1305	0.0015	0.30678	0.1158	0.0068	2123	16	2157	32	2215	120	2100	20	131.5	3.5	87.8	2.1	96.1	1.7	1.494	0.012
BOP1A - 44	6.83	0.13	0.3876	0.0068	0.44605	0.1281	0.0015	0.17653	0.1107	0.0064	2088	17	2111	31	2122	120	2068	20	153.4	4.5	105.6	3.7	110	3.4	1.465	0.017
BOP1A - 45	7.045	0.13	0.3971	0.007	0.35389	0.1287	0.0015	0.29839	0.1153	0.0067	2115	17	2155	32	2205	120	2076	21	158.7	2.3	117.5	1.7	127.9	2.2	1.354	0.019
BOP1A - 46	6.931	0.12	0.3912	0.0067	0.39236	0.1284	0.0012	0.29186	0.1106	0.0064	2101.2	16	2128	31	2119	120	2073	16	174.8	6	108.9	3.8	112.7	3	1.607	0.011
BOP1A - 47	6.802	0.14	0.3857	0.007	0.35362	0.1272	0.0018	0.38209	0.1084	0.0065	2085	18	2102	33	2079	120	2055	25	199.3	3.4	153.1	2.3	156.5	1.8	1.299	0.011
BOP1A - 48	7.137	0.14	0.3872	0.0067	0.31084	0.1327	0.0016	0.27245	0.1222	0.0072	2127	17	2109	31	2329	130	2129	21	137.8	4.8	98.5	3.9	112	3.1	1.404	0.019
BOP1A - 49	6.501	0.13	0.3649	0.0065	0.60294	0.1282	0.0013	0.10118	0.1068	0.0062	2044	17	2005	31	2051	110	2069	18	229.7	8.7	175.8	7	174.6	5.4	1.308	0.01
BOP1A - 50	6.811	0.12	0.3854	0.0068	0.28753	0.1268	0.0014	0.28792	0.111	0.0064	2085.5	16	2101	32	2127	120	2052	19	182.1	5.8	98.9	3.2	102.5	3	1.84	0.013
BOP1A - 51	6.97	0.14	0.3937	0.0079	0.82955	0.1266	0.0011	0.10892	0.116	0.0068	2105	18	2139	36	2217	120	2051	15	324	18	156.5	8.9	167	7.5	2.067	0.013
BOP1A - 52	6.62	0.14	0.3743	0.0071	0.69157	0.1269	0.0014	0.089769	0.108	0.0063	2059	19	2049	34	2076	110	2052	19	171.8	7.8	104.3	2.8	106.2	2.7	1.64	0.033
BOP1A - 53	8.889	0.16	0.4232	0.0075	0.2591	0.1506	0.0016	0.44706	0.474	0.028	2325.2	16	2274	34	7820	380	2351	18	132.7	4.8	71.6	1.6	324	12	1.818	0.027
BOP1A - 54	6.884	0.13	0.386	0.0068	0.29622	0.1276	0.0014	0.38623	0.1118	0.0066	2095	16	2104	32	2140	120	2063	21	126.8	3.5	76.4	2.2	79.1	1.9	1.661	0.014
BOP1A - 55	6.836	0.13	0.3826	0.0067	0.33042	0.1276	0.0013	0.28422	0.1111	0.0064	2089	16	2088	31	2129	120	2063	19	147	5.3	98	4.1	101.2	4.1	1.511	0.014
BOP1A - 56	6.891	0.13	0.3856	0.0067	0.3469	0.1279	0.0014	0.22387	0.1141	0.0066	2097	17	2102	31	2183	120	2065	20	180.9	5.8	132.1	4.5	139.3	3.5	1.3699	0.0092
BOP1A - 57	6.736	0.13	0.3821	0.0067	0.52998	0.1262	0.0013	0.006347	0.1071	0.0061	2076	17	2086	31	2055	110	2042	18	197.7	4.1	154.9	2.9	154	2.6	1.2722	0.0095
BOP1A - 58	6.996	0.12	0.3934	0.0068	0.35294	0.1271	0.0011	0.30136	0.1148	0.0065	2109.8	15	2138	31	2196	120	2057	15	224.6	5.8	151.6	2.7	161.2	2.3	1.471	0.015
BOP1A - 59	6.65	0.16	0.3661	0.008	0.69966	0.1301	0.0018	0.11454	0.1217	0.0082	2062	21	2010	38	2317	150	2093	24	144.2	7.8	98.4	7.6	114.2	5.6	1.558	0.038
BOP1A - 60	6.761	0.13	0.3801	0.0067	0.12398	0.1279	0.0016	0.43392	0.1154	0.0069	2079	16	2077	31	2207	120	2063	23	147.2	5.5	95.6	4.4	100.8	3.8	1.557	0.018
BOP1A - 61	6.64	0.14	0.3745	0.0078	0.80782	0.1275	0.0012	0.080639	0.1069	0.0062	2065	18	2049	37	2055	110	2063	16	255	16	193	11	186.5	8.3	1.307	0.011
BOP1A - 62	6.965	0.12	0.3887	0.0067	0.56104	0.12902	0.00096	0.18214	0.1119	0.0064	2105.9	15	2117	31	2143	120	2084	13	321	14	168.8	6.4	172.9	5.1	1.88	0.016
BOP1A - 63	7.104	0.14	0.4014	0.0071	0.40837	0.1281	0.0015	0.28693	0.1178	0.0069	2123	17	2175	33	2249	120	2069	21	159	7.8	109.5	6.8	116.1	5.8	1.486	0.021
BOP1A - 64	6.679	0.13	0.3786	0.0067	0.31496	0.1279	0.0015	0.23453	0.1081	0.0062	2068	17	2069	31	2074	110	2067	21	153.2	2	95.8	1.4	95.3	1.6	1.595	0.013
BOP1A - 65	6.69	0.12	0.3811	0.0066	0.22005	0.1282	0.0014	0.31274	0.1093	0.0063	2069.7	16	2081	31	2095	110	2073	19	190.7	4.1	123	2.4	123.3	2.2	1.543	0.01
BOP1A - 66	6.948	0.12	0.3958	0.0069	0.42721	0.1285	0.0012	0.21671	0.1141	0.0065	2103.3	16	2149	32	2183	120	2074	17	210.5	3.6	124.3	1.5	130.2	1.7	1.68	0.014
BOP1A - 67	6.691	0.12	0.3837	0.0067	0.10396	0.1278	0.0015	0.42869	0.1101	0.0063	2069.7	16	2093	31	2114	110	2063	21	173.1	8.2	113.7	6.8	113.9	6.2	1.554	0.021
BOP1A - 68	6.681	0.12	0.3775	0.0066	0.2599	0.13	0.0015	0.3195	0.1086	0.0063	2068	16	2064	31	2083	110	2093	21	160.8	4.9	107.8	4.1	106.2	3.4	1.5	0.015
BOP1A - 69	6.838	0.11	0.3896	0.0066	0.55688	0.12961	0.00078	0.26638	0.1137	0.0065	2089.9	14	2121	30	2176	120	2091	11	486	17	247.3	8.3	255.3	6.3	1.947	0.011
BOP1A - 70	6.706	0.13	0.3849	0.0068	0.32808	0.1288	0.0016	0.28862	0.1138	0.0065	2074	17	2100	31	2177	120	2075	21	159.6	4.2	95.9	2.8	99.5	2.5	1.66	0.012
BOP1A - 71	6.52	0.14	0.3696	0.0067	0.049876	0.1291	0.0021	0.39472	0.1038	0.0063	2047	19	2027	32	1995	120	2087	31	154.4	3.4	94.3	2.1	92	2.2	1.63	0.011
BOP1A - 72	6.645	0.12	0.3769	0.0068	0.32299	0.1299	0.0015	0.31327	0.1132	0.0066	2064	16	2061	32	2168	120	2093	20	175.2	2.3	89	1.3	90.1	1.5	1.96	0.016
BOP1A - 73	26.5	2.5	0.691	0.04	0.99717	0.26	0.013	-0.98337	1.18	0.16	3210	110	3380	160	14600	1500	3152	94	135.6	3.7	85.2	2.3	884	93	1.582	0.012
BOP1A - 74	6.856	0.13	0.3915	0.0069	0.41642	0.1287	0.0014	0.21752	0.1142	0.0067	2091	17	2129	32	2184	120	2076	19	152.5	5.5	84	3.6	86.9	2.9	1.811	0.02
BOP1A - 75	19	1.5	0.601	0.028	0.99453	0.2154	0.0099	-0.97852	1.28	0.17	2905	96	3000	120	14900	1700	2865	84	302	12	128.9	7.6	1190	110	2.428	0.049
BOP1A - 77	6.93	0.12	0.39	0.0068	0.4051	0.1299	0.0013	0.22519	0.1134	0.0065	2101	16	2122	31	2171	120	2093	18	306.7	5.4	242.2	5.9	259.7	7.4	1.264	0.013
BOP1A - 78	6.8	0.12	0.3877	0.0066	0.27152	0.128	0.0012	0.31914	0.1142	0.0065	2084.6	15	2111.9	31	2186	120	2067	17	212.2	4.8	129.3	3.5	135.3	3	1.638	0.013
BOP1A - 79	7.112	0.13	0.4023	0.0071	0.53796	0.1286	0.0011	0.23805	0.1263	0.0072	2124	16	2179	33	2403	130	2077	16	285.8	3.1	184.3	4.5	215	5.5	1.565	0.032
BOP1A - 80	6.96	0.14	0.3905	0.0071	0.35836	0.1299	0.0017	0.26383	0.1151	0.0067	2105	18	2125	33	2201	120	2093	23	167.4	4.3	108.7	1.8	116.1	1.8	1.53	0.02
BOP1A - 81	6.837	0.13	0.391	0.0067	0.33938	0.127	0.0014	0.24156	0.1149	0.0067	2090	17	2127	31	2197	120	2051	20	185.5	5.9	128.1	4.1	135.4	3.5	1.441	0.011
BOP1A - 82	6.996	0.13	0.3963	0.0069	0.35457	0.128	0.0014	0.31906	0.1179	0.0068	2109	16	2151	32	2252	120	2066	20	168.6	4.8	105.3	2.8	114.8	2.7	1.588	0.013
BOP1A - 83	7.051	0.13	0.3968	0.007	0.55151	0.1286	0.0014	0.19046	0.1143	0.0067	2116	17	2154	32	2187	120	2075	19	146.2	5.4	82.7	3.4	86.7	2.8	1.772	0.015
BOP1A - 84	7.007	0.13	0.3821	0.0066	0.30937	0.1327	0.0015	0.25147	0.1292	0.0076	2110.7	16	2086	31	2454	140	2130	19	208	5.5	121.7	3.4	145.7	2.4	1.7	0.011

% conc4

	Ratios									Ages									Concentrations (calculated from 91500)								
Sample - ar	207Pb/235	Propagatec	206Pb/238	Propagatec	Error Corre	207Pb/206	Propagatec	Error Corre	208Pb/232	Propagatec	207Pb/235	Propagatec	206Pb/238	Propagatec	208Pb/232	Propagatec	207Pb/206	Propagatec	U (ppm)	Internal 2 S	Th (ppm)	Internal 2 S	Pb (ppm)	Internal 2 S	U/Th	Internal 2 SE	
CLIB01 - 1	7.161	0.077	0.391	0.0056	0.27193	0.1328	0.0014	0.36332	0.1219	0.0042	2130.1	9.6	2127	26	2324	75	2132	19	180	4.2	63.6	1.6	74.1	2.2	2.832	0.024	
CLIB01 - 2	7.467	0.075	0.4027	0.0064	0.39087	0.1347	0.0014	0.49674	0.1363	0.0046	2167.7	9	2181	29	2582	81	2156	19	221.7	3.9	96.7	1.1	126.4	2.2	2.284	0.024	
CLIB01 - 3	6.81	0.1	0.3764	0.0063	0.55316	0.1308	0.0016	0.20052	0.1137	0.0042	2085	13	2059	30	2175	76	2106	22	145.6	7.5	63.6	3.6	67.3	2.8	2.308	0.023	
CLIB01 - 4	4.56	0.19	0.1804	0.0058	0.96019	0.1845	0.0035	-0.74815	0.1553	0.0099	1742	39	1067	31	2900	170	2689	32	503	27	261	14	372	16	1.934	0.012	
CLIB01 - 5	3.32	0.14	0.1857	0.0087	0.95649	0.1301	0.0015	0.17863	0.0658	0.0029	1467	33	1093	46	1291	55	2094	21	367	26	194	12	116.2	3.8	1.852	0.02	
CLIB01 - 6	5.841	0.062	0.2639	0.0046	0.019479	0.1605	0.0025	0.74556	0.1502	0.0069	1951	9.1	1509	23	2822	120	2453	26	304.9	5.2	112.3	2.2	160	3.3	2.716	0.02	
CLIB01 - 7	6.19	0.18	0.2674	0.0092	0.8984	0.1704	0.0026	0.43427	0.1731	0.007	1996	25	1522	47	3223	120	2554	26	219.2	2.7	91.7	1.6	153.7	2.4	2.392	0.026	
CLIB01 - 8	7.138	0.099	0.3953	0.0067	0.60142	0.1305	0.0013	0.22647	0.1144	0.004	2126	12	2146	31	2187	71	2106	19	193.5	9.5	105.5	5	115	3.9	1.824	0.013	
CLIB01 - 9	6.861	0.071	0.3831	0.0054	0.40045	0.1295	0.0013	0.17934	0.1048	0.0036	2092.1	9.5	2090	25	2014	66	2087	18	183.3	6.5	77.4	3.1	78.6	2.8	2.379	0.019	
CLIB01 - 10	7.71	0.12	0.4145	0.0068	0.4385	0.1356	0.002	0.15172	0.1245	0.0048	2197	15	2234	31	2369	86	2163	26	70.2	2.2	37.8	1.3	45.6	1.2	1.863	0.023	
CLIB01 - 11	6.09	0.12	0.3303	0.0069	0.81672	0.1335	0.0016	0.001579	0.112	0.0042	1983	17	1838	33	2144	76	2140	21	194.6	3.5	67	1.3	74.3	2.1	2.915	0.032	
CLIB01 - 12	7.41	0.1	0.408	0.0061	0.17604	0.1318	0.0019	0.36529	0.1202	0.0049	2160	12	2205	28	2299	88	2114	25	108.3	3.8	47.7	1.7	55.5	1.2	2.271	0.021	
CLIB01 - 13	6.718	0.093	0.3717	0.0061	0.63678	0.1314	0.0013	0.1392	0.1017	0.0036	2076	12	2037	29	1956	66	2113	18	170.7	8	83.1	5.2	82.3	4.8	2.127	0.037	
CLIB01 - 14	7.43	0.11	0.4215	0.0071	0.22245	0.1277	0.0018	0.26358	0.1118	0.0044	2162	15	2267	32	2140	78	2058	23	67.2	2.2	26.4	1.6	29.5	2	2.611	0.079	
CLIB01 - 15	7.23	0.1	0.3969	0.0062	0.29931	0.1323	0.0019	0.33022	0.1103	0.004	2138	13	2154	28	2113	74	2120	25	117.9	5.5	77.4	3.9	82	3.3	1.541	0.019	
CLIB01 - 16	7.115	0.095	0.4034	0.0059	0.25693	0.1281	0.0016	0.26028	0.1069	0.0039	2124	12	2184	27	2051	71	2066	23	110.8	3.5	55.4	1.7	57.2	1.4	2.002	0.018	
CLIB01 - 17	6.37	0.13	0.3556	0.0081	0.90391	0.1296	0.0011	0.021057	0.103	0.004	2023	19	1959	39	1979	73	2092	14	296	16	128.3	7.4	123	4.3	2.327	0.019	
CLIB01 - 20	7.22	0.12	0.4061	0.0065	0.37762	0.1287	0.0018	0.24095	0.1128	0.0042	2136	14	2196	29	2159	76	2079	25	114.6	3.8	37.5	1.4	39.9	1.3	3.083	0.035	
CLIB01 - 22	4.15	0.13	0.0973	0.0021	0.81633	0.3077	0.0057	-0.42426	0.1568	0.0067	1654	26	598.3	13	2937	120	3498	30	477	34	228	13	320.1	9.7	2.064	0.051	
CLIB01 - 24	7.2	0.11	0.4069	0.0069	0.57499	0.1286	0.0017	0.23461	0.1156	0.0043	2134	13	2200	32	2209	77	2073	23	120.9	5.3	56.3	2.6	59.3	2.1	2.157	0.018	
CLIB01 - 25	5.84	0.12	0.324	0.0073	0.86754	0.1304	0.0012	0.14801	0.0998	0.004	1948	18	1807	35	1920	74	2104	17	290	14	170.4	8.6	150.3	3.8	1.71	0.013	
CLIB01 - 26	6.84	0.12	0.3784	0.007	0.82933	0.131	0.0012	0.037313	0.1165	0.0042	2088	15	2067	33	2226	77	2109	16	234.1	9.3	107.3	4.2	112.8	2.8	2.183	0.014	
CLIB01 - 30	5.51	0.11	0.3027	0.0057	0.61965	0.132	0.002	0.15369	0.1017	0.0037	1897	16	1703	27	1956	67	2116	27	118.7	4.8	65.2	2.9	60.4	2.7	1.858	0.039	
CLIB01 - 31	5.81	0.19	0.3205	0.01	0.95078	0.1314	0.0012	-0.06873	0.0977	0.0041	1935	28	1787	50	1881	75	2114	16	328	25	191	19	152.3	9.8	1.868	0.05	
CLIB01 - 32	4.931	0.087	0.2769	0.0057	0.8412	0.1291	0.0012	0.10854	0.0874	0.0028	1806	15	1574	29	1693	53	2082	17	333.6	6.6	162.5	4.2	129.1	3.4	2.068	0.019	
CLIB01 - 33	4.92	0.059	0.2589	0.0044	0.6243	0.1379	0.0013	0.3975	0.0802	0.0027	1804.1	9.7	1483	23	1559	50	2198	17	639	42	412	22	300	16	1.527	0.019	
CLIB01 - 34	6.895	0.081	0.3877	0.0055	0.49259	0.1287	0.0013	0.096526	0.1119	0.0037	2096	10	2112	25	2143	67	2079	17	211.2	4	122.4	3.6	124.4	3.1	1.751	0.025	
CLIB01 - 35	7.22	0.11	0.4036	0.0066	0.53409	0.1298	0.0017	0.18537	0.1167	0.0042	2136	14	2185	30	2230	78	2089	23	136.3	6	63.9	2.8	66.8	2.3	2.142	0.019	
CLIB01 - 36	3.278	0.048	0.1823	0.0029	0.59847	0.1303	0.0016	0.056694	0.0601	0.0021	1474	11	1079.4	16	1182	39	2099	21	422	18	290	13	159.7	7.5	1.4572	0.0094	
CLIB01 - 38	6.1	0.15	0.3144	0.0087	0.87915	0.1412	0.0016	0.46122	0.126	0.0051	1984	21	1758	43	2394	92	2238	20	264	19	114	12	121.3	7.9	2.504	0.059	
CLIB01 - 39	7.254	0.096	0.4059	0.0062	0.33251	0.1296	0.0017	0.31093	0.1156	0.0041	2142	12	2197	28	2209	75	2089	23	133.3	5.2	61.4	2.4	65.5	2.2	2.175	0.02	
CLIB01 - 41	7.201	0.073	0.4	0.0058	0.48579	0.1306	0.0012	0.30215	0.1194	0.004	2135.3	8.8	2168	27	2279	72	2104	16	240.7	8.6	117.9	3.9	130.8	3.5	2.037	0.015	
CLIB01 - 42	6.28	0.18	0.3449	0.0089	0.90937	0.1312	0.0016	-0.33196	0.1103	0.0045	2004	25	1907	43	2113	82	2109	21	247	4.6	118	2.2	123	3.9	2.115	0.051	
CLIB01 - 43	8.31	0.11	0.4484	0.0073	0.70209	0.1342	0.0012	0.07475	0.1369	0.0047	2263	12	2387	32	2592	83	2153	16	262.6	2.7	118.1	1.8	152	3.7	2.24	0.027	
CLIB01 - 44	4.189	0.077	0.2099	0.0052	0.70202	0.1454	0.0022	0.48294	0.0779	0.0028	1668	15	1227	27	1516	52	2285	25	339	17	272	15	201	12	1.265	0.012	
CLIB01 - 45	7.21	0.13	0.405	0.0068	0.60906	0.1293	0.0018	0.022877	0.1162	0.0045	2133	16	2191	31	2219	83	2081	25	119.3	4.8	53.4	2.2	57.1	1.6	2.244	0.023	
CLIB01 - 46	20.3	2.2	0.686	0.047	0.98456	0.1973	0.0083	-0.87395	0.81	0.12	2930	100	3290	170	10800	1200	2740	72	66.7	6.4	27.3	3.2	139	14	2.634	0.064	
CLIB01 - 47	7.12	0.1	0.3576	0.0075	0.6981	0.1447	0.0018	0.56796	0.1421	0.0049	2124	12	1968	36	2685	86	2282	22	206.2	3.2	127.4	2.1	172.3	2.4	1.619	0.017	
CLIB01 - 48	2.356	0.075	0.0811	0.0015	0.21127	0.2117	0.0076	0.53143	0.0727	0.0039	1221	22	502.7	8.9	1415	74	2874	61	369	35	240	23	183	23	1.537	0.014	
CLIB01 - 49	5.74	0.17	0.3165	0.0088	0.91356	0.1314	0.0014	-0.10235	0.1119	0.0037	1926	24	1768	43	2144	67	2112	19	253	12	115.4	2.7	124.6	2.2	2.154	0.066	
CLIB01 - 50	6.628	0.081	0.3717	0.0053	0.23981	0.1293	0.0016	0.29178	0.1049	0.0035	2061	11	2037	25	2019	65	2083	22	178.9	4.4	89.3	2.3	90.4	2.2	2.005	0.015	
CLIB01 - 51	5.92	0.15	0.322	0.0088	0.88314	0.1336	0.0015	0.30223	0.1123	0.0044	1957	22	1796	44	2149	80	2142	20	212	16	101.4	8.7	102.8	5.9	2.155	0.029	
CLIB01 - 53	6.19	0.15	0.2917	0.0073	0.67203	0.1544	0.0028	0.29358	0.1712	0.0085	1996	21	1647	36	3180	150	2384	30	166.8	5.6	69.7	2.1	112.9	2.7	2.389	0.027	
CLIB01 - 54	6.624	0.076	0.3756	0.0053	0.37552	0.1277	0.0014	0.2522	0.1038	0.0034	2061	10	2055	25	1999	62	2062	20	174	2.3	113.2	1.6	115.6	1.8	1.5314	0.0097	
CLIB01 - 55	7.07	0.13	0.3942	0.0063	0.10311	0.1304	0.0025	0.4369	0.1155	0.0045	2117	15	2141	29	2207	83	2090	34	68.2	2	35.2	1.3	39.5	1.2	1.957	0.029	
CLIB01 - 56	3.421	0.091	0.0953	0.0047	0.9203	0.2703	0.006	0.80307	0.0995	0.0047	1509	21	585	28	1914	85	3292	36	686	11	464.3	7.7	457	12	1.485	0.027	
CLIB01 - 57	7.11	0.11	0.3915	0.007	0.66173	0.1317	0.0015	0.2287	0.1241	0.0045	2122	14	2128	32	2363	80	2116	20	172.8	6.9	87	3.1	105	2.3	1.973	0.019	
CLIB01 - 58	2.14	0.13	0.0953	0.0042	0.73028	0.1636	0.0055	0.13206	0.0583	0.0063	1139	37	585	25	1130	120	2450	61	618	18	359	34	176	12	2.23	0.18	
CLIB01 - 59	5.53	0.096	0.308	0.0056	0.78889	0.1301	0.0013	-0.04157	0.0983	0.0039	1902	15	1730	28	1893	72	2095	18	312	16	137.4	6.7	129.1	3.7	2.262	0.017	
CLIB01 - 60	6.723	0.091	0.3683	0.0059	0.63021	0.1323	0.0013	0.15997	0.1133	0.0043	2073	12	2021	28	2166	78	2127	17	273.7	9.7	114.5	5.4	125	3.4	2.426	0.03	
CLIB01 - 61	6.865	0.093	0.3786	0.0054	0.55986	0.1318	0.0014	-0.03889	0.112	0.0045	2092	12	2070	25	2151	83	2120	20	210.9	4.8	103	2	115	2.5	2.039	0.016	
CLIB01 - 62	7.59	0.11	0.4188	0.0065	0.48879	0.1315	0.0016	0.16334	0.1231	0.0046	2181	13	2254	29	2345	83	2112	22	138	2.5	57.2	1.1	69.6	1.2	2.412	0.023	
CLIB01 - 63	4.67	0.17	0.23	0.011	0.51406	0.1509	0.0045	0.44438	0.1103	0.0078	1748	29	1328	56	2100	140	2328	48	304	27	196	22	170	13	1.86	0.11	
CLIB01 - 64	10.91	0.93	0.351	0.018	0.93807	0.2269	0.0097	-0.40077	0.476	0.052	2479	73	1932	85	7850	730	2967	72	346	25	102.7	3.3	505	51	3.23	0.13	
CLIB01 - 65	4.308	0.095	0.2179	0.0056	0.86617	0.1436	0.0016	0.38312	0.1049	0.0036	1689	18	1269	30	2016	65	2268	19	351	19	134.1	6.9	137.4	5.6	2.609	0.02	
CLIB01 - 66	7.71	0.15	0.3835	0.0056	0.41967	0.1457	0.0025	-0.05236	0.1551	0.0083	2193	18	2092	26	2900	150	2285	31	157.1	3.9	78.8	2.1	116.9	3.2	1.994	0.017	
CLIB01 - 67	7.552	0.099	0.3937	0.006	0.42896	0.1391	0.0016	0.25267	0.1363	0.0051	2177	12	2139	27	2580	90	2214	20	125.1	4.5	57.8	2	76.7	1.9	2.157	0.021	
CLIB01 - 68	6.834	0.057	0.3831	0.0054	0.39092	0.1293	0.001	0.36045	0.1099	0.0036	2089.2	7.2	2091	25	2108	65	2085	14	295.9	8.6	131.2	3.6	141.6	3.3	2.247	0.014	
CLIB01 - 69	3.189	0.036	0.1439	0.0022	0.30031	0.1608	0.0019	0.36178	0.0897	0.0031	1453	8.7	866.7	12	1735	58	2459	20	586	26	260	12	230	12	2.259	0.019	
CLIB01 - 70	6.21	0.13	0.3498	0.008	0.91085	0.1287	0.0011	0.067516	0.0996	0.0038	2000	19	1931	38	1916	70	2077	15	286	17	145.8	8.6	135.5	5.3	1.97	0.016	
CLIB01 - 71	3.291	0.065	0.1927	0.0041	0.80658	0.1239	0.0013	0.11298	0.0644	0.0025	1475	15	1135	22	1260	47	2011	19	480	27	183	11	109.7	3.7	2.628	0.02	
CLIB01 - 72	6.9	0.1	0.3886	0.0057	0.32807	0.1287	0.0017	0.17624	0.1139	0.0039	2096	13	2116	26	2179	71	2074	24	126.1	4.6	58.3	2	64	1.8	2.156	0.023	
CLIB01 - 73	3.524	0.054	0.1798	0.0033	0.39874	0.1425	0.002	0.45867	0.0964	0.0033	1530	12	1066	18	1859	60	2250	26	253	14	117.7	4.8	108.4	4.2	2.115	0.035	
CLIB01 - 74	9.37	0.32	0.39	0.0066	0.74851	0.1732	0.0045	-0.52654	0.326	0.023	2358	32	2122	31	5610	350	2564	45	137.3	5.8	53.6	2.7	151.9	7.3	2.599	0.033	
CLIB01 - 75	7.19	0.13	0.408	0.0065	0.26109	0.1278	0.0023	0.25181	0.1125	0.0039	2131	17	2207	29	2154	71	2054	33	62.4	1.8	48.2	1.5	51.6	1.5	1.298	0.014	
CLIB01 - 76	3.643	0.063	0.2041	0.0043	0.80135	0.1299	0.0014	0.25997	0.0704	0.0029	1557	14	1196	23	1373	55	2092	19	373	20	205	19	126.8	6.5	1.972	0.049	
CLIB01 - 77	1.281	0.03	0.04731	0.00086	0.2073	0.1966	0.0046	0.30053	0.03356	0.0013	834	13	298	5.3	667	27	2790	40	762	53	747	57	228	13	1.035	0.011	
CLIB01 - 78	5.738	0.097	0.3214	0.0056	0.57612	0.1295	0.0018	0.12278	0.1021	0.0038	1933	15	1796	27	1964	69	2084	25	168	6.3	70.2	2.4	67.5	2.1	2.387	0.025	
CLIB01 - 79	4.8	0.11	0.2491	0.0066	0.82031	0.1401	0.0019	0.32277	0.1041	0.0043	1778	19	1431	34	1999	78	2222	23	326	18	141.4	8.2	132.2	3.6	2.322	0.02	
CLIB01 - 80	2.778	0.089	0.1055	0.0044	0.87132	0.1938	0.0037	0.50776	0.0809	0.0046	1343	23	645	26	1568	85	2762	31	812	12	454	14	333	8.9	1.843	0.064	
CLIB01 - 81	6.157	0.079	0.3468	0.0059	0.67672	0.1291	0.0011	0.29608	0.107	0.0036	1996	11	1918	28	2054	66	2082	16	236	12	112.3	6.9	110.1	5	2.141	0.025	
CLIB01 - 82	4.258	0.059	0.2425	0.004	0.59504	0.1272	0.0014	0.22198	0.0703	0.0024	1683	11	1399	21	1376	45	2057	20	287	11	181.7	6.3	120	3.9	1.573	0.015	
CLIB01 - 83	6.09	0.078	0.2642	0.0055	0.58309	0.1677	0.0022	0.68215	0.1674	0.006	1987	11	1510	28	3124	100	2532	23	452	18	186.6	9.5	287	11	2.464	0.03	
CLIB01 - 84	7.09	0.097	0.3901	0.0066	0.60783	0.1319	0.0014	0.22789	0.1332	0.0046	2120	12	2122	30	2525	81	2119	19	212	14	81	5.5	98.1	5.4	2.647	0.029	
CLIB01 - 85	6.366	0.098	0.3465	0.006	0.46268	0.1337	0.0018	0.35627	0.1197	0.004	2026	13	1917	29	2285	72	2140	24	164.8	7.7	77.1	3.7	84.1	3.3	2.143	0.018	
CLIB01 - 86	5.36	0.22	0.1964	0.0041	0.77578	0.1961	0.0059	-0.53491	0.1256	0.0075	1856	37	1155	22	2380	140	2758	54	395	17	249	11	265.9	8	1.585	0.011	
CLIB01 - 87	6.75	0.12	0.3808	0.0086	0.92656	0.1288	0.00087	0.19137	0.1107	0.0038	2075	16	2077	40	2121	70	2080	12	635	40	318	18	326	20	1.978	0.017	
CLIB01 - 88	7.083	0.082	0.395	0.0057	0.40005	0.1301	0.0013	0.25502	0.119	0.0038	2121	10	2146	26	2271	68	2097	19	204.1	6.8	97.2	3.1	104.9	3.1	2.102	0.015	

CLIB01 - 89	5.48	0.14	0.2921	0.0085	0.83642	0.1363	0.002	0.25526	0.1105	0.004	1888	23	1648	42	2117	72	2175	27	149.3	6.2	77.2	3.1	76	2.5	1.939	0.037
CLIB01 - 90	2.838	0.058	0.1514	0.0041	0.86624	0.1365	0.0016	0.57207	0.0732	0.0023	1362	16	908	23	1428	44	2178	21	470	32	185	11	121.8	7.6	2.518	0.025
CLIB01 - 91	6.23	0.18	0.3241	0.0068	0.90309	0.1389	0.002	-0.57257	0.1158	0.0066	2001	25	1808	33	2200	120	2206	25	317	12	184	7.5	177.9	3.7	1.736	0.014
CLIB01 - 92	3.77	0.35	0.1247	0.0081	0.99516	0.2179	0.0056	-0.85757	0.143	0.018	1556	60	753	44	2680	300	2950	39	832	44	377	22	508	87	2.231	0.022
CLIB01 - 93	1.084	0.023	0.06523	0.0011	0.49365	0.1205	0.0022	0.059487	0.02916	0.0011	743	11	407.3	6.8	581	21	1951	33	554	36	408	26	106.9	7.1	1.3582	0.0093
CLIB01 - 94	8.06	0.17	0.4276	0.0077	0.76996	0.1362	0.0019	-0.12656	0.1551	0.0071	2232	18	2293	35	2910	120	2172	24	112.1	2.2	59.3	1.6	83.8	4	1.909	0.028
CLIB01 - 96	4.94	0.15	0.236	0.012	0.88355	0.1575	0.0039	0.84761	0.1125	0.0042	1801	26	1358	60	2153	76	2408	42	258	35	129	17	127	16	1.961	0.025
CLIB01 - 97	4.15	0.055	0.2316	0.0042	0.7372	0.1301	0.0012	0.26639	0.0806	0.0025	1662	11	1342	22	1566	46	2098	16	461	19	219.5	8.8	158.2	5.4	2.099	0.014
CLIB01 - 98	9.5	0.15	0.4258	0.0071	0.72164	0.1614	0.0017	-0.05288	0.2489	0.0098	2384	15	2286	32	4480	160	2469	18	203.1	9	84.9	3.8	191.6	9.6	2.395	0.017
CLIB01 - 99	7.24	0.1	0.4075	0.0064	0.45324	0.1292	0.0017	0.23774	0.1191	0.004	2140	13	2202	29	2274	72	2080	24	106.5	3.3	46.7	1.5	50.4	1.4	2.285	0.021
CLIB01 - 10	7.16	0.11	0.4013	0.0067	0.46324	0.1291	0.0019	0.27676	0.1217	0.0042	2128	14	2176	31	2326	76	2081	26	73.7	2.6	56	2.1	61.4	1.7	1.321	0.015
CLIB01 - 10	4.26	0.14	0.1454	0.0052	0.89535	0.2137	0.0029	0.28923	0.2077	0.01	1673	28	873	29	3800	170	2930	22	304	26	106	10	179.2	8.9	2.942	0.036
CLIB01 - 10	6.42	0.12	0.3586	0.007	0.68951	0.1297	0.0017	0.12268	0.1129	0.0044	2030	17	1974	33	2160	79	2089	24	117	5.8	43.5	2.2	44.1	1.5	2.694	0.03
CLIB01 - 10	3.276	0.073	0.0917	0.0025	0.18455	0.2669	0.0091	0.74821	0.1082	0.0046	1473	17	565	15	2073	84	3250	55	877	34	525	21	511.3	9.2	1.668	0.014
CLIB01 - 10	5.77	0.15	0.2842	0.0085	0.93156	0.1474	0.0014	0.18669	0.1057	0.0042	1939	22	1609	43	2029	77	2313	17	371	24	229	17	221	12	1.672	0.016
CLIB01 - 10	6.761	0.067	0.3744	0.0056	0.39451	0.1309	0.0012	0.3773	0.1172	0.0041	2079.3	8.8	2050	26	2238	74	2107	16	250.5	5.4	98.6	2.7	108.7	1.9	2.543	0.026

	Ratios								Ages						Concentrations (calculated from 91500)									
Sample - ar	207Pb/235	Propagatec	206Pb/238	Propagatec	Error Corre	207Pb/206	Propagatec	Error Corre	208Pb/232	Propagatec	207Pb/235	Propagatec	206Pb/238	Propagatec	208Pb/232	Propagatec	207Pb/206	Propagatec	U (ppm)	Internal 2 S	Th (ppm)	Internal 2 S	Pb (ppm)	Internal 2 S	U/Th	Internal 2 SE
CLIB5_80 -	2.82	0.19	0.0714	0.0042	0.97982	0.2847	0.0046	-0.71018	0.1501	0.011	1346	49	444	25	2820	200	3385	25	1723	77	921	42	1280	46	1.865	0.03
CLIB5_35 -	2.223	0.17	0.0896	0.0055	0.73063	0.1772	0.0041	-0.2371	0.0966	0.012	1185	46	553	32	1850	220	2613	37	622	42	260	12	275	28	2.255	0.08
CLIB5_48 -	2.104	0.11	0.1289	0.0065	0.83909	0.1193	0.0021	-0.15397	0.0486	0.0036	1147	37	781	37	957	69	1943	31	630	28	228	10	104.7	4.7	2.693	0.035
CLIB5_71 -	2.929	0.16	0.1476	0.0079	0.87144	0.1465	0.0025	0.10138	0.0888	0.0057	1381	42	886	45	1724	110	2299	29	667	30	347	13	280	13	1.897	0.031
CLIB5_51 -	4.99	0.29	0.1502	0.0071	0.58252	0.2396	0.0078	-0.20166	0.901	0.11	1800	52	902	40	12000	1300	3084	56	709	11	131	12	779	44	6.96	0.52
CLIB5_56 -	2.738	0.13	0.1513	0.0072	0.77691	0.131	0.002	-0.05765	0.0731	0.0049	1337	37	909	41	1425	92	2111	28	471	25	165.8	9.3	109.4	3	2.836	0.039
CLIB5_32 -	2.637	0.13	0.1551	0.0071	0.70794	0.1219	0.0017	0.15724	0.05443	0.0032	1310.8	35	929.3	40	1071	62	1982	24	695	29	253	10	136.2	4.6	2.742	0.028
CLIB5_30 -	2.79	0.14	0.159	0.0078	0.88451	0.1271	0.0019	-0.03804	0.0549	0.0032	1349	37	950	43	1080	62	2054	26	504	12	262.7	6.8	139.7	3.7	1.948	0.02
CLIB5_60 -	7.99	0.38	0.1615	0.0078	0.90874	0.3592	0.0044	0.27419	0.443	0.026	2226	44	965	43	7405	370	3745.1	18	865	37	390	15	1580	63	2.194	0.025
CLIB5_3 -	3.204	0.16	0.169	0.0083	0.69945	0.1372	0.0023	0.62872	0.0867	0.0055	1456	37	1006	46	1679	100	2189	28	459	15	179.1	6	159.5	4.2	2.654	0.022
CLIB5_41 -	3.006	0.26	0.1742	0.014	0.7666	0.1254	0.0018	0.027024	0.062	0.005	1407	52	1035	73	1215	93	2030	25	362	11	164.6	5.7	99.4	3.1	2.125	0.039
CLIB5_8 - 1	2.994	0.14	0.175	0.0081	0.86597	0.12513	0.0016	0.073651	0.0597	0.0034	1404	36	1039	45	1172	65	2029	23	736	35	319	14	179.1	6.1	2.389	0.02
CLIB5_70 -	3.161	0.17	0.1796	0.0093	0.89984	0.1295	0.002	0.16418	0.0766	0.0051	1441	39	1063	51	1490	95	2087	27	889	42	400	23	257.3	5.8	2.257	0.045
CLIB5_49 -	3.389	0.16	0.1912	0.0089	0.8921	0.1284	0.0019	0.10739	0.0564	0.0035	1500	37	1127	48	1108	67	2074	24	1089	44	1080	40	601	30	0.984	0.014
CLIB5_82 -	3.261	0.16	0.1912	0.0091	0.85068	0.1247	0.0018	-0.08744	0.0686	0.0041	1468	39	1127	49	1340	77	2021	25	534	19	189.5	6.3	119.3	4.2	2.794	0.048
CLIB5_11 -	6.17	0.31	0.1933	0.0092	0.88758	0.2304	0.0033	-0.29876	0.389	0.024	1994	44	1139	50	6610	350	3054	23	431	21	153.4	8	550	23	2.938	0.032
CLIB5_59 -	3.568	0.2	0.2035	0.012	0.69061	0.1269	0.003	0.23382	0.0633	0.0071	1540	53	1194	67	1241	130	2051	37	325.7	7	138.2	3.6	83.3	2	2.353	0.053
CLIB5_61 -	5.543	0.27	0.2136	0.011	0.67664	0.1882	0.0042	0.26157	0.2668	0.018	1905	46	1247	59	4776	290	2723	33	409.7	8.7	145.3	2.9	358.6	6.6	2.818	0.048
CLIB5_75 -	5	0.24	0.2293	0.012	0.59732	0.1596	0.0074	0.11	0.141	0.021	1815	45	1330	66	2660	270	2442	66	269	13	109.1	6.3	147.3	9.2	2.481	0.062
CLIB5_68 -	4.061	0.21	0.233	0.012	0.75039	0.1276	0.0016	0.19101	0.0854	0.0053	1645	47	1350	63	1657	99	2064	23	917	24	709	14	567	11	1.287	0.038
CLIB5_50 -	4.51	0.21	0.2533	0.012	0.81532	0.1292	0.0017	0.076472	0.0767	0.0049	1730	40	1455	61	1492	91	2085	23	558	25	337	16	245.1	9.1	1.642	0.022
CLIB5_28 -	5.026	0.25	0.2541	0.012	0.64162	0.1445	0.0027	-0.10577	0.1506	0.011	1825	44	1459	62	2830	180	2281	33	372.8	8.8	123.1	4.1	178	12	3.118	0.062
CLIB5_52 -	4.675	0.22	0.2608	0.012	0.83726	0.1295	0.0017	0.073543	0.0892	0.0057	1760	40	1493	63	1726	110	2088	24	413	18	149.3	6.5	126.8	3.6	2.729	0.037
CLIB5_25 -	7.33	0.38	0.2711	0.013	0.40802	0.1978	0.0043	0.11597	0.787	0.057	2149	54	1546	67	11630	720	2799	38	494	18	90.2	2.7	670	42	5.571	0.087
CLIB5_15 -	4.92	0.23	0.2762	0.013	0.72245	0.1279	0.0018	0.010314	0.0823	0.005	1803	40	1572	64	1597	92	2068	25	362.8	8.1	132.7	2.6	108.4	1.9	2.83	0.028
CLIB5_72 -	5.289	0.25	0.2803	0.013	0.67788	0.1391	0.002	0.23121	0.1275	0.0076	1865	41	1592	66	2431	140	2212	24	401	18	176.5	8.5	201	9.2	2.279	0.031
CLIB5_5 -	5.075	0.24	0.285	0.013	0.78548	0.1294	0.0018	0.11661	0.0935	0.0059	1829	40	1616	66	1805	110	2087	25	233	11	114.2	6.5	101.9	3.1	2.177	0.035
CLIB5_40 -	5.491	0.25	0.2961	0.014	0.65229	0.1348	0.0019	0.16986	0.1481	0.0089	1897	42	1672	68	2790	160	2157	25	283	9.1	77.6	2.3	111	3.4	3.511	0.066
CLIB5_65 -	7.99	0.44	0.308	0.014	0.024375	0.1878	0.0077	0.46427	0.349	0.025	2222	49	1730	72	6020	380	2716	57	415	10	135.2	7.8	436	41	3.2	0.11
CLIB5_12 -	6.088	0.29	0.3094	0.014	0.70005	0.142	0.0021	0.23562	0.1652	0.011	1986	42	1737	71	3080	190	2250	26	273	11	104.3	5	154.7	2.1	2.768	0.042
CLIB5_76 -	5.51	0.34	0.3141	0.019	0.79756	0.1281	0.0019	-0.20908	0.0998	0.0067	1900	60	1760	95	1922	130	2068	25	235.5	4.7	114.7	4.6	110.1	5.5	2.073	0.096
CLIB5_47 -	6.04	0.28	0.3193	0.016	0.67898	0.1376	0.0031	0.27749	0.1728	0.016	1979	48	1785	81	3220	260	2193	36	242.8	6.8	65.2	2.2	102.2	3.4	3.64	0.1
CLIB5_78 -	5.68	0.27	0.3276	0.015	0.83454	0.1263	0.0017	0.049517	0.1034	0.006	1925	45	1825	76	1988	110	2044	23	282	14	94.5	4	93.1	3.9	2.965	0.065
CLIB5_79 -	6.11	0.3	0.3412	0.016	0.84146	0.1306	0.002	-0.02635	0.1274	0.009	1988	43	1891	79	2420	160	2103	28	377	13	140.9	4.3	162.4	3.6	2.661	0.046
CLIB5_44 -	6.11	0.34	0.3428	0.019	0.84073	0.1296	0.002	0.055833	0.1059	0.0064	1988	64	1899	100	2033	120	2090	26	376	10	157.8	5.7	156.8	4.2	2.342	0.074
CLIB5_53 -	6.6	0.31	0.3499	0.016	0.67398	0.1361	0.002	0.24998	0.1528	0.0094	2059	43	1937	79	2871	160	2174	26	189.9	6.7	74.5	2.2	112.1	2.4	2.525	0.049
CLIB5_14 -	6.5	0.31	0.3519	0.016	0.49766	0.1332	0.0024	0.21615	0.1287	0.0081	2047	44	1943	78	2443	140	2136	31	83.8	2.1	28.83	0.65	35.35	0.85	3.025	0.049
CLIB5_74 -	6.37	0.31	0.3552	0.017	0.77153	0.1317	0.002	0.21448	0.1255	0.0075	2025	44	1958	84	2388	140	2116	27	220.5	5.4	100.6	2.8	116.8	3	2.21	0.063
CLIB5_67 -	6.76	0.33	0.3596	0.017	0.66392	0.1377	0.0022	0.20786	0.1524	0.01	2079	43	1979	80	2861	180	2194	29	254	14	86.7	2.1	115.8	2.8	2.87	0.12
CLIB5_77 -	6.53	0.32	0.3606	0.017	0.82873	0.1327	0.0019	0.085239	0.1437	0.0087	2047	43	1983	82	2713	150	2132	25	196.5	3.8	71.56	0.94	94.6	1.7	2.725	0.052
CLIB5_21 -	6.53	0.4	0.3647	0.022	0.7785	0.1308	0.0026	-0.05379	0.106	0.0083	2047	82	2003	110	2036	160	2105	36	214.4	4.6	76.8	2.7	77.7	3.1	2.89	0.099
CLIB5_31 -	6.64	0.31	0.3684	0.017	0.75096	0.1296	0.0017	0.16262	0.1056	0.0063	2063	42	2021	82	2029	110	2090	23	307.2	9.1	134.9	4	138.9	3.2	2.301	0.025
CLIB5_62 -	6.76	0.37	0.369	0.021	0.791	0.1317	0.0024	-0.15302	0.1228	0.0074	2076	59	2024	100	2341	130	2122	31	204.9	5	94.8	2.7	107.7	3.9	2.162	0.053
CLIB5_46 -	7.06	0.5	0.3719	0.019	0.67662	0.138	0.017	0.32907	0.1485	0.077	2117	52	2036	94	2810	970	2199	110	175	6.3	76.7	1.4	107.3	4.2	2.215	0.07
CLIB5_73 -	6.91	0.35	0.3723	0.018	0.56032	0.1362	0.0077	0.37613	0.1431	0.023	2097	45	2039	89	2700	370	2173	71	201.4	7.4	70.8	2.3	95.3	6.5	2.849	0.062
CLIB5_6 - 1	6.586	0.31	0.3724	0.017	0.58824	0.1284	0.0017	0.2496	0.1054	0.0062	2055.9	41	2040	81	2025	110	2073	24	248.4	6.3	124.5	3.6	129.5	2.9	2.089	0.029
CLIB5_20 -	6.66	0.31	0.3732	0.02	0.71277	0.1301	0.0048	0.018705	0.1077	0.014	2065	47	2044	100	2065	230	2095	56	109.4	4.7	48	2.2	51.8	2.3	2.356	0.047
CLIB5_4 -	6.707	0.32	0.374	0.017	0.59448	0.1296	0.0018	0.12177	0.1047	0.0063	2071	41	2048	81	2012	120	2089	25	136.5	7	67	5.1	70.1	4.2	2.214	0.046
CLIB5_69 -	6.61	0.31	0.3744	0.018	0.7691	0.1293	0.0018	0.24467	0.1149	0.0068	2059	42	2051	81	2197	120	2085	24	294	14	101.3	4.5	101.4	3.2	2.877	0.043
CLIB5_54 -	6.88	0.33	0.3754	0.018	0.71856	0.1322	0.0021	0.17672	0.131	0.0095	2092	43	2053	84	2485	160	2126	27	172.3	5.6	57.5	2.2	72.2	1.9	3.011	0.054
CLIB5_1 - 1	6.775	0.32	0.3763	0.017	0.55245	0.1298	0.0018	0.16567	0.1062	0.0066	2081	42	2058	82	2039	120	2092	25	145.7	2.8	79	1.2	87.3	1.5	1.891	0.022
CLIB5_9 - 1	6.764	0.32	0.3766	0.017	0.55521	0.1314	0.002	0.11712	0.1177	0.0067	2079	42	2060	82	2248	120	2113	26	165.6	5.9	112.6	3.2	124.2	2.3	1.522	0.017
CLIB5_37 -	6.89	0.35	0.3761	0.019	0.7266	0.1312	0.002	0.11709	0.1145	0.0068	2096	48	2060	91	2190	120	2109	27	170	10	95.8	5.3	108.3	5	1.739	0.031
CLIB5_18 -	6.78	0.32	0.3795	0.018	0.73977	0.1299	0.0018	0.026291	0.1076	0.0066	2080	43	2073	84	2064	120	2093	25	195.9	4.8	81.2	2.6	86.8	2.3	2.513	0.037
CLIB5_23 -	7	0.35	0.3959	0.019	0.91284	0.12943	0.0017	-0.0969	0.1091	0.0068	2110	45	2148	87	2091	120	2088	22	323	11	163.6	5.5	170.1	6.4	2.023	0.034
CLIB5_45 -	7.24	0.4	0.4027	0.023	0.80965	0.1304	0.002	0.12473	0.1297	0.0076	2139	72	2180	120	2464	140	2100	26	373	19	150.8	8.5	182.9	8	2.402	0.061
CLIB5_81 -	9.88	0.52	0.4444	0.021	0.82565	0.1613	0.0031	-0.34368	0.287	0.021	2413	51	2368	96	5070	330	2460	33	177.2	5	84.4	3.7	212.3	4.3	2.146	0.06

	Ratios								Ages								Concentrations (calculated from 91500)								
Sample - ar	207Pb/235	Propagatec	206Pb/238	Propagatec	Error Corre	207Pb/206	Propagatec	Error Corre	208Pb/232	Propagatec	207Pb/235	Propagatec	206Pb/238	Propagatec	208Pb/232	Propagatec	207Pb/206	Propagatec	U (ppm)	Internal 2 S	Th (ppm)	Internal 2 S	Pb (ppm)	Internal 2 S	U/Th	Internal 2 SE
CLIB7 - 1	5.86	0.29	0.3291	0.014	0.79388	0.1293	0.0017	0.017276	0.0976	0.0018	1952	48	1833	70	1882	32	2086	22	284.4	6.3	118.2	3.5	336	14	2.52	0.031
CLIB7 - 2	5.965	0.37	0.3282	0.02	0.59279	0.1313	0.0021	0.1846	0.1019	0.0037	1969	80	1829	100	1960	68	2115	27	261.5	9.7	122.1	4.9	361	12	2.203	0.022
CLIB7 - 3	6.194	0.3	0.3445	0.013	0.16488	0.13	0.0017	0.3767	0.1087	0.0017	2003.5	43	1908.2	64	2084	31	2094	23	290.7	6.3	131.6	2.6	406.4	5.6	2.265	0.022
CLIB7 - 4	4.13	0.23	0.219	0.01	0.56152	0.1359	0.0017	0.18064	0.0821	0.0019	1659	43	1276	54	1594	36	2175	23	459	15	204	6.4	503	27	2.28	0.022
CLIB7 - 5	6.872	0.33	0.3842	0.015	0.44984	0.129	0.0015	0.23145	0.1098	0.0015	2093.9	43	2095	68	2105	28	2083	19	274	10	128.3	4.5	405	11	2.158	0.017
CLIB7 - 6	6.649	0.32	0.3665	0.014	0.29094	0.131	0.0017	0.30604	0.1165	0.0017	2064	43	2012	65	2226	30	2110	24	196.9	9.6	133.9	6.8	448	17	1.491	0.02
CLIB7 - 7	6.801	0.33	0.3783	0.015	0.44261	0.1295	0.0014	0.14943	0.1094	0.0013	2084.7	44	2068	69	2098	24	2091	20	348.6	8.3	164.2	3.8	519.4	8.6	2.134	0.018
CLIB7 - 10	4.15	0.2	0.212	0.0083	0.74257	0.14134	0.0013	0.26225	0.07647	0.00095	1663.6	41	1239.3	45	1489	18	2242.7	16	1380	82	1274	86	2870	170	1.086	0.011
CLIB7 - 12	4.988	0.25	0.2748	0.011	0.79863	0.1312	0.0016	0.009777	0.0904	0.0018	1814	43	1564	55	1748	34	2111	21	321.5	8.9	159	3.9	428.2	7.9	1.992	0.036
CLIB7 - 13	6.589	0.32	0.3688	0.014	0.35998	0.1297	0.0016	0.38179	0.1121	0.0017	2058	43	2024	68	2146	31	2090	21	228.3	8.7	128	7.2	421	18	1.786	0.039
CLIB7 - 15	6.305	0.31	0.354	0.014	0.74864	0.1288	0.0015	0.095655	0.1042	0.002	2017	43	1953	66	2002	37	2081	20	317	14	205.4	9.8	634	20	1.506	0.014
CLIB7 - 16	6.439	0.31	0.3583	0.014	0.17277	0.1302	0.0015	0.13234	0.1144	0.0018	2036.3	42	1974	65	2189	33	2098	20	241.4	6.2	112.5	3.3	392.4	7.8	2.09	0.018
CLIB7 - 17	6.067	0.3	0.3414	0.014	0.61452	0.1289	0.0016	0.19483	0.1101	0.0015	1984	43	1893	65	2111	28	2079	22	262	6.6	132.1	4.9	442	15	1.948	0.029
CLIB7 - 19	6.73	0.33	0.3794	0.015	0.37724	0.1287	0.0017	0.3005	0.1081	0.0015	2075	44	2073	68	2075	27	2078	23	168.2	3.5	89.2	1.7	296.7	4.8	1.826	0.015
CLIB7 - 20	1.872	0.095	0.1182	0.0047	0.58773	0.115	0.0018	0.052832	0.04473	0.00074	1069	34	720.3	27	884	14	1873	29	494	21	194	8.3	267	10	2.472	0.019
CLIB7 - 21	4.105	0.2	0.2325	0.009	0.70711	0.1285	0.0017	-0.05196	0.0948	0.0035	1654	41	1347	47	1827	65	2073	23	360	14	112.1	4.1	317.3	5	3.116	0.029
CLIB7 - 22	6.511	0.32	0.3654	0.014	0.54048	0.1299	0.0016	0.21625	0.1123	0.0018	2046	45	2007	69	2150	34	2094	22	229	4.5	129	2.7	438.8	8.9	1.73	0.027
CLIB7 - 23	6.86	0.33	0.3869	0.015	0.578	0.1291	0.0016	0.15516	0.1172	0.0024	2093	44	2108	69	2238	44	2085	21	169.1	7.1	99.9	6	350	14	1.707	0.033
CLIB7 - 24	3.863	0.2	0.2119	0.0087	0.89428	0.1324	0.0015	-0.15087	0.096	0.0027	1602	41	1238	46	1852	50	2127	20	477	18	189.6	5.1	566	23	2.444	0.035
CLIB7 - 25	6.972	0.34	0.3915	0.015	0.47127	0.1296	0.0015	0.24819	0.1083	0.0015	2106.5	43	2129	70	2081	28	2091	21	181.1	5.7	100.9	4.3	334	12	1.795	0.03
CLIB7 - 26	2.46	0.12	0.1308	0.0055	0.60297	0.1381	0.0025	0.66815	0.0559	0.0015	1258	35	792	31	1099	28	2193	31	492	48	361	35	650	74	1.341	0.013
CLIB7 - 27	6.065	0.29	0.3442	0.013	0.51099	0.1283	0.0015	0.23739	0.1072	0.0013	1984	43	1907	65	2059	25	2072	21	309.2	3.5	205.8	2.2	671	13	1.484	0.016
CLIB7 - 28	7.154	0.35	0.3942	0.015	0.43229	0.132	0.0018	0.26634	0.1239	0.002	2129	44	2142	70	2361	36	2120	24	158.5	4.9	78.9	2.2	296.8	6.4	1.989	0.022
CLIB7 - 29	6.728	0.33	0.3763	0.015	0.55353	0.1303	0.0016	0.23895	0.1169	0.0029	2076	44	2058	68	2232	52	2098	22	243	6.5	118.5	3.3	417.5	7.3	2.05	0.021
CLIB7 - 30	7.67	0.41	0.3316	0.015	0.53784	0.1682	0.0033	0.43875	0.2967	0.015	2192	46	1845	70	5250	250	2537	37	233.8	4.1	82.7	1.5	764	14	2.83	0.048
CLIB7 - 31	3.059	0.15	0.1743	0.0072	0.8361	0.1275	0.0014	0.17122	0.0503	0.0012	1422	38	1035	39	992	24	2062	19	822	50	600	46	945	83	1.429	0.037
CLIB7 - 32	3.19	0.16	0.1776	0.0071	0.75559	0.1308	0.0016	0.1273	0.05334	0.00077	1452	39	1053	39	1050	15	2105	22	595	38	431	31	674	39	1.42	0.022
CLIB7 - 33	5.971	0.3	0.3262	0.014	0.43586	0.1336	0.0016	0.29885	0.1176	0.0039	1970	52	1820	72	2246	71	2142	22	274	12	142	12	487	35	2.037	0.07
CLIB7 - 34	4.93	0.26	0.2546	0.011	0.84515	0.1406	0.0019	-0.32084	0.1155	0.0049	1799	46	1461	55	2201	89	2230	25	392	19	148	5.8	527	37	2.625	0.036
CLIB7 - 35	4.815	0.24	0.2658	0.01	0.71708	0.1315	0.0015	0.21967	0.0914	0.0016	1787	40	1519	53	1767	29	2115	20	342	17	193	8.4	524	20	1.759	0.022
CLIB7 - 36	6.578	0.32	0.3632	0.014	0.6364	0.132	0.0016	0.47399	0.1195	0.0016	2054.8	43	1996	67	2281	30	2124	21	243.7	6.2	126.8	2.1	461	11	1.896	0.025
CLIB7 - 37	6.872	0.34	0.3846	0.015	0.61128	0.1296	0.0016	0.19045	0.1124	0.002	2094	43	2097	70	2151	37	2091	21	208.6	2.8	82.8	1	280.8	4.8	2.51	0.027
CLIB7 - 38	5.616	0.27	0.3066	0.012	0.76023	0.133	0.0016	0.27454	0.1263	0.0035	1917	43	1723	60	2403	63	2136	21	501	13	127.6	3.6	485	10	3.863	0.069
CLIB7 - 39	5.3	0.25	0.2943	0.012	0.33192	0.1309	0.0017	0.3283	0.1033	0.0022	1870	47	1663	63	1985	40	2112	22	225	7	99.1	3.6	322	14	2.214	0.038
CLIB7 - 40	2.938	0.17	0.1668	0.009	0.93761	0.1274	0.0014	-0.20622	0.04852	0.0015	1387	55	994	51	957	29	2060	20	1182	66	1041	61	1562	90	1.103	0.011
CLIB7 - 42	6.665	0.33	0.376	0.015	0.49984	0.129	0.0017	0.36026	0.1081	0.0016	2066	44	2057	69	2075	29	2080	23	210.5	5.5	102.4	2.8	333.8	8.2	2	0.021
CLIB7 - 43	6.91	0.35	0.3704	0.015	0.76714	0.1349	0.0017	0.054868	0.1351	0.0034	2097	45	2033	71	2558	61	2162	22	292	21	139	11	532	29	2.072	0.025
CLIB7 - 44	6.722	0.33	0.3719	0.014	0.53847	0.1309	0.0015	0.18072	0.115	0.0014	2074	43	2038	67	2200	26	2107	20	284.7	6.6	140.5	2.7	483.4	8.5	1.973	0.021
CLIB7 - 45	6.842	0.33	0.3833	0.015	0.52864	0.1292	0.0015	0.30324	0.1154	0.0017	2089.7	43	2091	69	2207	31	2086	21	254.2	7.2	121.5	3.3	415	8.1	2.06	0.023
CLIB7 - 46	6.255	0.31	0.344	0.014	0.82655	0.1318	0.0015	0.14938	0.0746	0.0013	2009	43	1904	66	1454	25	2119	20	320	18	266	14	584	27	1.186	0.024
CLIB7 - 48	6.531	0.32	0.3566	0.014	0.54732	0.1329	0.0017	0.26044	0.119	0.002	2048	48	1965	68	2272	37	2133	22	238	11	134.7	5.2	469	16	1.746	0.032
CLIB7 - 49	3.553	0.17	0.2046	0.0081	0.74393	0.1259	0.0014	0.04249	0.0834	0.0021	1539	41	1200	44	1617	38	2038	21	402	22	170.5	9.8	416	16	2.367	0.028
CLIB7 - 50	6.367	0.32	0.3531	0.014	0.59755	0.1308	0.0017	0.080057	0.1073	0.0016	2027	46	1949	69	2060	30	2107	22	180.3	4.5	107.3	2.7	338.7	7.1	1.686	0.021
CLIB7 - 51	6.934	0.34	0.3917	0.015	0.59791	0.1283	0.0016	0.2789	0.112	0.0015	2101	44	2130	71	2146	28	2071	22	258.5	5.5	122	2.8	404.7	7.2	2.125	0.021
CLIB7 - 52	4.607	0.24	0.2355	0.01	0.83738	0.1418	0.002	0.10392	0.1134	0.0036	1745	44	1362	53	2168	65	2244	24	414	18	182	11	577	32	2.374	0.057
CLIB7 - 53	6.68	0.33	0.347	0.014	0.68237	0.1398	0.0017	0.02945	0.1672	0.004	2067	47	1920	68	3121	70	2221	21	214.9	7.1	90.4	3.4	450.5	8.2	2.404	0.037
CLIB7 - 54	6.794	0.34	0.3835	0.015	0.66195	0.1285	0.0016	0.086907	0.1101	0.0019	2083	44	2092	70	2110	34	2074	22	169.4	4.2	90.2	2.3	295.1	6.4	1.888	0.023
CLIB7 - 56	5.767	0.29	0.3192	0.013	0.67309	0.131	0.0017	0.16317	0.1108	0.0016	1939	43	1787	63	2123	29	2109	23	262.1	9.4	141.5	5.7	462	15	1.847	0.022
CLIB7 - 57	2.103	0.11	0.0994	0.0046	0.86482	0.1541	0.0022	0.55856	0.1785	0.0051	1146	36	610	27	3314	87	2386	25	763	36	131.6	8.3	655	20	5.92	0.12
CLIB7 - 59	6.714	0.33	0.3774	0.015	0.73944	0.1295	0.0014	0.065593	0.1099	0.0015	2075	46	2063	70	2107	27	2089	19	324.1	9.7	148.3	4.7	478	13	2.157	0.026
CLIB7 - 60	4.807	0.26	0.2754	0.013	0.88131	0.1263	0.0013	0.077406	0.0872	0.0021	1783	54	1567	69	1689	40	2045	18	863	22	459	10	1195	29	1.862	0.026
CLIB7 - 61	6.929	0.34	0.386	0.015	0.60192	0.13	0.0017	0.29225	0.1229	0.0025	2100	44	2103	71	2341	45	2094	24	164.8	5.8	75.2	2.8	265.9	6.9	2.207	0.031
CLIB7 - 62	6.92	0.35	0.3769	0.015	0.74697	0.1329	0.0018	0.16292	0.1377	0.0025	2097	44	2060	71	2606	44	2132	24	175.8	7.7	66.5	2.2	265.7	8.3	2.648	0.048
CLIB7 - 63	6.539	0.32	0.356	0.014	0.75725	0.1329	0.0015	0.16467	0.114	0.0025	2049	45	1962	69	2180	45	2134	19	308	11	123.7	2.6	418	12	2.505	0.051
CLIB7 - 64	6.182	0.31	0.3381	0.013	0.66202	0.1321	0.0018	0.15689	0.1121	0.0018	1999	44	1876	64	2151	34	2124	23	200	4.2	112.3	1.9	366.8	6.1	1.883	0.028
CLIB7 - 68	4.341	0.24	0.2268	0.011	0.82344	0.1379	0.0016	0.25784	0.0855	0.0014	1698	43	1317	58	1658	25	2197	21	369	23	195	11	494	29	2.056	0.033
CLIB7 - 69	6.5	0.32	0.354	0.014	0.75781	0.1319	0.0016	0.21164	0.1105	0.0022	2043	45	1953	68	2117	40	2120	21	237.3	9	132.1	4.1	430	14	1.95	0.039
CLIB7 - 70	5.481	0.27	0.3011	0.012	0.81966	0.1308	0.0015	0.073167	0.099	0.002	1894	43	1695	60	1906	36	2106	21	351	11	195.8	6.1	554.2	8.8	1.945	0.028

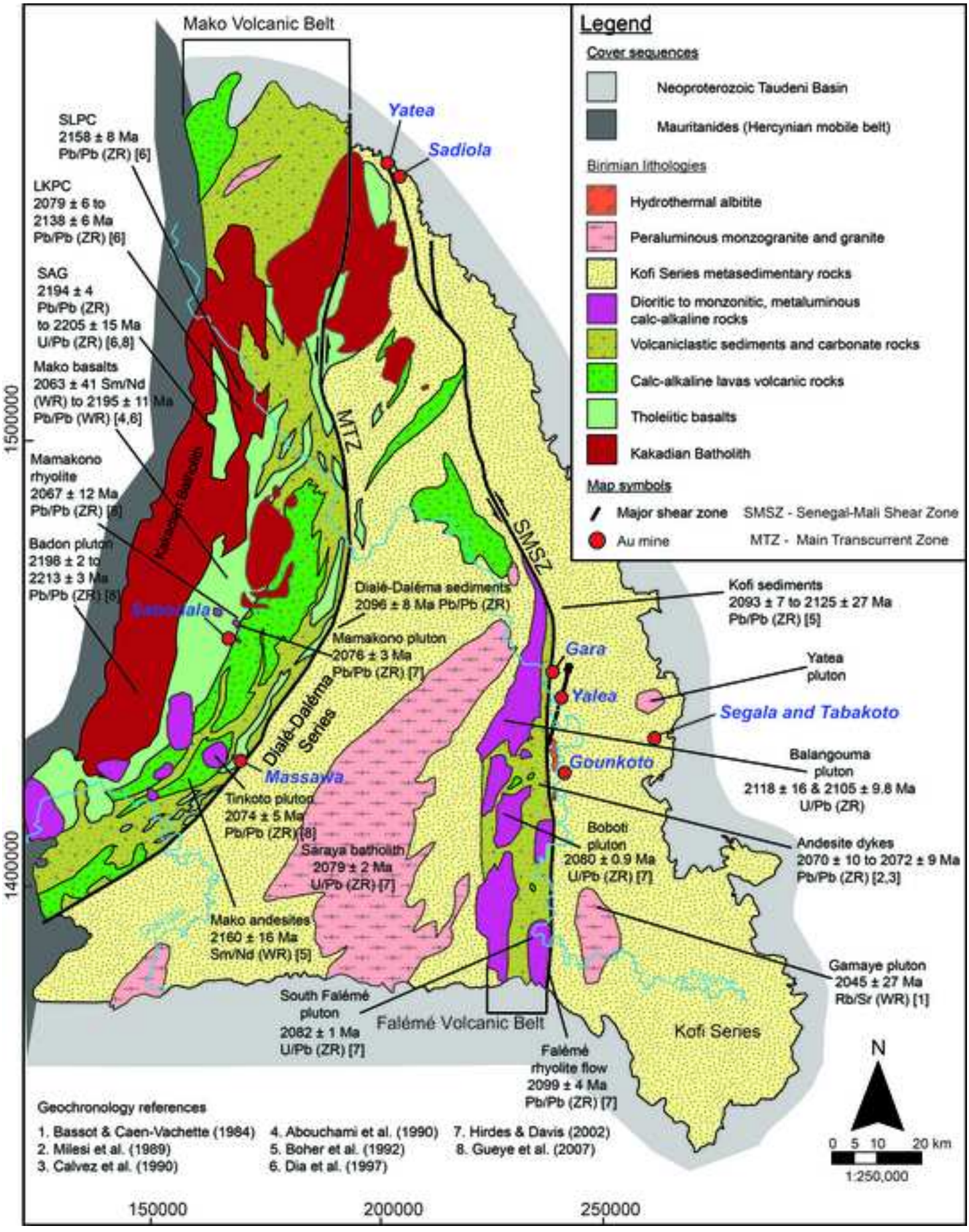

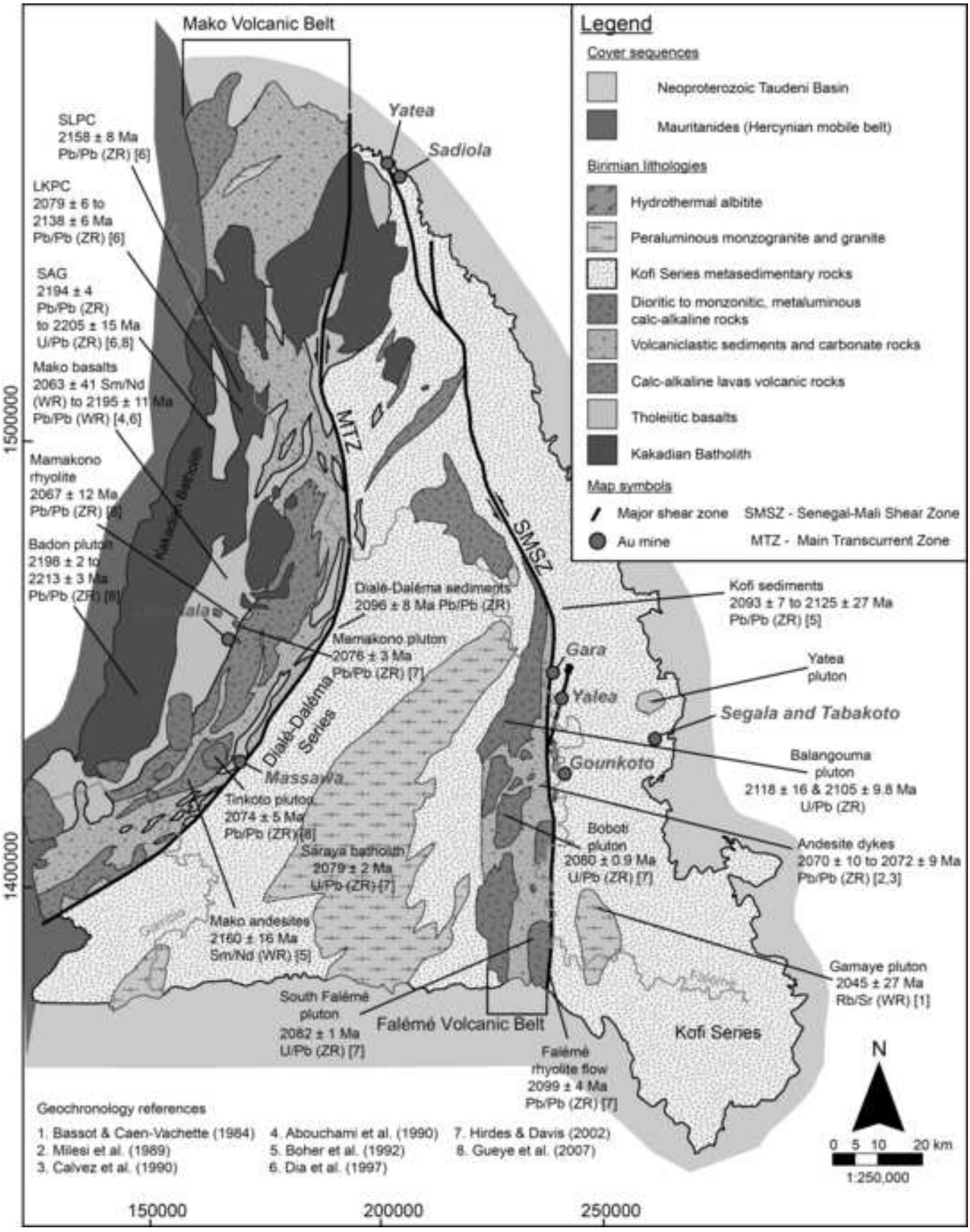

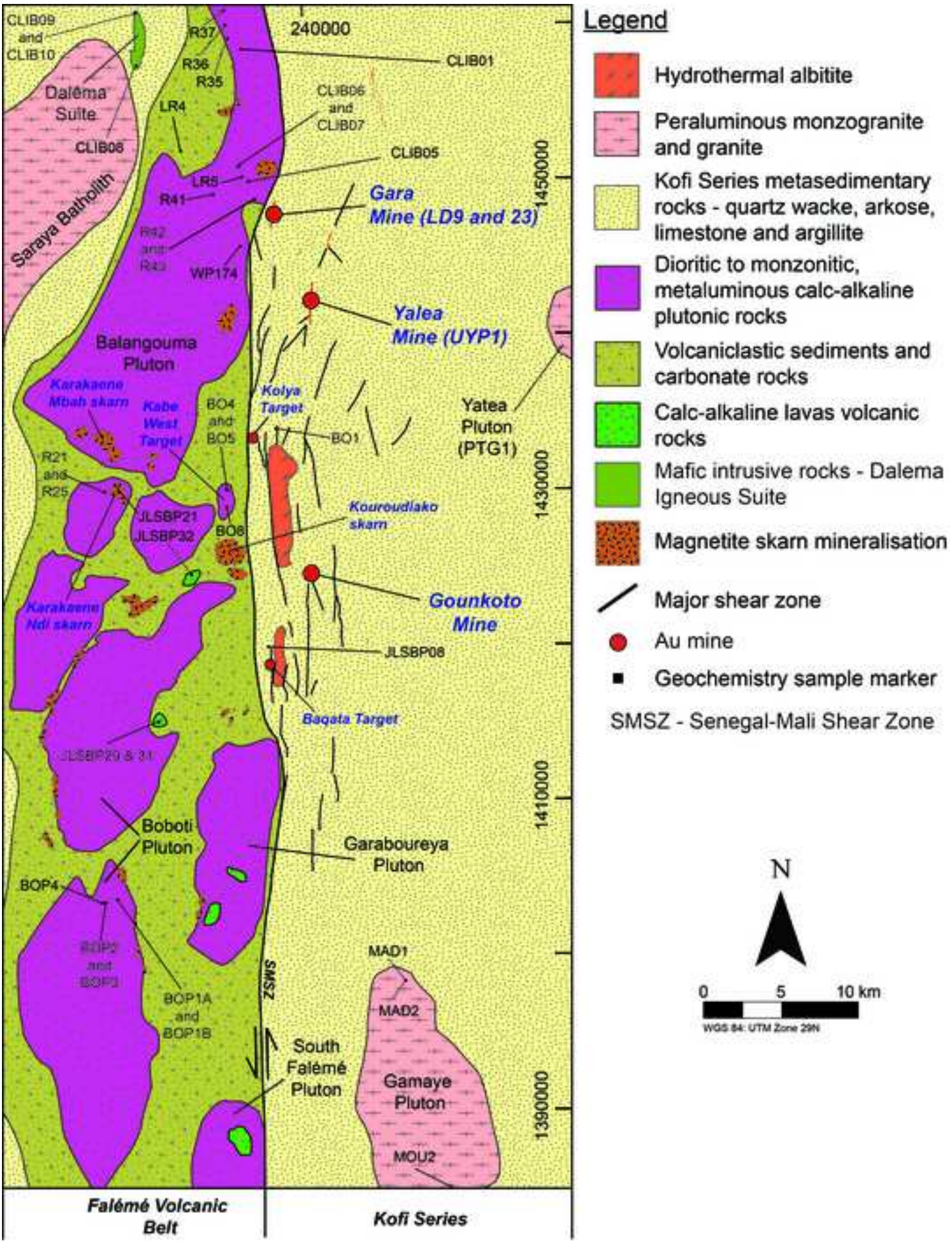

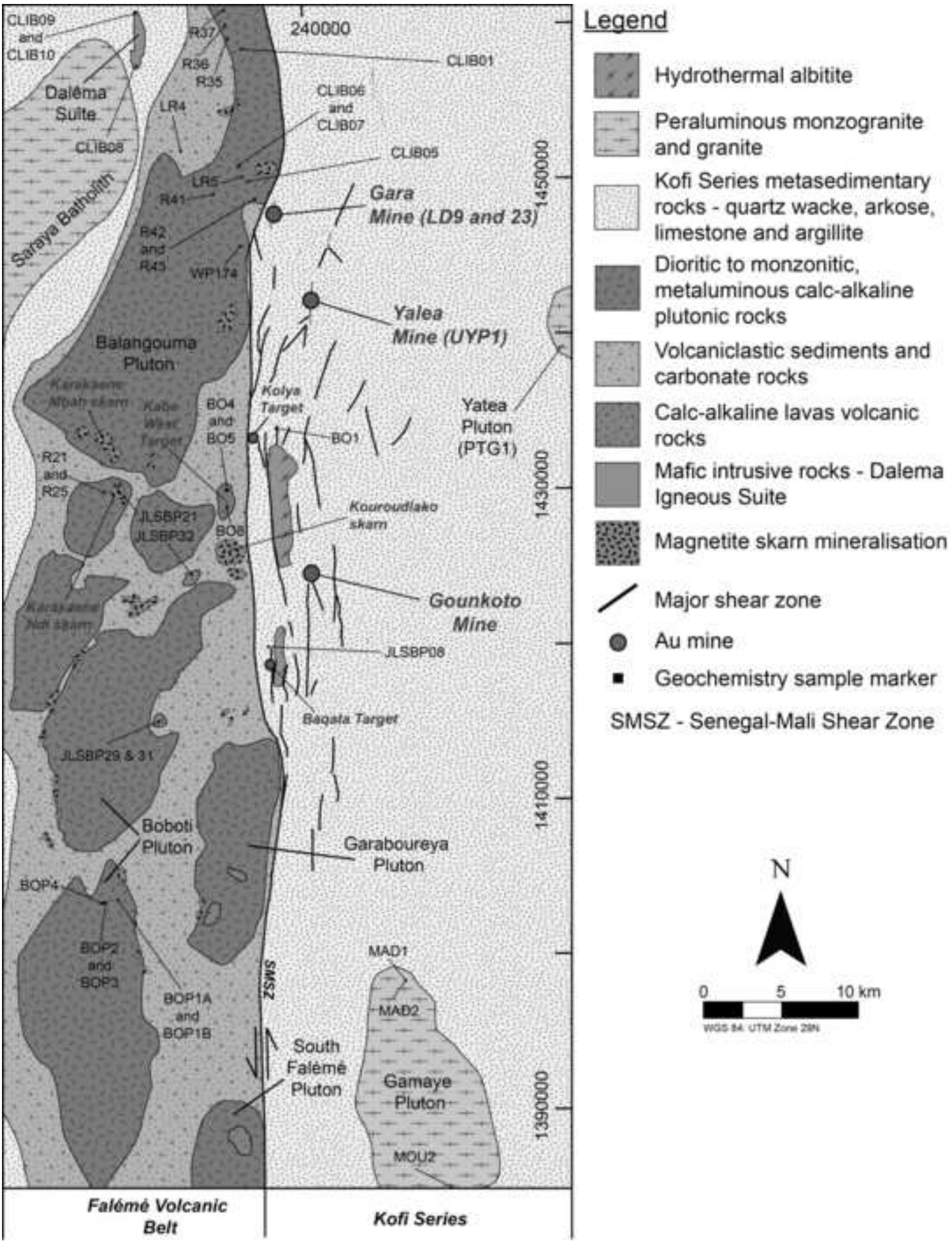

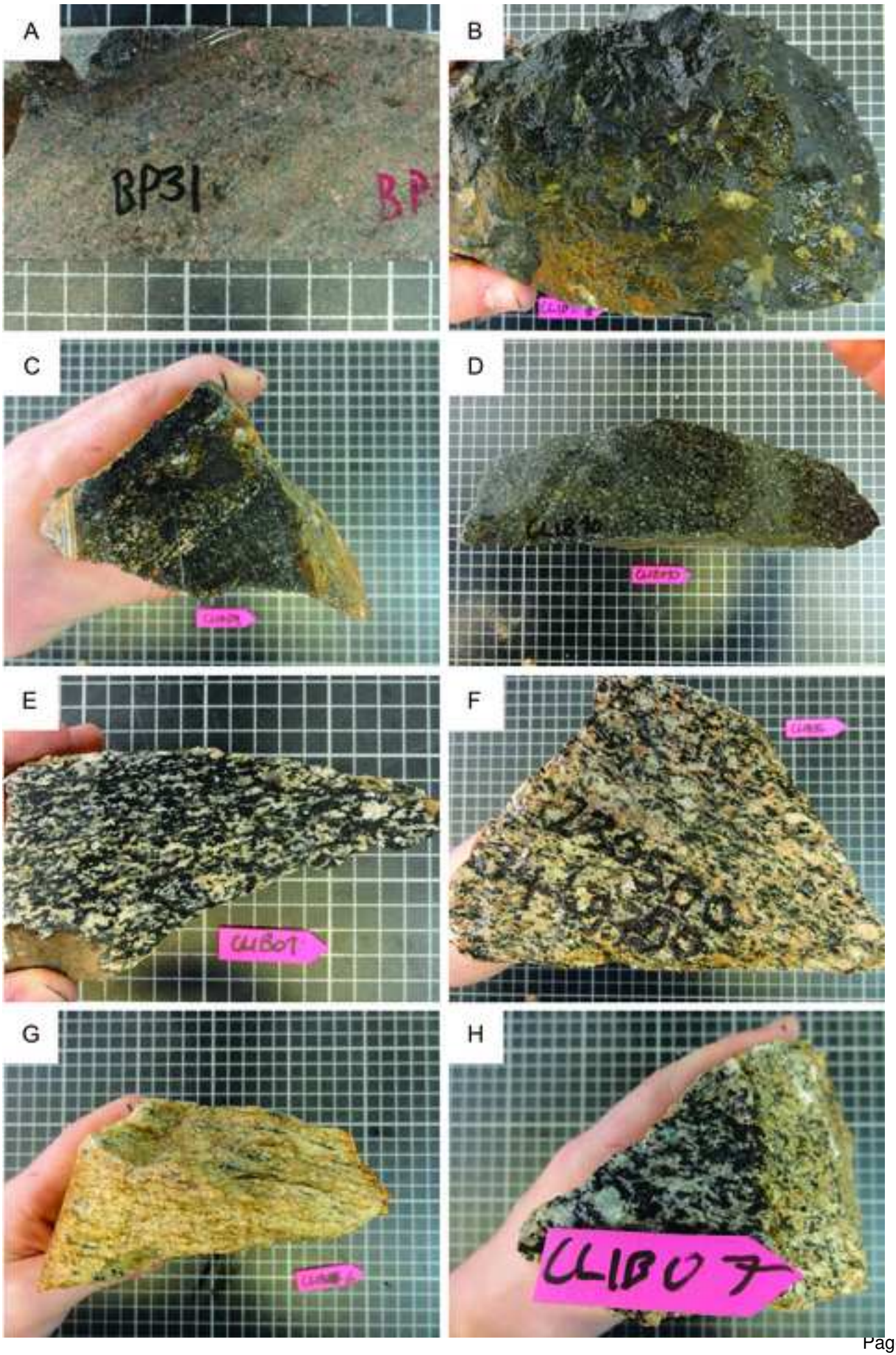

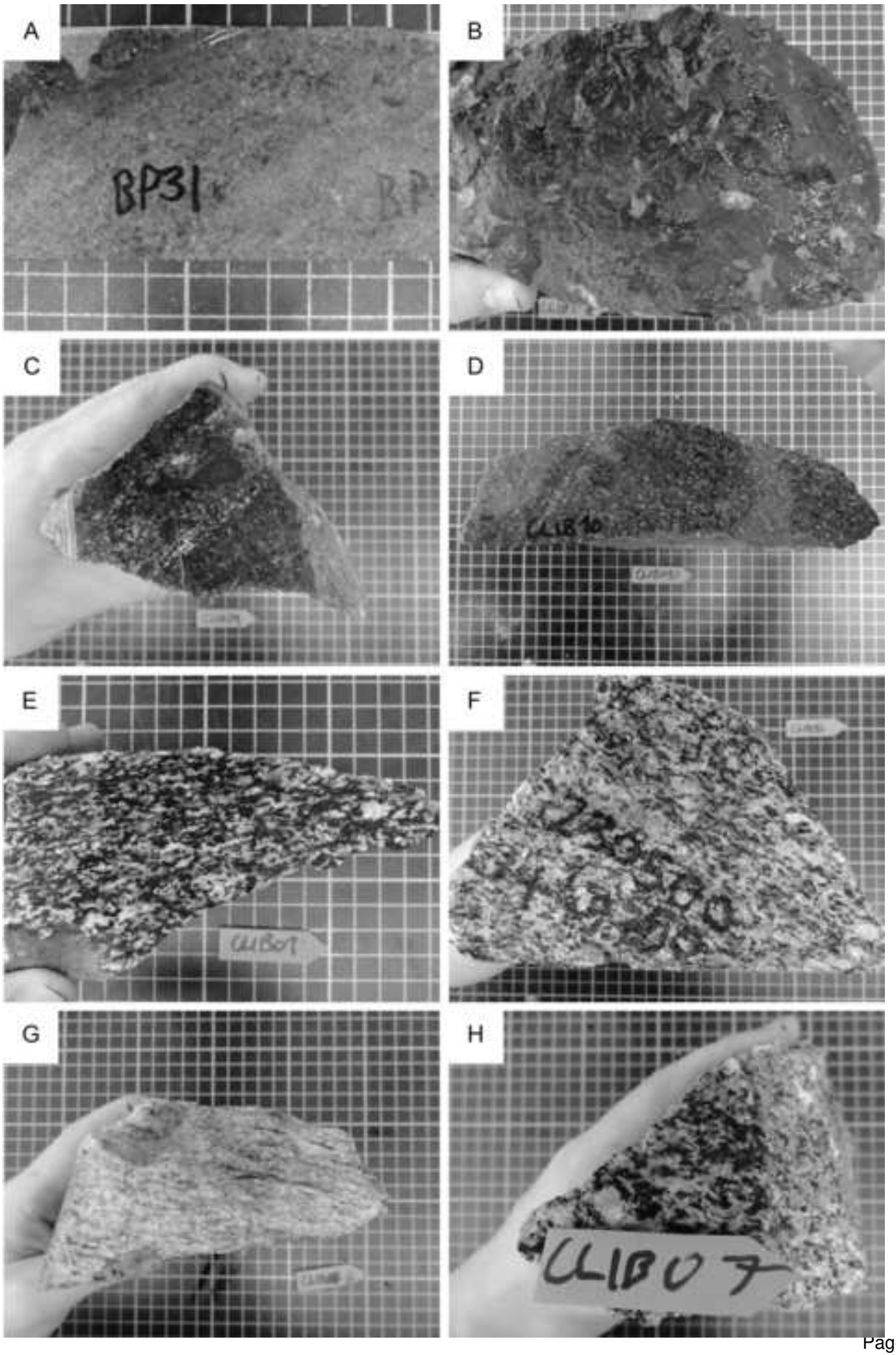

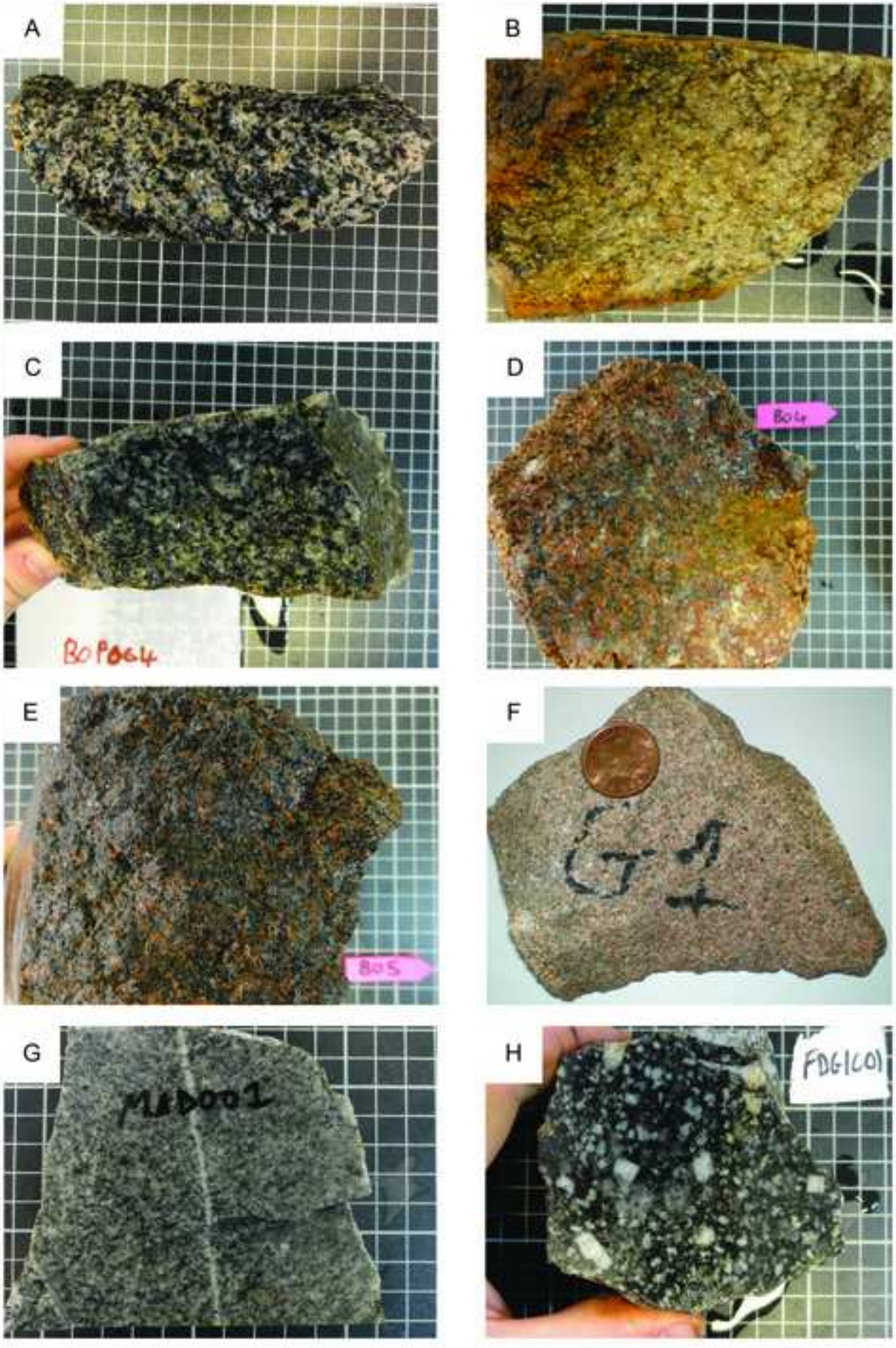

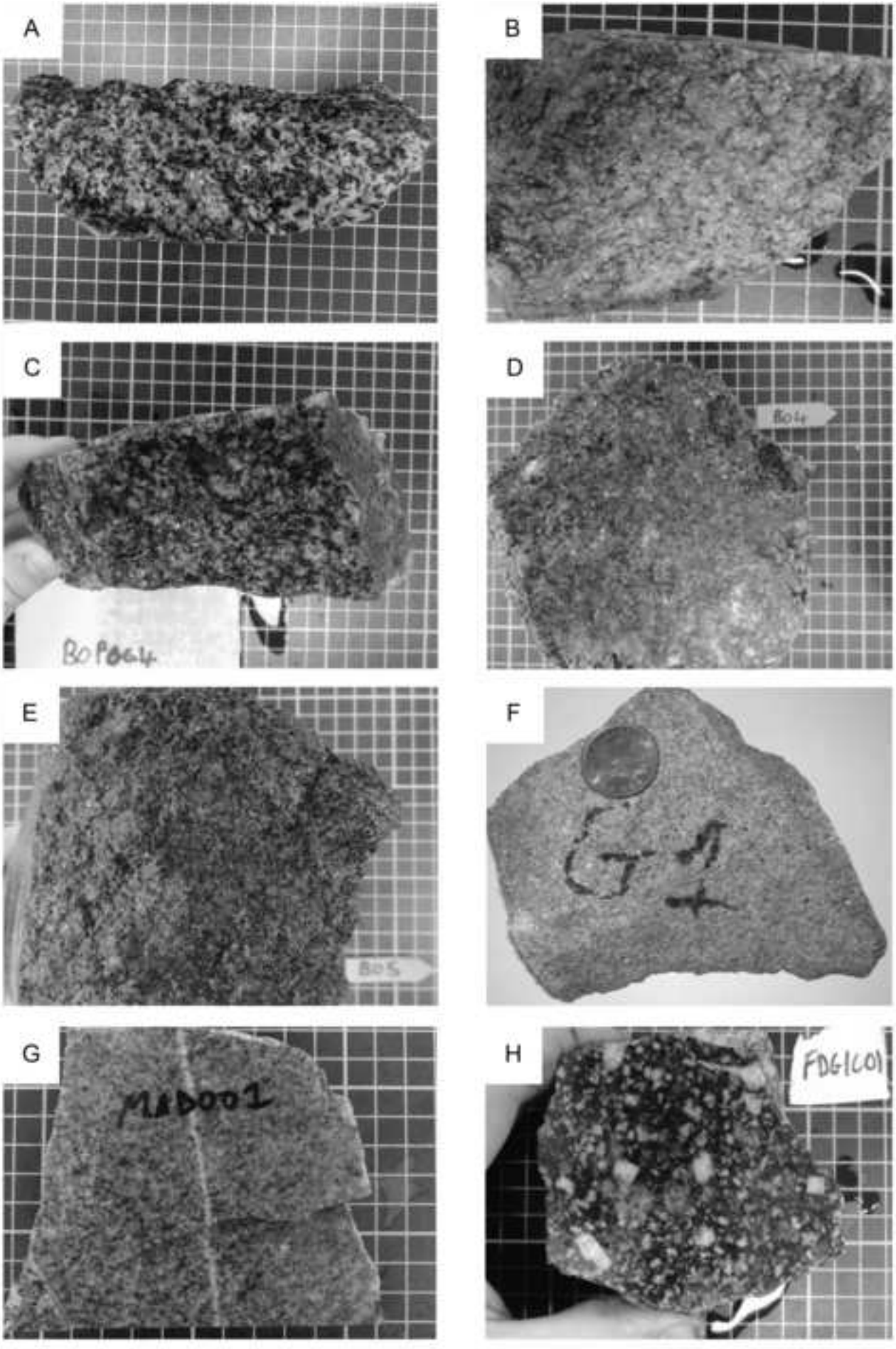

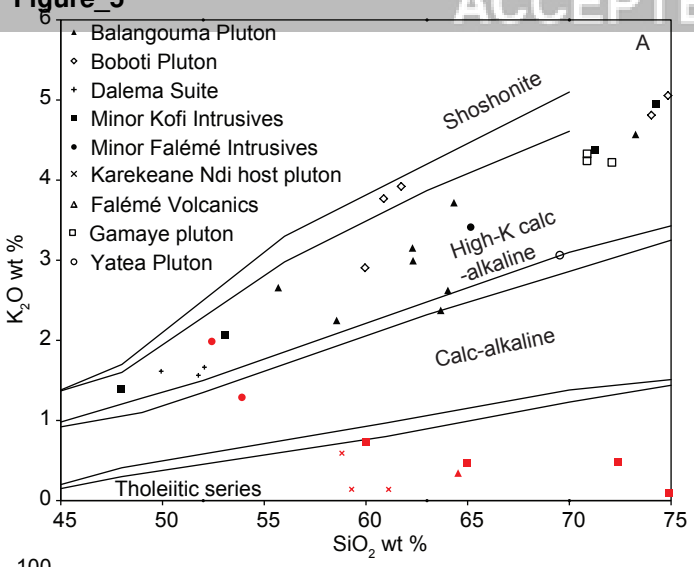

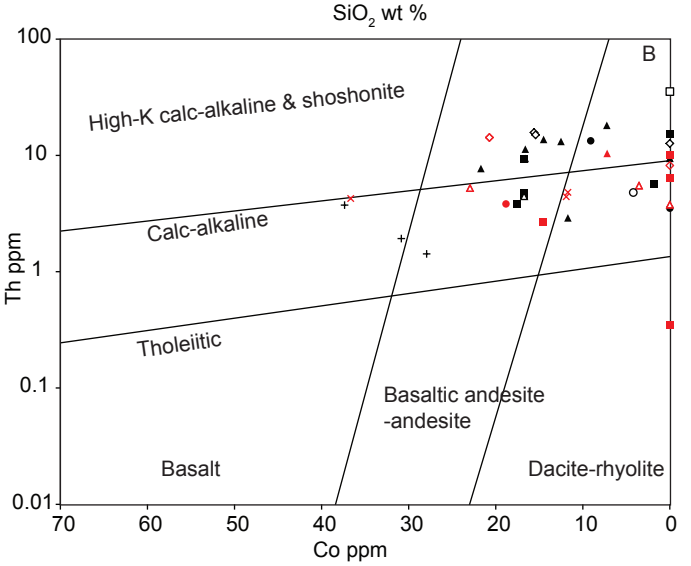

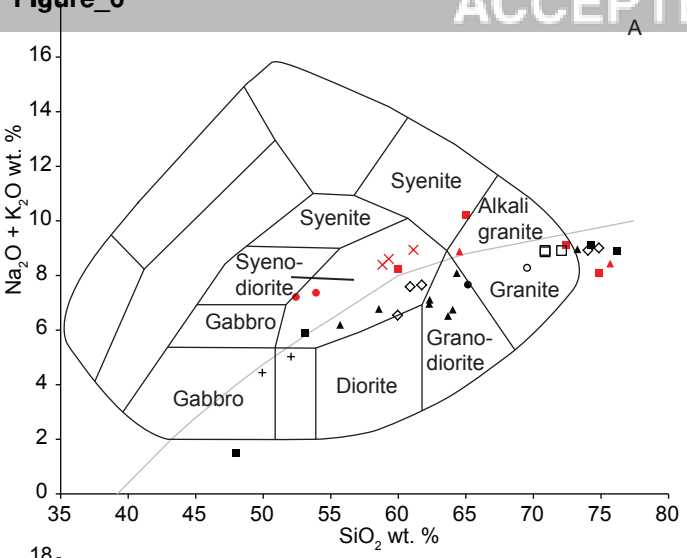

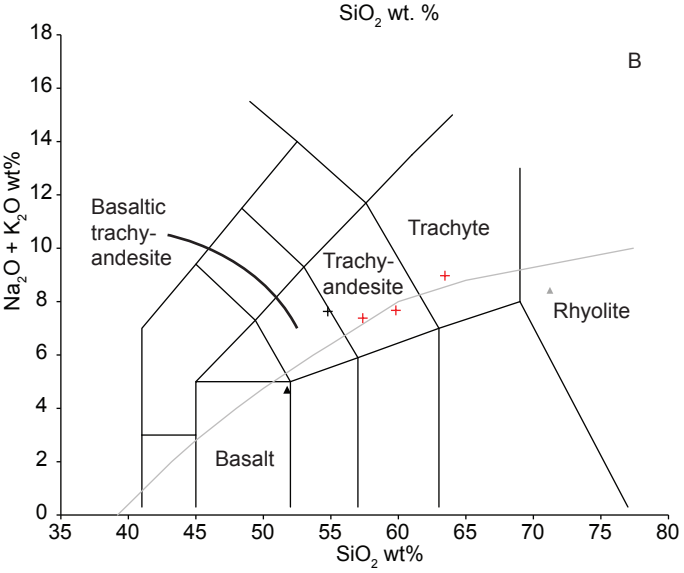

Legend

Plutonic rocks

- ▲ Balangouma
- ◇ Boboti
- \+ Dalema Suite
- ■ Minor Kofi Intrusives
- ● Minor Falémé Intrusives
- □ Gamaye pluton
- × Karekeane Ndi host pluton
- ○ Yatea

Volcanic rocks

- ▲ Dalema Suite
- ▲ Fadougou rhyolite
- \+ Falémé Volcanics

— Alkali-Sub-alkali division

Figure_7

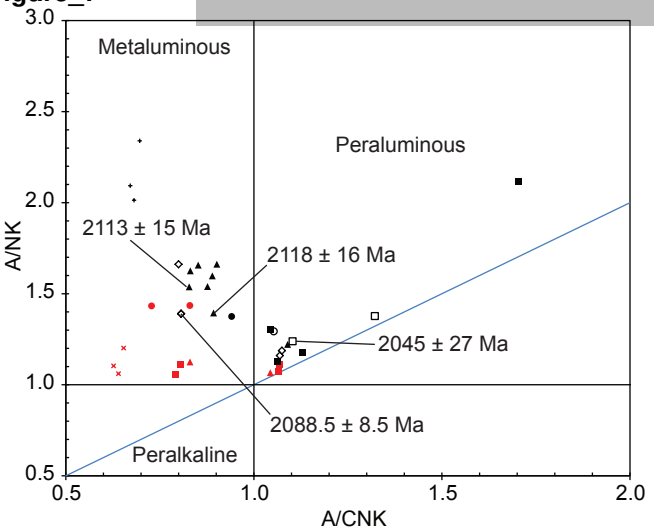

Legend

- ▲ Balangouma Pluton
- ◇ Boboti Pluton
- \+ Dalema Suite
- ■ Minor Kofi Intrusives
- ● Minor Falémé Intrusives
- □ Gamaye pluton
- × Karekeane Ndi host pluton
- ○ Yatea Pluton

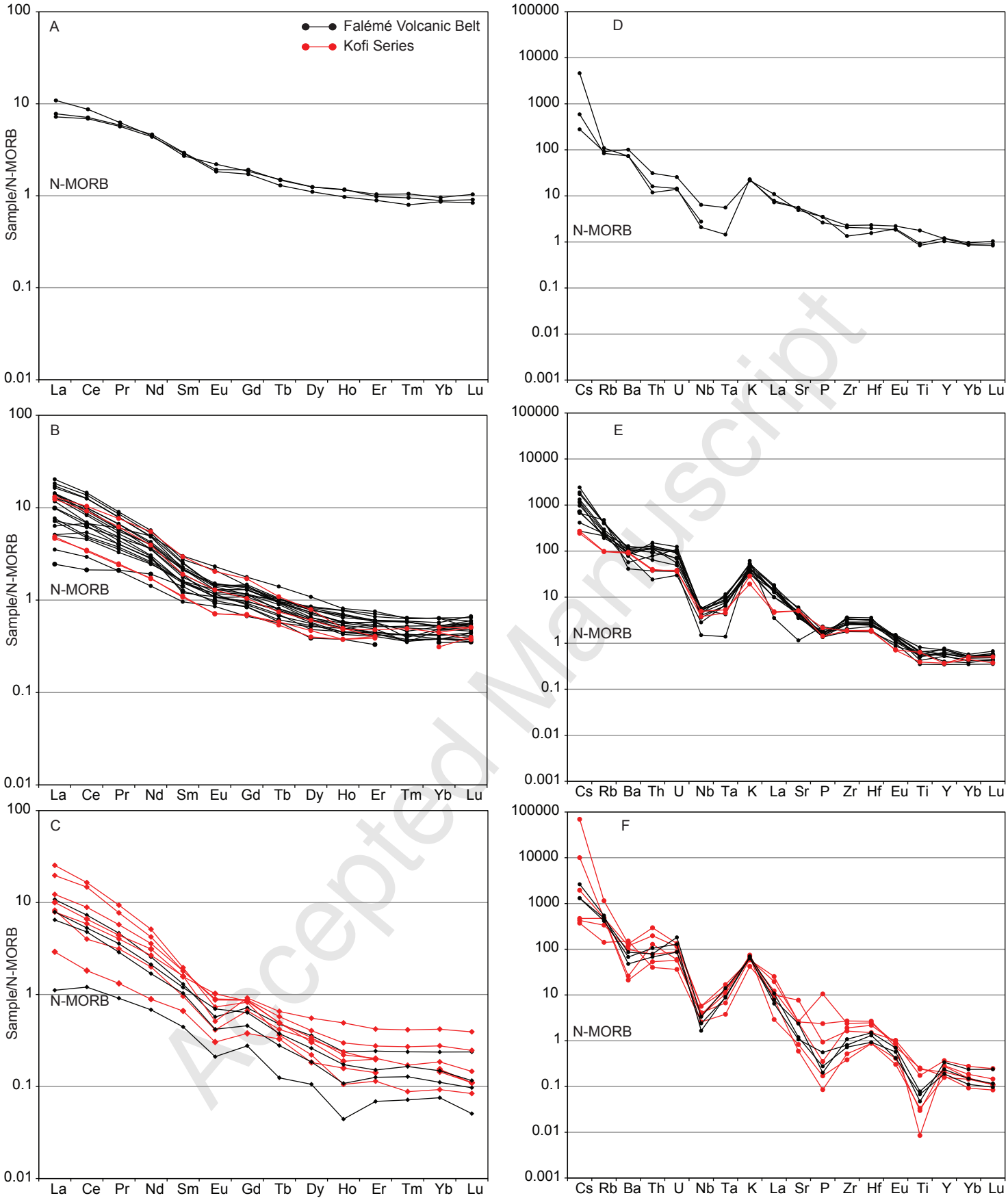

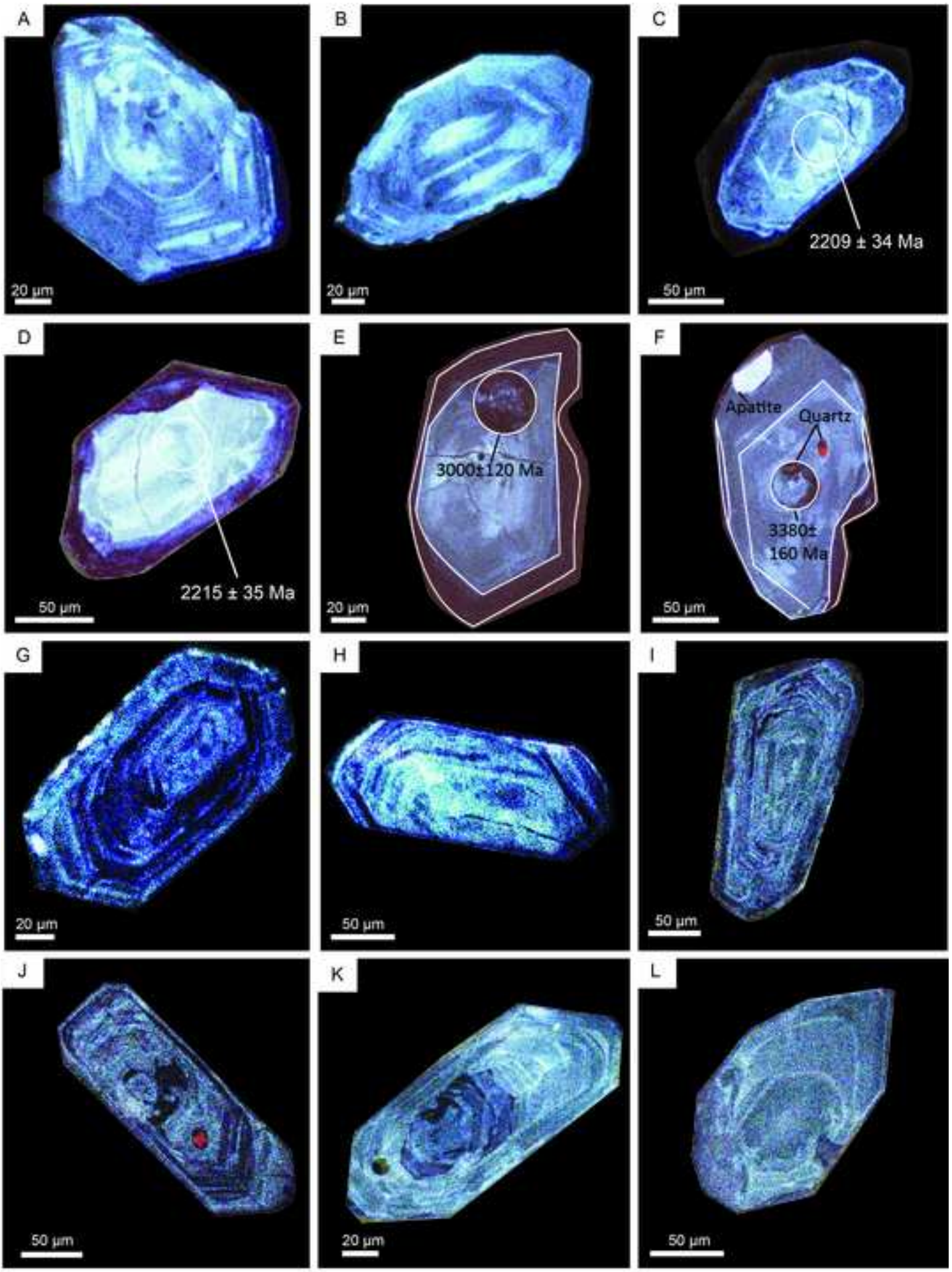

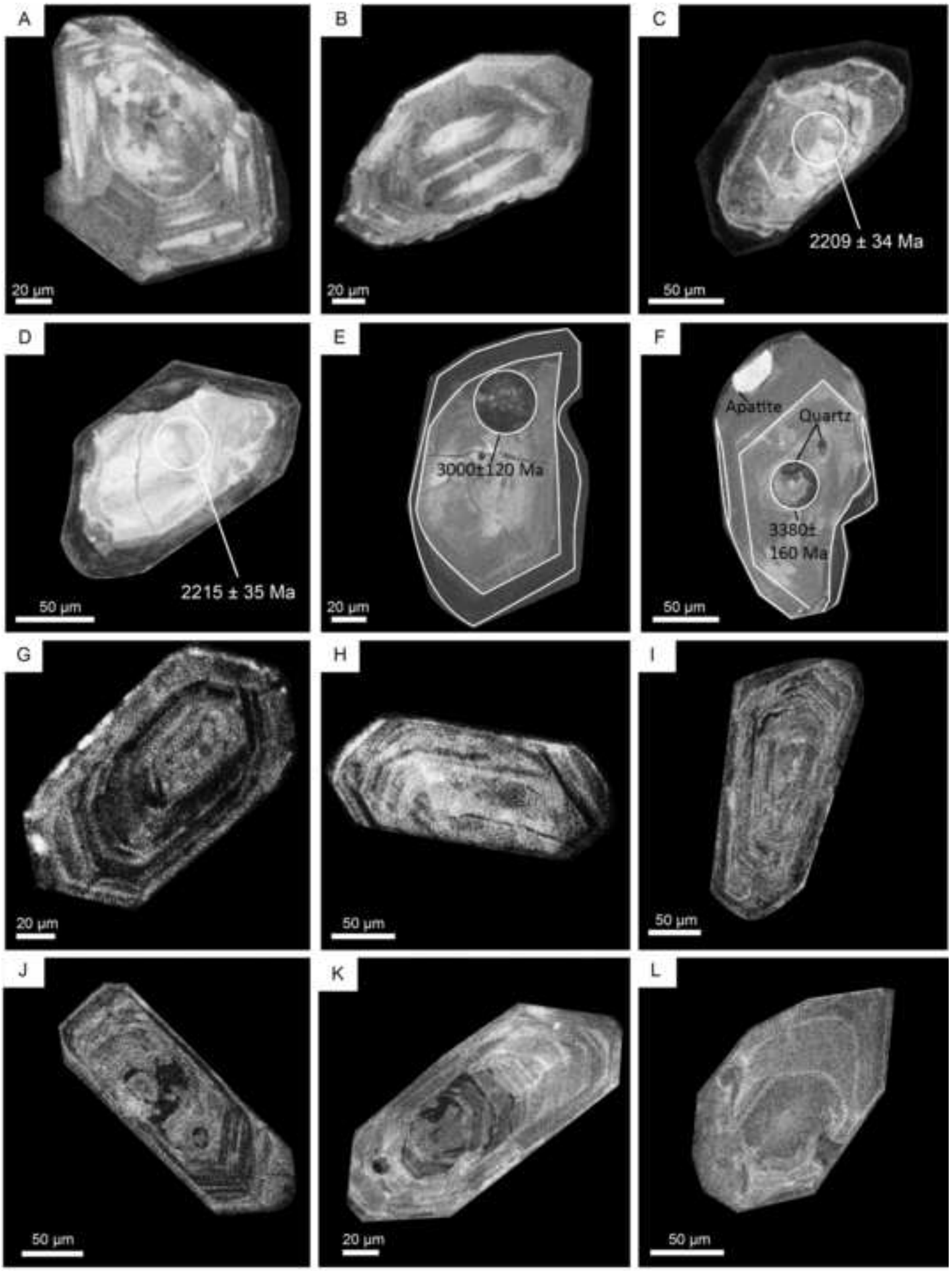

Figure 10

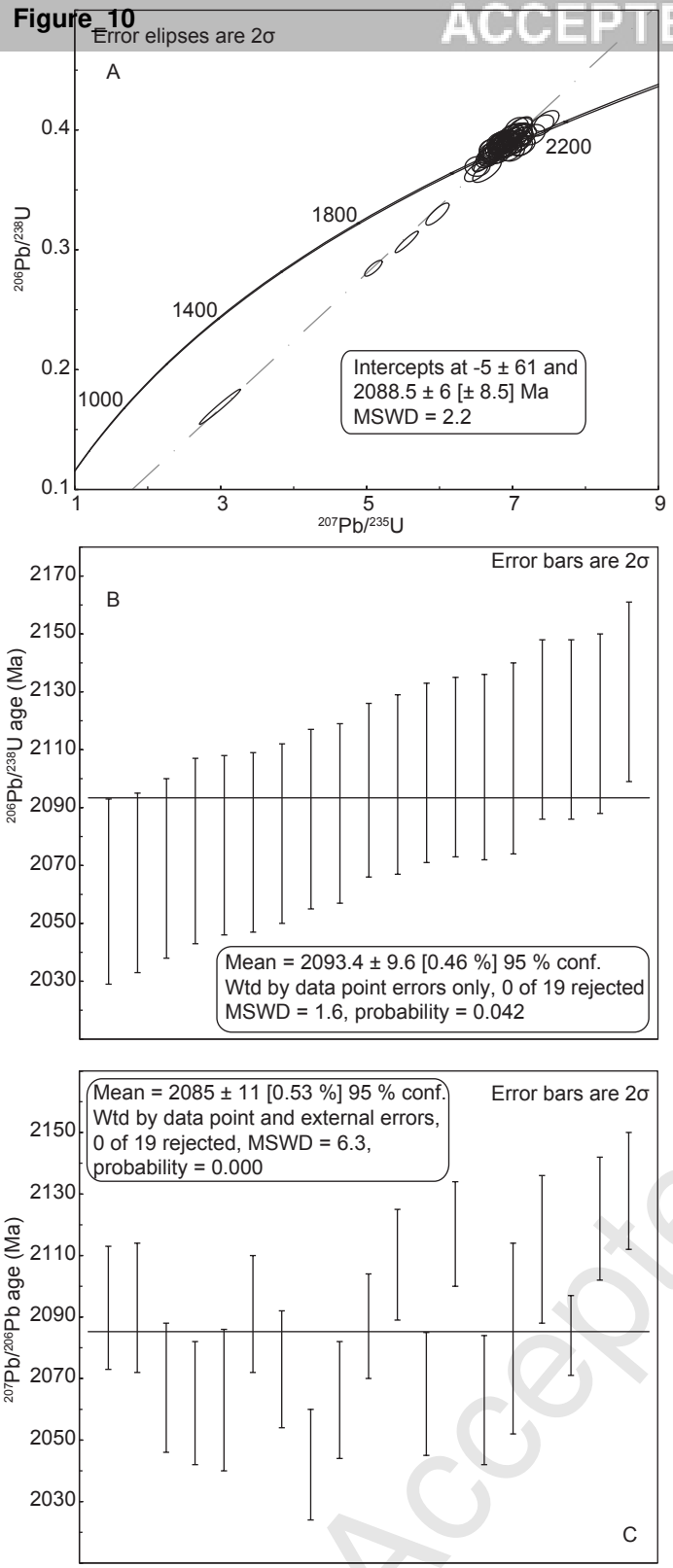

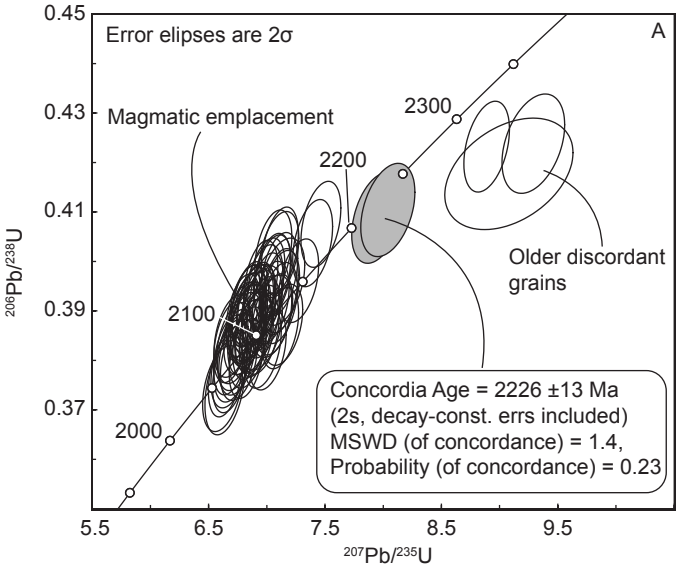

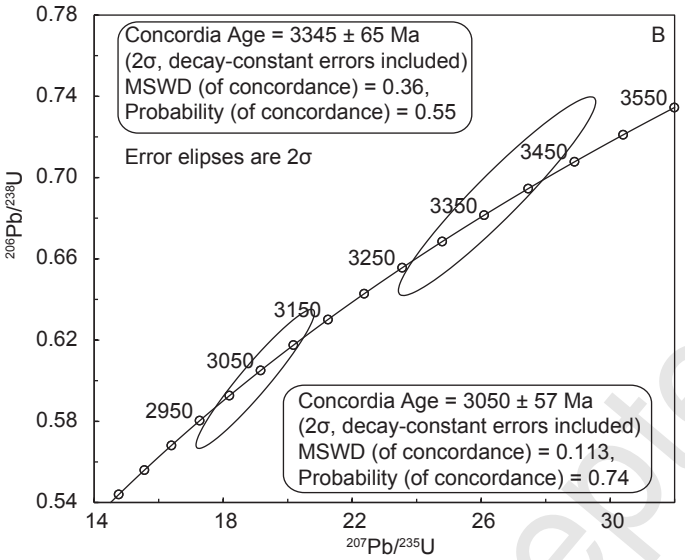

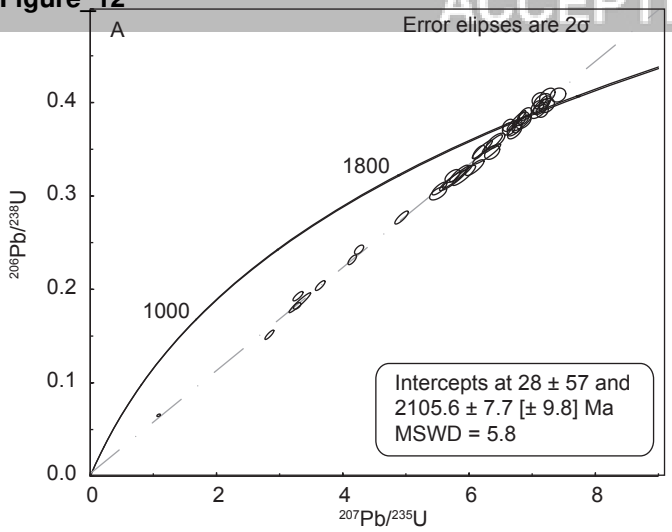

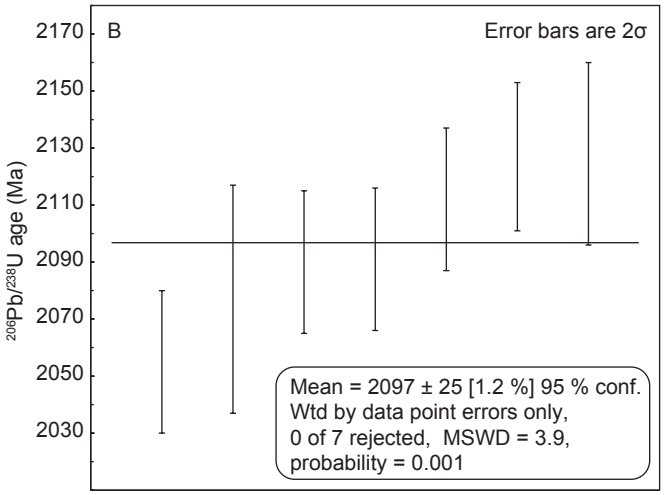

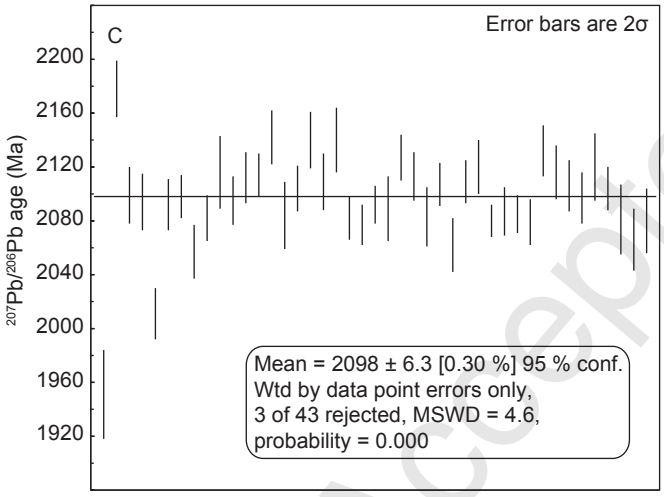

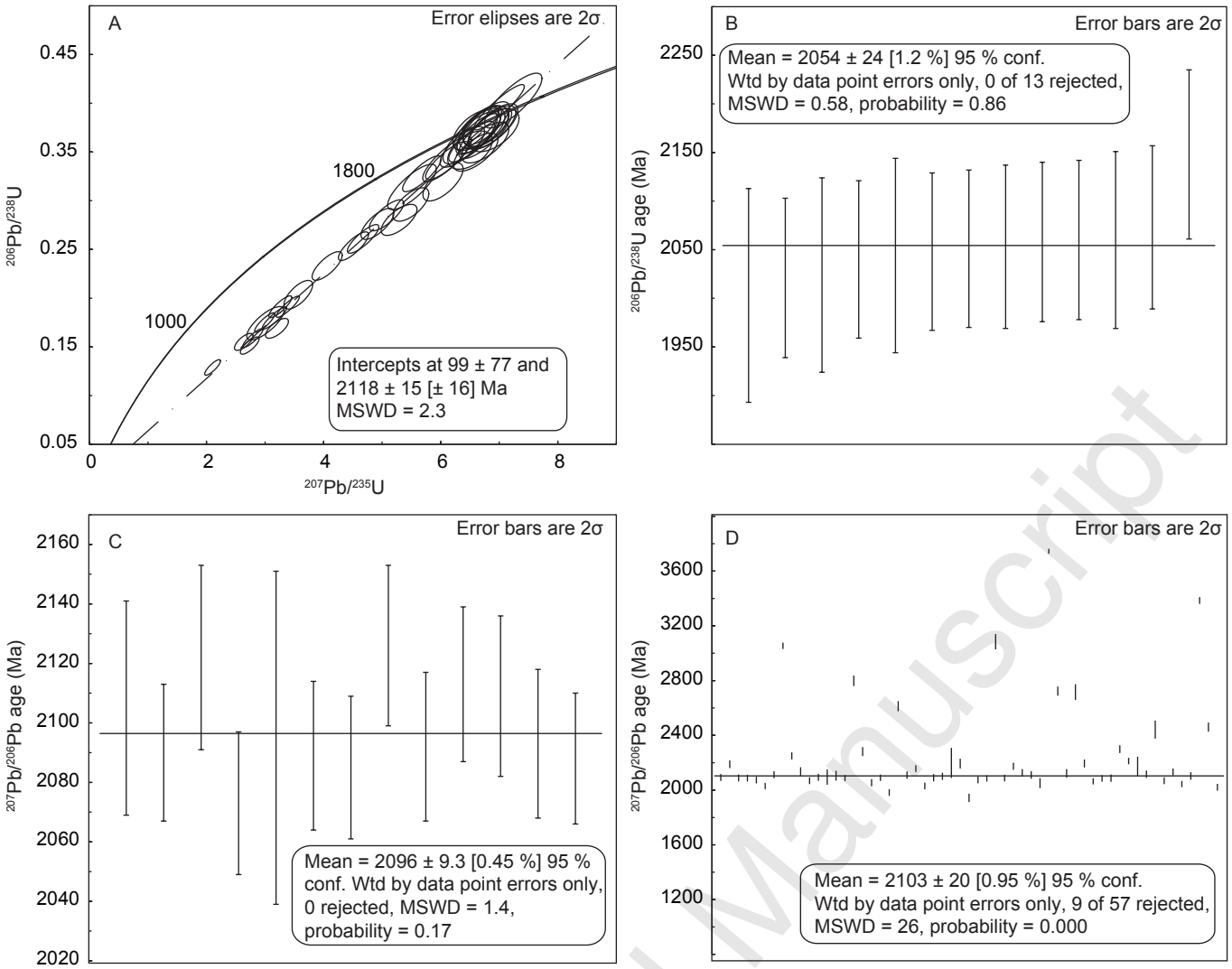

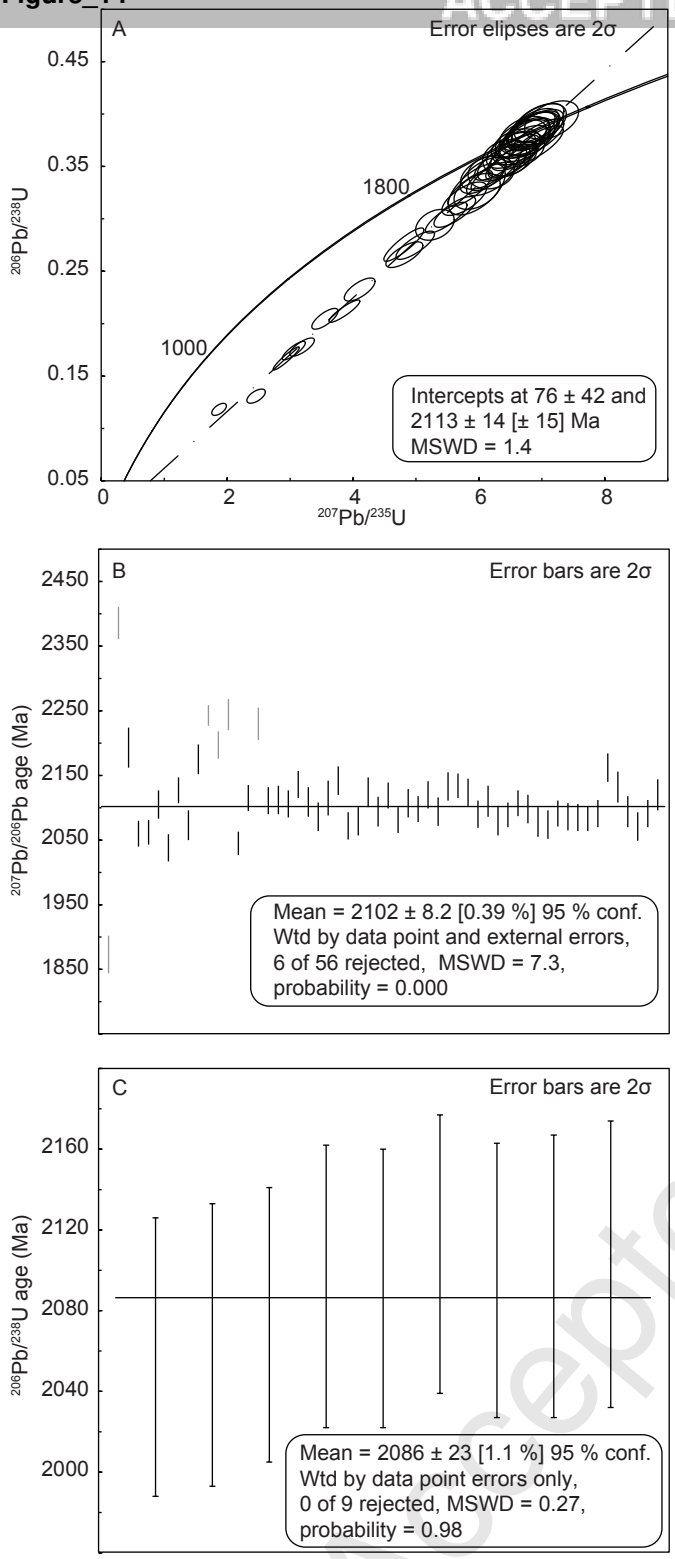

Figure_15

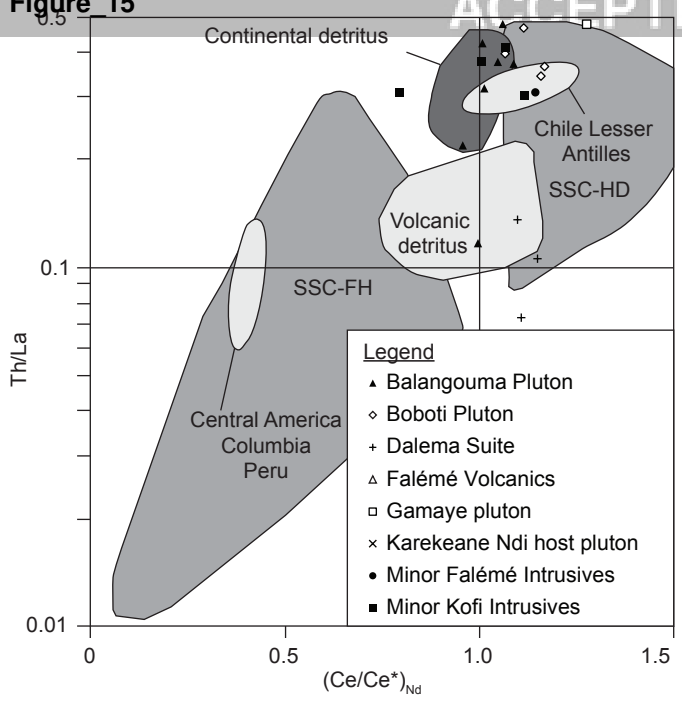

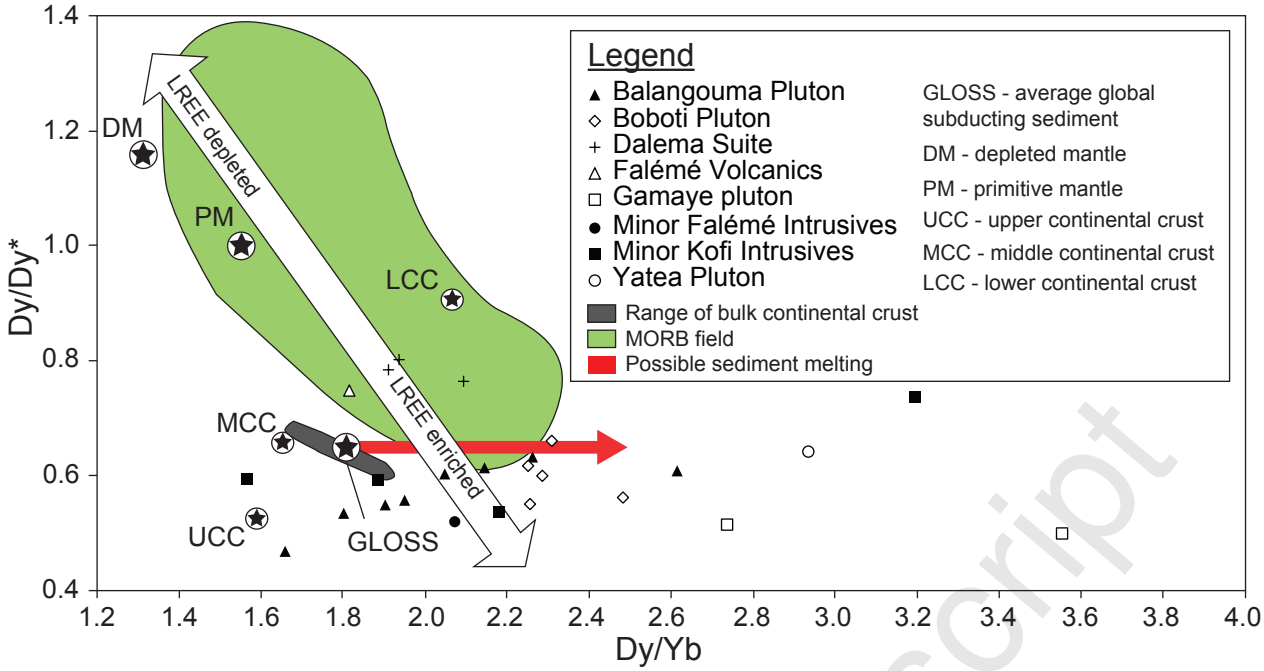

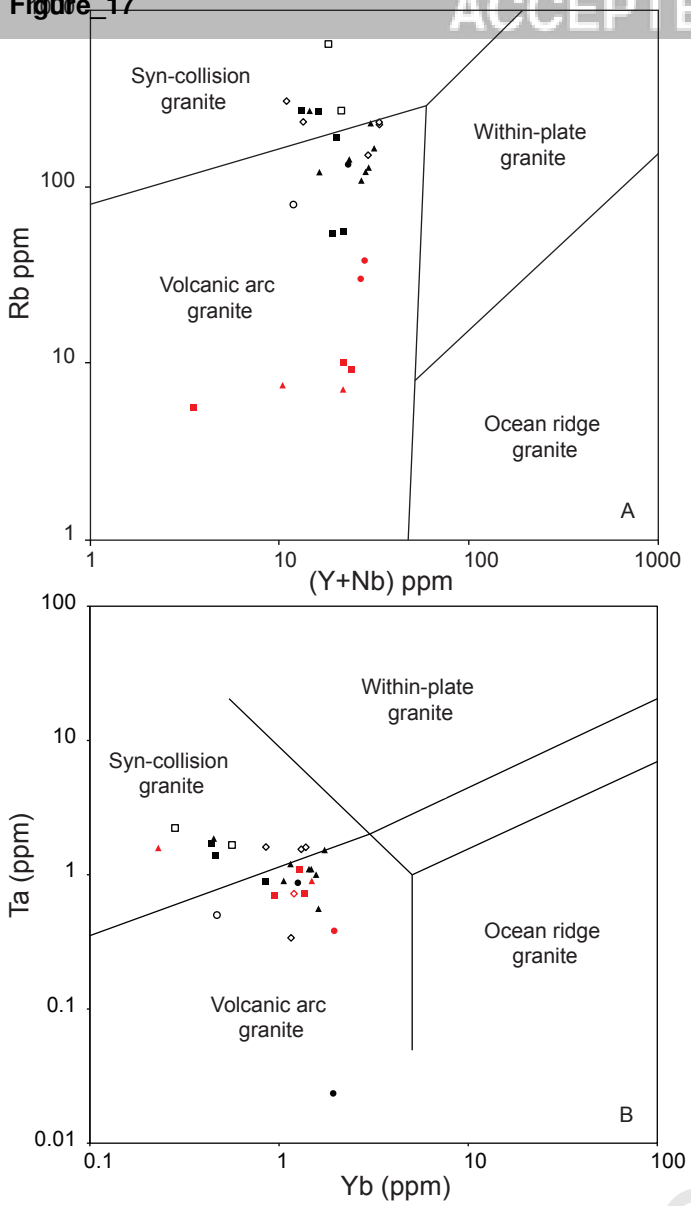

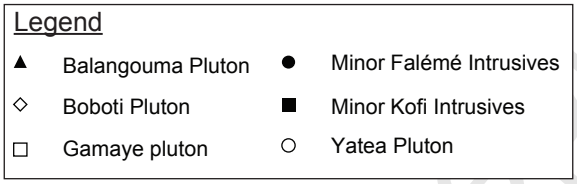

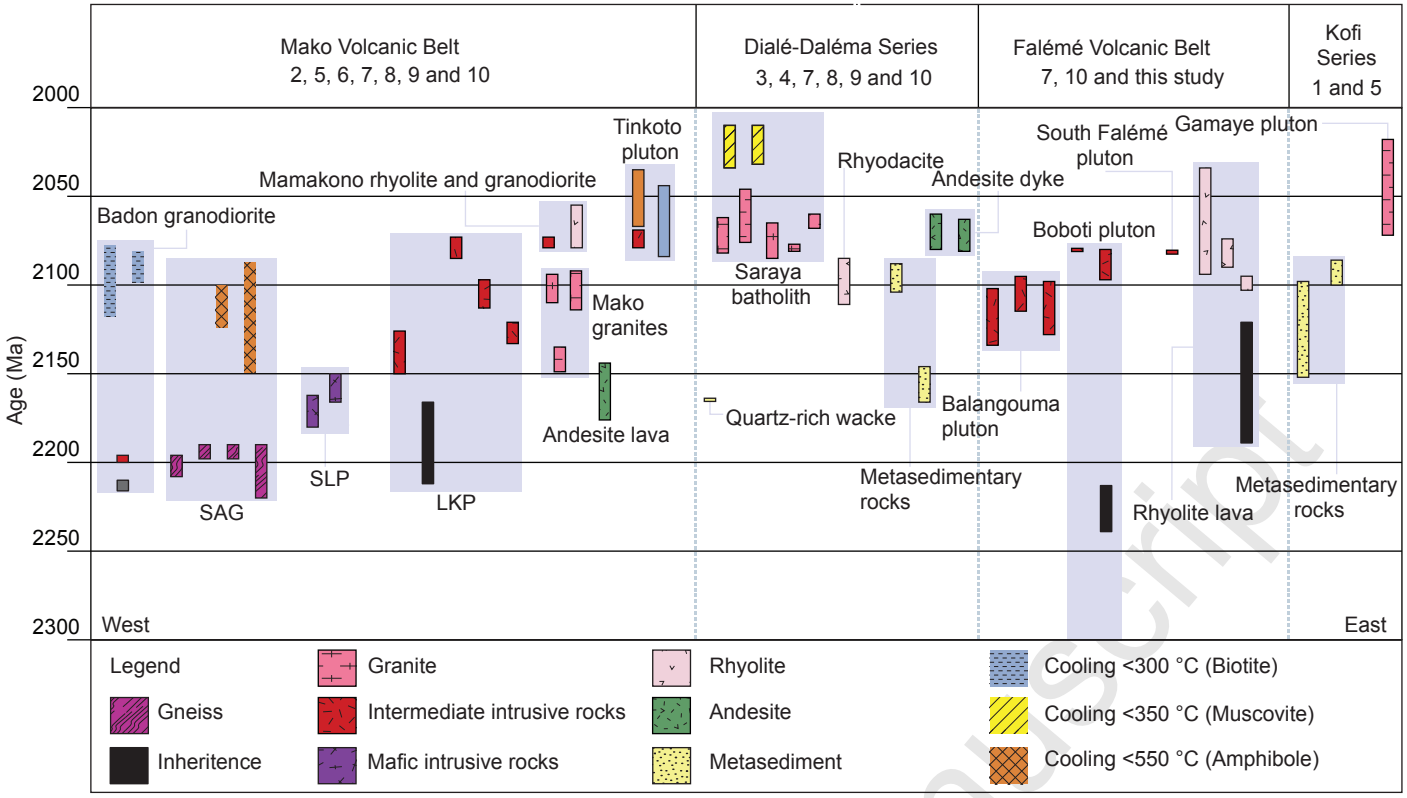

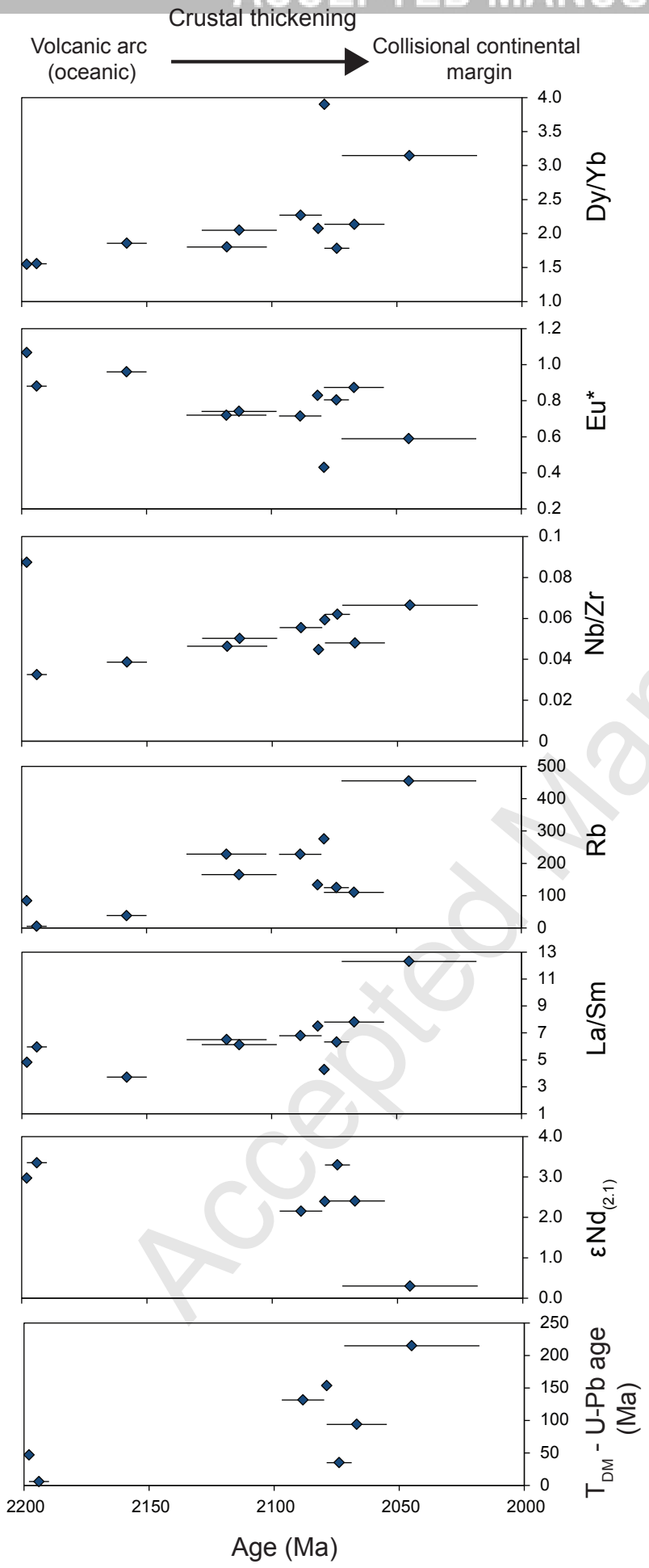

- Highlights
- New U-Pb age data indicate the Balangouma pluton crystallised at 2112 ± 13 Ma.
- Inherited zircons indicate magmatic activity in the Falémé Belt at 2226 ± 13 Ma.
- The KKI evolved from a volcanic island arc environment to an active continental margin.
- Crustal thickening generated peraluminous, granitic melts with a crustal component.
- The Daléma igneous rocks may have formed in an extensional back arc setting.